Space Sci Rev (2013) 180:101–175
DOI 10.1007/s11214-013-0020-8

Complementary and Emerging Techniques for Astrophysical Ices Processed in the Laboratory

M.A. Allodi · R.A. Baragiola · G.A. Baratta · M.A. Barucci · G.A. Blake · P. Boduch · J.R. Brucato · C. Contreras · S.H. Cuylle · D. Fulvio · M.S. Gudipati · S. Ioppolo · Z. Kaňuchová · A. Lignell · H. Linnartz · M.E. Palumbo · U. Raut · H. Rothard · F. Salama · E.V. Savchenko · E. Sciamma-O'Brien · G. Strazzulla

Received: 2 January 2013 / Accepted: 26 August 2013 / Published online: 26 September 2013

Abstract Inter- and circumstellar ices comprise different molecules accreted on cold dust particles. These icy dust grains provide a molecule reservoir where particles can interact and react. As the grain acts as a third body, capable of absorbing energy, icy surfaces in space have a catalytic effect. Chemical reactions are triggered by a number of possible processes; (i) irradiation by light, typically UV photons from the interstellar radiation field and

M.A. Allodi · G.A. Blake
Division of Chemistry & Chemical Engineering, California Institute of Technology, 1200 E. California Blvd., Pasadena, CA 91125, USA

M.A. Allodi
e-mail: mallodi@caltech.edu

G.A. Blake
e-mail: gab@gps.caltech.edu

R.A. Baragiola · D. Fulvio · U. Raut
Laboratory for Atomic and Surface Physics, University of Virginia, Thornton Hall B-103, Charlottesville, VA 22904, USA

R.A. Baragiola
e-mail: raul@virginia.edu

D. Fulvio
e-mail: df6vz@virginia.edu

U. Raut
e-mail: raut@virginia.edu

G.A. Baratta · Z. Kaňuchová · M.E. Palumbo · G. Strazzulla (✉)
Osservatorio Astrofisico di Catania, INAF, Catania, Italy
e-mail: gianni@oact.inaf.it

G.A. Baratta
e-mail: gbaratta@oact.inaf.it

Z. Kaňuchová
e-mail: zkanuch@ta3.sk

M.E. Palumbo
e-mail: mepalumbo@oact.inaf.it

Ly-α radiation emitted by excited hydrogen, but also X-rays, (ii) bombardment by particles, free atoms (most noticeably hydrogen, but also N, C, O and D-atoms), electrons, low energy ions and cosmic rays, and (iii) thermal processing. All these effects cause ices to (photo)desorb, induce fragmentation or ionization in the ice, and eventual recombination will make molecules to react and to form more and more complex species. The effects of

M.A. Barucci
Paris Observatory, LESIA, Paris, France
e-mail: antonella.barucci@obspm.fr

G.A. Blake · S. Ioppolo
Division of Geological & Planetary Sciences, California Institute of Technology, 1200 E. California Blvd., Pasadena, CA 91125, USA

G.A. Blake
e-mail: gab@gps.caltech.edu

S. Ioppolo
e-mail: ioppolo@caltech.edu

P. Boduch · H. Rothard
Centre de Recherche sur les Ion, les Matériaux et la Photonique (CEA/CNRS UMR 6252/ENSICAEN/UCBN), CIMAP-CIRIL-Ganil, BP5133, 14070 Caen Cedex 05, France

P. Boduch
e-mail: boduch@ganil.fr

H. Rothard
e-mail: rothard@ganil.fr

J.R. Brucato
Osservatorio Astrofisico di Arcetri, INAF, Florence, Italy
e-mail: jbrucato@arcetri.astro.it

C. Contreras · F. Salama · E. Sciamma-O'Brien
Ames Research Center, Space Sciences & Astrobiology Division, NASA, Moffett Field, CA 94035-1000, USA

F. Salama
e-mail: farid.salama@nasa.gov

S.H. Cuylle · H. Linnartz
Raymond & Beverly Sackler Laboratory for Astrophysics, Leiden Observatory, University of Leiden, 2300 RA Leiden, The Netherlands

H. Linnartz
e-mail: linnartz@strw.leidenuniv.nl

M.S. Gudipati · A. Lignell
Jet Propulsion Laboratory, California Institute of Technology, Pasadena, CA 91109, USA

M.S. Gudipati
e-mail: murthy.gudipati@jpl.nasa.gov

M.S. Gudipati
IPST, University of Maryland, College Park, MD 20742, USA

E.V. Savchenko
Verkin Institute for Low Temperature Physics & Engineering NASU, Lenin Ave. 47, Kharkov 61103, Ukraine
e-mail: elena.savchenko@gmail.com

this solid state astrochemistry are observed by astronomers; nearly 180 different molecules (not including isotopologues) have been unambiguously identified in the inter- and circumstellar medium, and the abundances of a substantial part of these species cannot be explained by gas phase reaction schemes only and must involve solid state chemistry. Icy dust grains in space experience different chemical stages. In the diffuse medium grains are barely covered by molecules, but upon gravitational collapse and darkening of the cloud, temperatures drop and dust grains start acting as micrometer sized cryopumps. More and more species accrete, until even the most volatile species are frozen. In parallel (non)energetic processing can take place, particularly during planet and star formation when radiation and particle fluxes are intense. The physical and chemical properties of ice clearly provide a snapshotroot to characterize the cosmological chemical evolution.

In order to fully interpret the astronomical observations, therefore, dedicated laboratory experiments are needed that simulate dust grain formation and processing as well as ice mantle chemistry under astronomical conditions and in full control of the relevant parameters; ice morphology (i.e., structure), composition, temperature, UV and particle fluxes, etc., yielding parameters that can be used for astrochemical modeling and for comparison with the observations. This is the topic of the present manuscript. Laboratory experiments simulating the conditions in space are conducted for decades all over the world, but particularly in recent years new techniques have made it possible to study reactions involving inter- and circumstellar dust and ice analogues at an unprecedented level of detail. Whereas in the past "top-down scenarios" allowed to conclude on the importance of the solid state for the chemical enrichment of space, presently "bottom-up approaches" make it possible to fully quantify the involved reactions, and to provide information on processes at the molecular level. The recent progress in the field of "solid state laboratory astrophysics" is a consequence of the use of ultra high vacuum systems, of new radiation sources, such as synchrotrons and laser systems that allow extensions to wavelength domains that long have not been accessible, including the THz domain, and the use of highly sensitive gas phase detection techniques, explicitly applied to characterize the solid state such as fluorescence, luminescence, cavity ring-down spectroscopy and sophisticated mass spectrometric techniques.

This paper presents an overview of the techniques being used in astrochemical laboratories worldwide, but it is incomplete in the sense that it summarizes the outcome of a 3-day workshop of the authors in November 2012 (at the Observatoire de Meudon in France), with several laboratories represented, but not all. The paper references earlier work, but it is incomplete with regard to latest developments of techniques used in laboratories not represented at the workshop.

Keywords Laboratory astrophysics · Solid state astrochemistry · Inter- and circumstellar medium · Molecular astrophysics · Astronomical ice analogues

1 Introduction

Solid phase molecules (often referred to as "ices") are present both in the inter- and circumstellar medium as mantles on silicatic and/or carbonaceous dust and in/on many objects in the Solar System (including the Earth! see e.g. Bartels-Rausch et al. 2012).

The first icy species discovered to be present in the interstellar medium (ISM) was amorphous solid water (ASW) through the observation in the mid-IR spectrum of an absorption feature at about 3300 cm^{-1}, due to the O–H symmetric and anti-symmetric stretching modes (Merrill and Soifer 1974). The peak position of that band is in fact different from the one

observed for gas phase water molecules. In the solid (or liquid phase) the H-bond occurring between the H atom of a molecule and the O atom of a different molecule causes a shift of the O–H stretching modes band. This simple fact permitted, since the 70's of last century, to observe the O–H stretching modes band in ground based IR observations of many astrophysical objects otherwise prohibited by the presence of abundant water vapor in the Earth atmosphere. This opened a new era in the study of the interstellar medium and since then an enormous number of Earth based and space observations have been confirmed the presence of 10–15 solid state molecules (e.g. Öberg et al. 2011). However, it is thought that many more, even complex, molecules are present and released into the gas phase upon warm-up e.g. around protostars. The inventory of nearly 180 molecules largely detected by radio observations (and much more are foreseen to be detected by the in-progress Atacama Large Millimeter/submillimeter Array-ALMA project) have important contributions from the evaporation of molecular species from the solid phase. In a paper that includes the last finding from the IR detectors on board of the Spitzer space telescope, Öberg et al. (2011) found that the median ice composition H_2O:CO:CO_2:CH_3OH:NH_3:CH_4:XCN is 100:29:29:3:5:5:0.3 and 100:13:13:4:5:2:0.6 toward low- and high-mass protostars, respectively, and 100:31:38:4:X:X:X in cloud cores.

Formation and evolution of interstellar ices are driven by a number of processes. The ice formation phase is characterized by hydrogenation of atoms, which results in an H_2O-dominated ice, and by the contemporary energetic (UV photolysis and fast ion radiolysis) processing. Such a processing allows the formation of ices on the cold dust only at gas densities greater than about 10^4 H-atoms/cm^3. At later prestellar times, CO freezes out and the subsequent CO-based chemistry explains most of the observed ice abundance variations. The final important ice evolution stage is thermal processing around protostars, resulting in CO desorption, ice segregation, and the release, in the gas phase, of complex organic molecules produced by surface reactions induced by radiolysis and photolysis.

In between "ices" and "dust" there is a component in the ISM that will be also discussed in some detail in this paper: Polycyclic Aromatic Hydrocarbons (PAHs). PAHs include elements that extend from the molecular size up to the solid phase where they are often mixed with other icy species. PAHs are the best-known candidates to account for the infrared emission bands (UIR Allamandola et al. 1999) and PAH spectral features are now being used as probes of the interstellar medium (ISM) in extra-galactic environments (Smith et al. 2007). In the models dealing with the interstellar spectral features, PAHs are present as a mixture of radicals, ions and neutral species. PAH ionization states reflect the ionization balance of the medium while PAH size, composition, and structure reflect its energetic and chemical history. PAHs are also thought to be among the carriers of the diffuse interstellar absorption bands (DIBs). Their specific contribution to the interstellar extinction and to the DIBs in particular remains, however, unclear. The DIBs are ubiquitous spectral absorption features observed in the line of sight of stars that are obscured by diffuse interstellar clouds (Salama et al. 1996; Salama et al. 2011). PAHs constitute the building blocks of interstellar carbonaceous dust grains and play an important role in mediating the energetic and chemical processes in the ISM.

Ices are also abundant on a large number of objects in the Solar System; for a recent review see e.g. Dalton et al. (2010), Gudipati and Castillo-Rogez (2013). Water ice and carbon dioxide are present in large areas surrounding the Martian poles. Water ice dominates the composition of the surfaces of the icy satellites in the outer Solar System that show also the presence of other species such as hydrated salts (e.g. sulfuric acid) and carbon and sulfur dioxide. Trans Neptunian objects present a variegated coloration attributed to the presence

of ices "colored" by complex organic molecules. The composition of cometary ice inferred from the observation of molecular species released during the approach to perihelion, is consistent with the idea that most cometary ices have a protostellar origin. Icy surfaces in the Solar System are also exposed to a number of energetic processes such as UV photolysis, thermal annealing, micrometeoritic bombardment and irradiation by energetic ions and electrons.

In the interstellar medium grains act as a third body, capable of absorbing energy, and icy surfaces have a catalytic effect. Chemical reactions are triggered by a number of possible processes; (i) irradiation by light, typically UV photons from the interstellar radiation field and Ly-α radiation emitted by excited hydrogen, but also X-rays, (ii) bombardment by particles, free atoms (most noticeably hydrogen, but also N, C, O and D-atoms), electrons, low energy ions and cosmic rays, and (iii) thermal processing. All these effects cause ices to (photo)desorb, induce fragmentation or ionization in the ice, and eventual recombination will make molecules to react and to form more and more complex species.

Laboratory experiments conducted for some decades in several laboratories worldwide have shown that photolysis and radiolysis of ices produce a number of relevant and observable effects such as the erosion of the target, i.e. sputtering or photo-sputtering, the modification of the structure (crystalline or amorphous) of the sample as well as a number of non-thermal, "hot" chemical reactions that can lead to the formation of a large number of molecules and also organic refractory residues. These laboratory experiments simulate relevant targets "irradiated" under physical conditions as close as possible to the astrophysical ones.

While a large amount of experiments have been performed, this research field still needs further efforts. In particular, radiolysis and photolysis of icy mixtures resulted in the synthesis of several specific, also complex, molecules. However it is a common feeling that much more molecules are still to be revealed. In fact, the detection techniques used up to now, mostly IR spectroscopy, are sensitive only to the synthesized species whose abundance is larger than several thousandths with respect to the original species. This paper is a review of the effort that is ongoing in some selected laboratories in the world to build up and use experimental apparatus based on techniques different from the traditional and widely used IR spectroscopy (that however is still extremely relevant). These techniques include novel ones that are more sensitive and that can better evidence the formation of additional (complex) molecules and/or fragments that could be of primary relevance, e.g. for astrobiology. Also important is the opportunity to use available techniques but in a complementary way for a more in depth characterization and understanding of icy grains from dust grain formation, to ice mantle growth on the surface of the grains, and to the in-depth characterization of irradiated targets.

The paper is organized along a number of common topics. It starts with the description of new techniques. In Sect. 2 a simulation chamber to study aerosol and grain formation is described. Although this is not directly connected to the study of ices it introduces the concept of simulating ice mantle accretion on dust and this is important to perform experiments in which ices are grown on substrates that are realistic analogous of the astrophysical dust.

Section 3 focuses on new spectroscopic developments. The composition and structure of inter- and circumstellar ice is largely known from combining observational and laboratory studies in the infrared. Here ongoing efforts are described to extend ice spectroscopy to the TeraHertz (THz) domain. Here interstellar ices can be in fact detected in emission through their thermal radiation. With the ongoing exploration of this wavelength domain by HIFI

on board of Herschel (Batchelor et al. 1996; van der Tak 2012), SOFIA (Erickson 1995) and ALMA (van Dishoeck and Jørgensen 2008) this is a timely development.

The next part reviews techniques that are particularly useful to study (photo)sputtering. In fact, the measurement of sputtering yields requires the knowledge of the total mass removed from a target after a given ion fluence as well as of the kind and amount of molecular species that are sputtered. These studies benefit from the use of quartz micro-balances (Sect. 4) that allow measuring the (loss of) deposited mass and mass spectrometers that are used to measure molecular species emitted from the bombarded targets (Sect. 5).

Section 6 reviews a time of flight technique used to measure secondary ions emitted by materials during ion irradiation. The technique has not yet been applied to the study of ices but it is presently in a test phase, and promises to give a relevant contribution in a next future.

Laboratory measurements of luminescence and fluorescence require the use of techniques that can give important information on the composition of ices, particularly on minor species e.g., PAHs embedded in water ice, and/or on the details of the physico-chemical processes governing the absorption of energy and its emission at different wavelengths. The luminescence of electron irradiated ices is discussed in Sect. 7 and laser-induced fluorescence in Sect. 8.

The structural properties of ices i.e. crystalline, damaged or fully amorphized, compact or porous, depend on many parameters such as pressure, temperature cycling, and energetic processing. In addition, the structure of the ices (e.g., comprising water) determines the capability to trap other, minor, species and their chemical evolution. As detailed in Sect. 9, Raman spectroscopy is a technique very sensitive to the structure of materials, particularly those rich in carbon.

In the final part, Sect. 10, experiments are described simulating reactions in inter- and circumstellar ices and these show that molecules, such as methanol, can be formed upon hydrogenation reactions of CO ice and that subsequent ion/UV irradiation results in the generation of larger species with up to 10 atoms, such as methyl formate, acetic acid, ethylene glycol, and glycol aldehyde. These laboratory studies follow experiments by Greenberg and others who irradiated ices containing many different astronomically relevant components with UV broadband light for days. The resulting residues—known in literature as 'yellow stuff'—were analyzed by gas chromatography and showed evidence for amino acid formation and other biologically relevant species in the resulting organic refractory material (e.g. Greenberg et al. 1995; Muñoz Caro et al. 2002). The experiments presented here provide a more in depth analysis of the actual processes taking place. In parallel experiments are discussed in which more complex species are simply embedded in the ice and UV/VIS spectroscopy allows to study chemical processes in the ice in situ and in real time.

The paper follows the outcome of a three-day workshop of the authors in November 2012 at the Observatoire de Meudon in France. As outlined this is a review of a selected set of techniques currently applied or foreseen to be used soon, for the spectroscopic and dynamical study of chemical processes in astrophysical ices. In the next sections quite a number of different applications are discussed, but obviously these largely reflect the work done by the authors. The extensive list of references tries to put the work presented here within the general context of laboratory based research including other groups, not involved in this paper but active in solid state astrochemistry. This list is not complete, it cannot be, as currently interstellar ices are a hot topic and the literature in this field has become very extensive. Instead, we would like to mention LASSIE, a large European FP7 ITN (*Initial Training Network*) focusing on 'Laboratory Astrochemical Surface Science in Europe' (www.lassie.u-cergy.fr/) that will come to an end in 2014. In that year two special issues will be fully dedicated to the astrochemistry of dust, ice and gas, covering not only the laboratory side of the story. In April 2014 the Faraday Discussions 168 will cover this topic and

around the same time a special issue by PCCP will be released. The present article introduces selected examples on the underlying laboratory work but as a whole aims at providing a large cross section of the laboratory work currently going on in this field. Further results of experiments and observations are also available from two recent books: (1) the proceedings of the first European conference on laboratory astrophysics (ECLA; Stehl et al. 2012); and (2) the science of solar system ices (Gudipati and Castillo-Rogez 2013).

2 COSmIC: Cosmic Simulation Chamber—Combining time-of-flight mass spectrometry with cavity ringdown spectroscopy to study aerosol and grain formation in the laboratory

Main contributors: authors at NASA-Ames

This section is devoted to an experimental set-up for the study of the formation, growth and destruction mechanisms of cosmic dust. Dust particles span a continuous size distribution from large molecules to nanometer-sized particles to μm-sized particles and influence many processes in the evolution of the ISM such as the energy balance through the photoelectric effect, the ionization balance through recombination with electrons and ions, and the chemical composition of molecular clouds (Tielens 2005; Verstraete 2011; Bierbaum et al. 2011). The carbonaceous component of cosmic dust plays an important role in the universe (Henning and Salama 1998). Carbon particles are thought to be primarily formed in the outflow of carbon stars, through a combustion-like process where small carbon chains (e.g., acetylene) form polycyclic aromatic hydrocarbons (PAHs) that nucleate into larger-size PAHs and, ultimately, into nanoparticles (Frenklach et al. 1989; Pascoli and Polleux 2000; Jäger et al. 2011). According to the model, that was developed to account for the formation of carbonaceous meteoritic materials, nucleation occurs above 2000 K, followed by the growth of amorphous carbon on the condensation nuclei in the 2000–1500 K temperature range. As the temperature falls to around 1100 K, aromatic molecules begin to form in the gas phase and condense onto the growing particles forming graphitic microstructures that will ultimately aggregate into larger structures such as seen in soot formation (Cherchneff 2011).

Although a large amount of laboratory data exists on the formation and the properties of solid dust analogs and in particular of Si-based materials (e.g. Michael et al. 2003), very little is known, about the specific properties (structure, size and spectral signatures) and the formation mechanisms of the key intermediate range of the size distribution (nanoparticles) of cosmic dust. The scarcity of relevant laboratory data on the transition from gas-phase molecules to solid grains is due to the difficulty of forming and isolating these large species and in tracking their evolutionary path under astrophysically realistic laboratory conditions. Recent attempts have been initiated to address these shortcomings (Contreras et al. 2011).

Here we describe new laboratory studies that have been performed to address these key issues and describe the experimental set-up that has been developed to measure the formation and destruction mechanisms of carbonaceous grains from molecular precursors in an environment with key physical parameters expected to exist in circumstellar regions where molecular formation is observed. In a future, follow-up study, we will monitor in-situ, ice-mantle formation on the dust grains. We briefly present and discuss the preliminary results that were obtained in the laboratory (for a detailed discussion of the results refer to Contreras and Salama 2013). This new phase of laboratory astrophysics offers tremendous opportunities for the analysis of astronomical data.

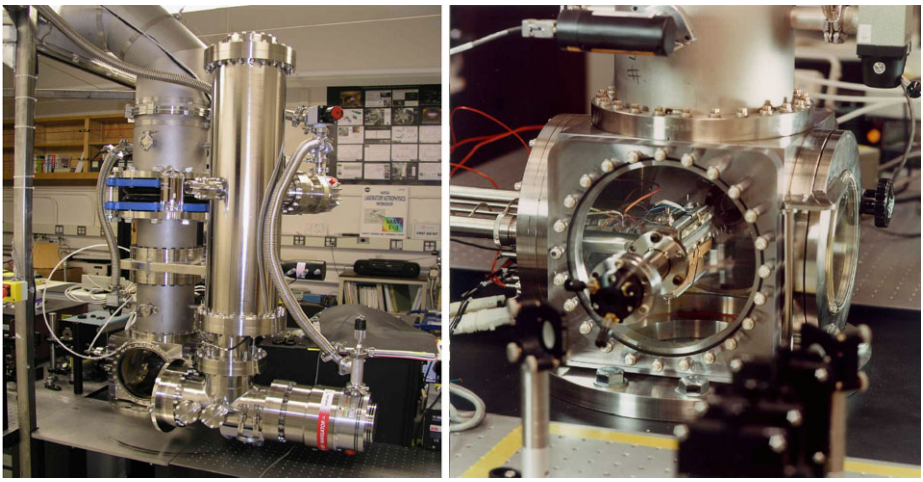

Fig. 1 Configuration of the Laboratory Facility, COSmIC. (*Left panel*) View of the oRETOF-MS rotating to face the Pulsed Discharge Nozzle (PDN) expansion chamber. (*Right panel*) Close-up view of the Chamber consisting of a Pulsed Discharge Nozzle (PDN) coupled to a Cavity Ringdown Spectrometer apparatus and Reflectron time-of-flight mass spectrometer

2.1 The Technique

The laboratory facility COSmiC, or cosmic simulation chamber, is a multicomponent system that studies the role of PAHs and, more generally, of carbon-bearing molecules in space by mimicking interstellar, circumstellar or planetary conditions in the laboratory. COSmIC is composed of three major components: a Pulsed Discharge Nozzle (PDN) where molecules, ions and radicals are formed in a free supersonic jet exposed to a plasma discharge, a high-sensitivity cavity ringdown spectrometer (CRDS) that measures the spectral signature of the products and an orthogonal Reflectron Time-of-Flight Mass Spectrometer (oReTOF-MS) that characterizes the mass and the structure of the products. The full system, PDN-CRDS-oReTOF-MS, is shown in Fig. 1 and described in this section.

In its original configuration, COSmIC was composed of the pulsed discharge supersonic expansion source coupled to the pulsed cavity ringdown spectrometer (PDN-CRDS component) and was used to measure the first electronic spectra of neutral and ionized PAHs under conditions that realistically simulate astrophysical environments (for a review Salama 2008, and references therein). These initial gas phase experiments also showed that, in addition to forming cold isolated molecules and ions, the cold plasma in the PDN produced complex chemistry. Monitoring these processes in-situ became important as soon as it was observed that the cold plasma discharge was producing soot, evidenced by the accumulation of solid deposits on the electrodes of the PDN apparatus (Biennier et al. 2005). As a result, the third component of the system, a custom-built orthogonal Reflectron time-of-flight mass spectrometer (oReTOF-MS) was added to the apparatus (Ricketts et al. 2011) to provide a complementary analytical tool for the analysis of the products of plasma chemistry.

A schematic of the experimental arrangement of the combined components of COSmiC is shown in Fig. 2. The PDN produces a supersonic free jet that is submitted to an ionizing electronic discharge. The net result is the generation of a plasma that is supersonically expanded to astrophysically relevant pressure and temperature regimes upon which the products of the expansion can be probed by cavity ringdown spectroscopy or time-of-

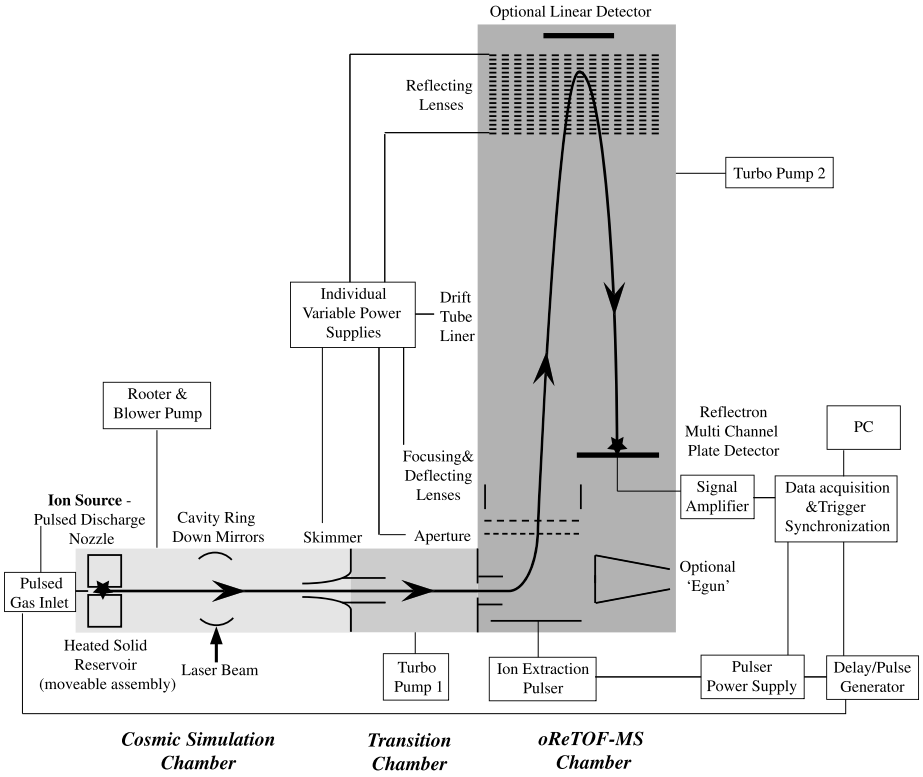

Fig. 2 Schematic of the COSmiC apparatus showing the main components. Note the ion flight path originating from the PDN into the transition chamber, followed by orthogonal acceleration and reversal of flight path toward MCP detector. From Ricketts et al. (2011)

flight mass spectrometry or a combination of both. The jet flow dynamics and the plasma expansion generated by the PDN are well characterized (Remy et al. 2003; Biennier et al. 2003, 2006; Broks et al. 2005a, 2005b). The species that are generated in the hot, confined, plasma from carbonaceous precursors are suddenly frozen by the expansion (Jost 1996; Biennier et al. 2006) providing a very efficient cooling over short distances (a few mm) and an ideal simulation tool for astrophysical environments. The current geometry of the PDN leads to a residence time of a few microseconds for the particles in the active region of the discharge. Two stainless steel knife-edge electrodes are mounted outside the PDN on each side of the slit. The two electrodes are separated by an even gap of 400 μm and configured as the cathode of a high-voltage pulse generator. This design enables the generation of atomic and molecular ions and radicals in the jet expansion by application of a high voltage (typically between −500 and −1000 V) as the carrier gas is introduced into the PDN. A custom-built orthogonal ReTOF-MS (Jordan TOF, Inc.) has been used to monitor and detect the products (neutral molecules and ions) produced in the slit discharge nozzle (PDN).

The particle flight path originating from the PDN and visible in Fig. 2 can be briefly described as follows. The molecular precursors are expanded in a free supersonic beam (pressure 10^{-2}–10^{-1} Torr) and exposed to an ionizing electronic discharge in the plasma of the PDN. A fraction of the ionic and neutral products generated in the PDN travels

through the aperture of the skimmer facing the output of the PDN (pressure in the range 10^{-5}–10^{-4} Torr). The skimmed products are then guided through a second aperture plate and into the extraction region of the ReTOF-MS (pressure of the order of 10^{-5}–10^{-6} Torr). Both the skimmer and the plate are connected to external power supplies in order to polarize and hence actively attract the ions generated in the plasma. From the extraction region the ions are accelerated, perpendicular to their original direction of motion, and focused into the drift tube of the ReTOF-MS towards the reflectron assembly of the ReTOF-MS, where the reflecting lenses turn the ions by approximately 180 degrees and the ions continue to drift to the Multi Channel Plate (MCP) detector. The MCP signal is amplified using a pre-amplifier (ORTEC VT-120) and mass spectra are recorded using a fast digital signal analyzer (ORTEC FastFlight-2) with a computer-driven acquisition program. A Digital Delay and Pulse Generator DG-535 (Stanford Instruments) is used to synchronize the gas plasma discharge with the CRDS and ReTOF-MS components. The ReTOF-MS extraction pulse event is timed to coincide with the discharge event and the time it takes the ions to reach the mass spectrometer. In typical experiments, the high voltage discharge is 300 μs long and is applied within a gas pulse that lasts 1.2 ms. The extraction pulse occurs 200 μs after the discharge starts. The FastFlight-2 hardware monitors all events after the extraction pulse, with the MCP detection time typically set to collect mass spectra up to 2000 m/z (mass units). Averages of 3000 scans per spectrum are routinely taken to optimize the signal-to-noise.

Neutral species are also generated in the plasma and travel with the ions in the cold free jet expansion. Neutral PAHs, for example, have been detected and probed with CRDS (Tan and Salama 2005). Hence, the ReTOF-MS is equipped with an electron ionization (EI) source that ionizes the cold neutral molecules in the extraction region of the ReTOF-MS. The EI source uses a tungsten filament to produce electrons at 70 eV (tunable from 40 to 80 eV), which in turn produce ions via electron-neutral collisions. When operating in the EI or internally generated ion mode, the neutrals travel from the PDN chamber into the ReTOF-MS without the application of voltage to the skimmer or plate apertures in the transition chamber. Since the extraction plate is set to ground, only ions formed internally with EI are detected. The timing and pulsing procedures with the repeller plate and the introduction of the internally generated ions into the drift tube are similar to that described for the externally generated ions.

COSmiC was used in this first phase of the program to look at the formation and the destruction processes of carbon-bearing molecules and ions that are potential precursors of carbonaceous grains. Various types of molecular precursors that are related to the formation of PAH-type structures have been studied.

2.2 Results Obtained So Far

Due to the nature of the plasma and to the various processes (ionization, fragmentation, and recombination) that can occur in that environment, a variety of products are expected to be formed from each molecular precursor injected into the PDN. The products include, neutrals, radicals and ions of the molecular precursors as well as neutrals, radicals and ions of the fragments formed due to spontaneous dissociation of the molecular precursors. We have previously shown that ions are formed through direct ionization or through soft penning ionization (Remy et al. 2005). Other processes, such as recombination (bond formation) between atomic and molecular fragments, are observed for each molecular precursor.

The laboratory species that are generated in the expanding discharge plasma experience a strong temperature gradient that ranges from a few thousand degrees Kelvin to 100 K over a short distance (1.5–2.5 mm) from the edge of the plasma chamber to the probing zone

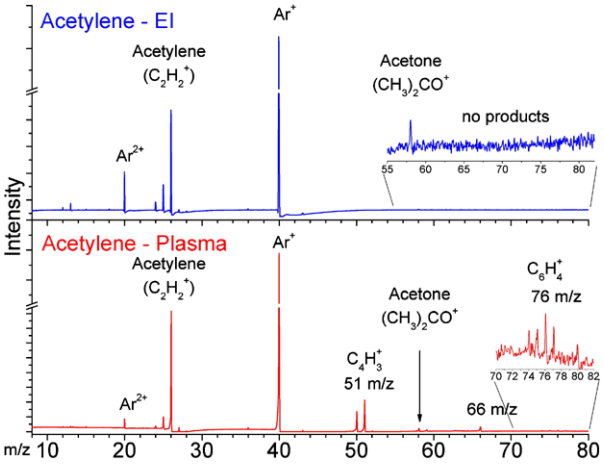

Fig. 3 Time-of-flight mass spectra of ionization experiments of argon seeded with acetylene show the differences observed in the products detected as a function of the ionization method. *Bottom*: plasma ionization; *Top*: electron ionization (EI). *The peaks due to the acetone in the acetylene sample are indicated at 58 and 59 m/z

where the particles are detected (Remy et al. 2003; Broks et al. 2005a, 2005b; Biennier et al. 2006). This temperature domain corresponds to the domain where aromatic molecules begin to form in the gas phase and condense onto the growing particles forming graphitic microstructures that will ultimately aggregate into larger soot-like structures as we observe. This temperature variation is similar to the temperature variation observed from the surface of a carbon star to the edges of the cooling stellar outflow envelope (Pascoli and Polleux 2000).

Plasma discharges were conducted with small hydrocarbons, methane, ethane, ethylene, and acetylene representative of the alkane, alkene, and alkyne groups, respectively. The formation of larger molecules and carbon grains was probed by the addition of benzene, toluene and pyridine precursors and small PAH precursors (naphthalene, 1-methylnaphthalene, and acenaphthene) into the hydrocarbon-seeded Ar gas mixture. In all experiments, the molecular precursors are seeded into Ar and supersonically expanded through the PDN. Solid and liquid PAH samples are held in the bottom reservoir of the PDN and are heated to increase their vapor pressure. Heating of the reservoir has been shown not to alter the expansion temperature of the gas. Previous studies indicate a rotational temperature of 52 K for the gas in the supersonic expansion, measured at a distance of 4 mm from the opening of the slit (Tan and Salama 2005). In typical experiments, the high voltage discharge is 300 μs long and is applied within a gas pulse that lasts 1.2 ms. The ReTOF-MS extraction pulse event is timed to coincide with the discharge and the time it takes the ions to reach the mass spectrometer. The extraction pulse occurred 200 μs after the discharge. An illustrative mass spectrum is shown in Fig. 3.

The preliminary experiments performed for the investigation of the formation of carbon grains from molecular precursors in the circumstellar shells of carbon star outflows by combining the effects of a plasma discharge into a seeded gas with the efficient cooling-down of a supersonic expansion jet have shown that this laboratory approach offers a reasonable approximation for the physical parameters (density and temperature) known to be associated with a cooling circumstellar envelope of a carbon star (Pascoli and Polleux 2000). It also demonstrates that adding a reflectron time-of-flight detector to the Cosmic Dust Simulation Chamber (COSmiC) constitutes a powerful tool to probe the formation and fragmentation processes of the laboratory analogs of interstellar and circumstellar dust formed in this simulated environment. It was observed that the reaction products are highly dependent on the

molecular nature of the precursors. The molecular products observed in the COSmIC experiments tend to support the assumptions that were made so far in the models that describe the chemical pathways to the formation of PAHs in circumstellar environments (Frenklach et al. 1989, see also Cherchneff 2011 for a recent review). The product ions formed from small molecular precursors (linear hydrocarbons such as acetylene) have maximum masses that correspond to the masses associated with the formation of benzene-type and toluene-type molecular structures (Contreras and Salama 2013). This observation seems to indicate that the most promising routes for molecular growth and for the formation of large molecular species in the outflows of carbon stars are indeed the routes that begin with small unsaturated carbon chains leading to the formation of benzene rings and the subsequent formation of small polycyclic aromatic hydrocarbon structures that act as seed units for the formation of larger grains. Future laboratory studies with COSmIC will focus on the study of the chemical pathways that involve small unsaturated hydrocarbons precursors, in particular acetylene that is thought to be abundant in space (e.g. Knacke et al. 1989), and the optimization of the formation of the one- and two-ring aromatic structures that are the building blocks of the larger molecular (grain-like) structures (Bera et al. 2011).

3 THz Time-Domain Spectroscopy of Interstellar Ice Analogs

Main contributors: authors at CALTECH

The portion of the electromagnetic spectrum commonly known as the far-infrared, submillimeter, or TeraHertz (THz) region extends roughly from 0.1 → 10 THz (3 mm → 30 μm) and lies between the microwave and infrared windows. Until recently, the THz region has not been particularly amenable to laboratory spectroscopy because of the lack of intense radiation sources and fast, sensitive detectors. As a result, this region has been referred to, for quite some time, as 'the gap in the electromagnetic spectrum'. Historically, THz spectroscopy was first used by chemists and astronomers to characterize the rotational or torsional resonances and thermal-emission lines of simple molecules, especially hydrides. More generally, THz frequencies are suitable for probing low energy light-matter interactions. Over the past 20 years, advances in terahertz technology have provided new and high-power sources with potential applications in sectors as diverse as the semiconductor, medical, manufacturing, space, and defense industries (Ferguson and Zhang 2002; Zhang and Xu 2010).

For remote sensing, spectroscopy at THz frequencies holds the key to our ability to remotely sense different environments, such as primeval galaxies, star and planet-forming molecular cloud cores, comets, and planetary atmospheres. In the dense interstellar medium (ISM), scattering of visible/UV light by dust grains renders dense molecular clouds (the cradle of new stars and planets) optically opaque and lowers their internal temperature to only a few tens of Kelvin (Blake 2001). Observations of ices in the ISM have typically been performed in the near- and mid-infrared. These observations are limited, however, to lines-of-sight along which infrared absorption spectroscopy is possible (i.e., toward a source of light such as a protostar or a field star). Moreover, ground-based infrared observations are limited because of telluric absorption and thus airborne/space observatories have served as the primary means of identifying solid-phase species in space. Mid-infrared observations with the Infrared Space Observatory (ISO) (Gibb et al. 2000, 2004) in particular and, more recently, with the Spitzer Space Telescope combined with laboratory data (e.g., see Leiden Ice-Database; http://home.strw.leidenuniv.nl/~linnartz/ice_database.html) have characterized in detail the main molecular content of icy grain mantles (Boogert et al. 2008;

Pontoppidan et al. 2008; Öberg et al. 2008; Bottinelli et al. 2010; Zasowski et al. 2009), leading to an unambiguous identification of the simplest and most abundant species in the ice (i.e., H_2O, CO, CO_2, CH_4, CH_3OH, and NH_3). The identification of more complex, potentially prebiotic species in the mid-IR is difficult because of their low expected interstellar abundances in the solid phase. Moreover, complex molecules present a forest of absorption peaks in the mid-IR that overlap with each other and the more abundant simple species and, therefore, make the identification of an individual compound even harder.

Interstellar ices can be detected in emission in the THz region through their thermal radiation without need of a background source of light (i.e., towards any direction in the sky) (Siegel 2007). Spectroscopy at THz frequencies has the potential to circumvent the limitations mentioned above, and thus astrochemists have been looking at the THz range with extreme interest since recent observations with Herschel Space Telescope (Batchelor et al. 1996), the Stratospheric Observatory For Infrared Astronomy (SOFIA) (Erickson 1995) and the Atacama Large Millimeter/submillimeter Array (ALMA) (van Dishoeck and Jørgensen 2008) will enable access to both quantitatively and qualitatively new tracers of dense and diffuse gas, dust, and ice in the ISM (van Dishoeck et al. 2011; Posch et al. 2005).

To interpret the huge amount of new spectral data (to be) collected by Herschel, SOFIA and ALMA, laboratory spectra of the same compounds are needed for comparison to observational data. Such spectra, however, are largely lacking, and this severely restricts the scientific impact of the astronomical observations. The Jena databases include the optical properties of several interstellar dust analogs at low temperatures in the range between 25–110 μm (e.g., Posch et al. 2007; Mutschke et al. 2008). Some pioneering laboratory far-IR ice work has been also done in the past (e.g., Moore and Hudson 1994). These works are however limited in their THz coverage (typically far-infrared spectra are available from 20–150 μm), while large facilities such as Herschel can cover up to 210 μm with PACS and 670 μm with the SPIRE and HIFI instruments. Moreover, the far-IR work on ices does not include spectra of prebiotic species, and the spectra are typically acquired at low resolution, while high resolution is needed for a better comparison with observations.

In summary, a complete THz map of the sky combined with quantitative THz laboratory studies of the interstellar gas, ice, and dust has the potential to reveal the molecular evolution of the Universe, answering open questions, e.g., on the origin and fate of complex molecules in space. Laboratory data are urgently needed. Toward this end, an integrated time and frequency domain THz facility has been developed at Caltech that allows the investigation of interstellar relevant dust, ice, and gas across the full wavelength region accessible to Herschel/SOFIA/ALMA instruments and for astronomically relevant temperatures (10–300 K). This facility is, to the best of our knowledge, unique and has myriad applications in astronomy, physics, chemistry, and biology (Blake 2009).

3.1 The Technique

The Caltech THz Time Domain Spectroscopy (THz-TDS) facility is based on ultrafast, pulsed Titanium:Sapphire (Ti:Sapph) lasers. Two systems are in operation: A dual oscillator high spectral resolution instrument based on ASynchronous OPtical Sampling (ASOPS) and a high peak power instrument. The latter has a larger spectral grasp, such as is necessary for ice analog studies, and so is described here. As shown in Fig. 4, a mode-locked Ti:Sapph oscillator (Coherent Mantis) produces near-IR (800 nm) broad bandwidth, ultrashort pulses that are subsequently amplified by a regenerative amplifier (Coherent Legend Elite) to provide approximately 4 mJ of <35 fs near-IR pulses at a repetition of 1 kHz. The amplifier

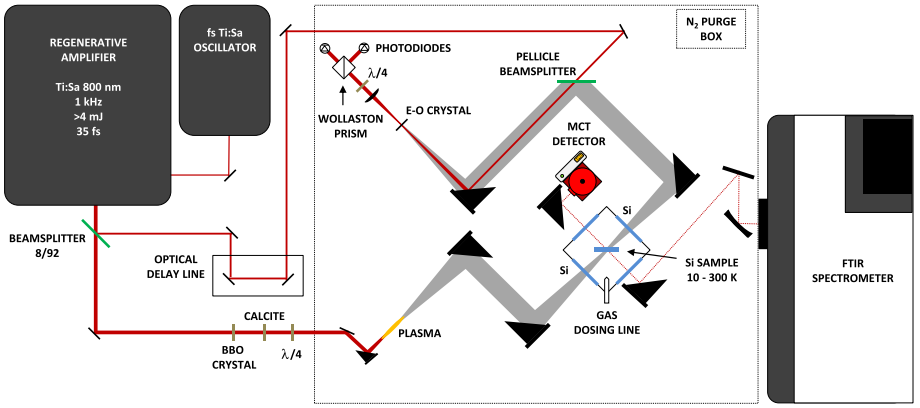

Fig. 4 Schematic top-view of the experimental apparatus

output is split into generation and detection (also called pump and probe) beams, where the former is used to generate THz pulses in an N_2 purge box, while the latter is used to detect the THz field strength. Two different techniques have been used at Caltech to generate a THz pulse beam with this system. In the first case, the THz generation beam excites a zinc telluride (ZnTe) crystal to produce intense THz pulses over areas of $\sim$1 cm^2 via electro-optic (E-O) rectification (Rice et al. 1994). Alternatively, THz pulses are produced by plasma filamentation in air (Xie et al. 2006). To generate THz pulses via plasma filamentation, the 800 nm near-IR pulses pass through a barium borate (BBO) crystal to generate the second harmonic of the 800 nm beam. Then, both the second harmonic and the remaining unconverted fundamental 800 nm light pass through a calcite plate to compensate for the different phase delays for blue and red light. Finally, the two colors are focused on the same zone producing THz wave generation in ionized air (mainly N_2, see Fig. 4). The main advantages of using THz air-plasma generation over E-O rectification is a higher intensity of the THz pulse beam and a much broader bandwidth (>50 THz). Thus, we will use THz air-plasma generation in order to investigate interstellar ice analogs over the full far-IR range accessible to Herschel and SOFIA.

After generation, THz pulses pass through the sample at an angle of 45° and are then reflected and focused onto a ZnTe or GaP (gallium phosphate) crystal where the THz pulses interact with the probe beam. The THz pulse causes a rotation in the polarization of the probe beam in a non-linear optical material such as ZnTe. This phenomena is called the Pockels effect or first order E-O effect. A Wollaston prism is used to split the incoming probe beam into orthogonal polarization components. Two matched 800 nm-sensitive photodiodes detect the two components separately and measure the degree of polarization rotation of the probe beam. The degree of polarization rotation is linearly proportional to the THz electric field on the detector at sufficiently low THz pulse energies (Wu and Zhang 1995; Lu et al. 1997).

Since they are derived from the same source, the probe and pump beams have a well defined temporal relationship. Adding pathlength along the probe arm by using an opto-mechanical delay line allows one to step through the entire THz waveform. Therefore, the electric field is measured as a function of delay time, and a fast Fourier transform (FFT) of the temporal waveform gives spectral distribution of the THz pulse in the frequency domain. After appropriate processing the resulting spectrum yields both the real and imaginary indices of refraction of the sample under study, since it is the field strength and phase of the THz pulse that are measured and not the intensity.

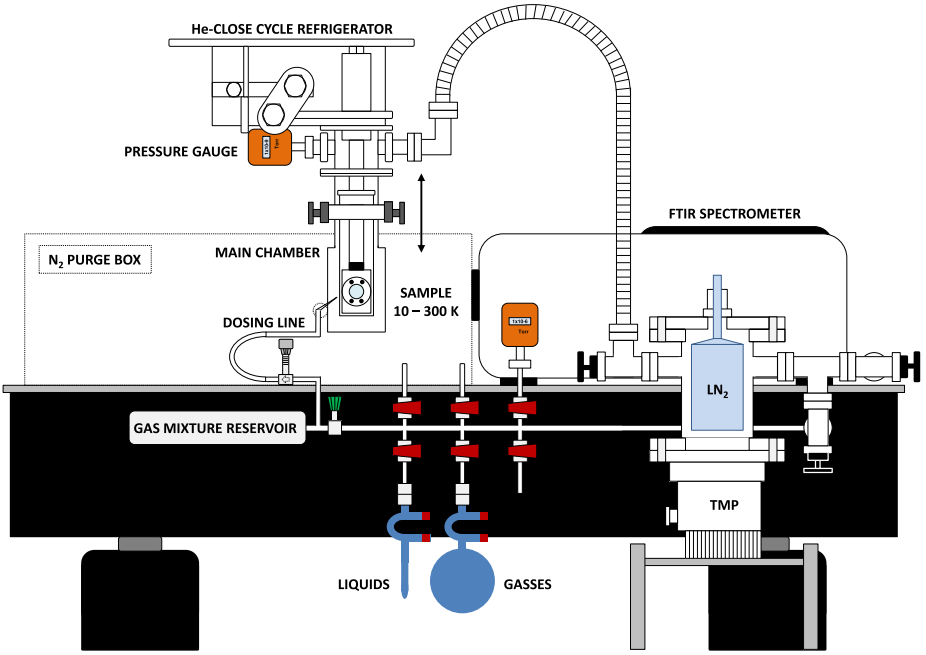

Fig. 5 Schematic side-view of the experimental apparatus

For astrophysically-motivated studies of interstellar ice analogs, it is essential to achieve low temperatures and high vacuum. Here, the ice sample is deposited through a metal deposition line onto a silicon (Si) window placed in the center of a high vacuum chamber (base pressure $\sim 10^{-8}$ Torr) and in thermal contact with the cold finger of a helium closed-cycle cryostat (see Fig. 5). The substrate temperature is varied between 10 and 300 K with a precision of 0.5 K through a cryogenic temperature controller. To achieve such a low temperature, an aluminum thermal shield, kept at $\sim$77 K, surrounds the cold finger and partially the sample. To change and monitor the temperature of the sample, heating wires are mounted around the cold finger close to the substrate, and a KP-type thermocouple wire is connected to the window substrate holder. The absolute temperature accuracy is better than 2 K.

Simple gases or gas mixtures are prepared and stored in the metal deposition line prior deposition. Gas and mixture pressures are controlled mass independently through two capacitance manometers. A liquid nitrogen trap (LN_2) is placed between the main chamber and the turbo-molecular pump (TMP) in order to minimize water pollution in the system. The TMP is assembled in the system in such a way that it can be shared with different experimental setups as well as with the gas dosing line. Ice thicknesses are monitored during deposition with a helium-neon (He–Ne) laser.

The position of the sample allows the simultaneous and *in situ* acquisition of THz spectra with the THz-TDS system and mid-IR spectra by using a Fourier Transform-InfraRed (FT-IR) spectrometer, which covers the range between 4000 and 600 cm^{-1} (2.5–16 μm). A spectral resolution of between 0.5 and 4 cm^{-1} is generally used, and of order 128 → 512 scans are typically co-added. As shown in Fig. 4, a series of $\lambda/4$ precision silver-coated mirrors (Thorlabs) is used to focus the beam onto the sample firstly, and onto the liquid N_2 cooled Mercury Cadmium Telluride (MCT) detector secondly. The FT-IR and all the external optics and detector are purged with N_2 to prohibit atmospheric absorptions.

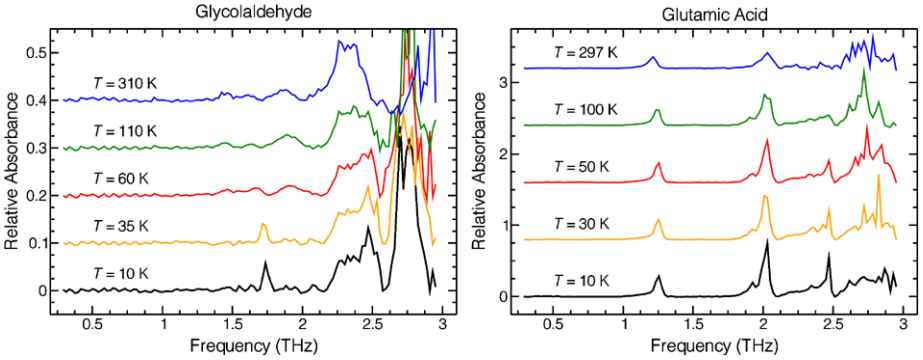

Fig. 6 Relative absorbance of glycolaldehyde (*left panel*) and glutamic acid (*right panel*) versus frequency from 10 to 310 K. The spectra are off-set for clarity

3.2 Results Obtained So Far

Figure 6 shows the potential of the system by presenting THz spectra of solid glycolaldehyde and glutamic acid (left-panel and right-panel, respectively) over the 0.3–3 THz range and for temperatures between 10–310 K. In both panels the signal-to-noise ratio is lower above 2.5 THz than in the rest of the spectral range here presented. This is a result of the phase walk-off of the THz and near-IR detection beam in the ZnTe detector crystal. The difference of the phase velocity of the THz pulse relative to the group velocity of the 800 nm detection pulse causes this phase walk-off and thus reduces the detectable bandwidth. Therefore, the features present in this region of the spectra cannot be interpreted as clear absorptions. In this preliminary study, the THz beam is generated by means of optical rectification in ZnTe. As previously mentioned, the use of plasma filamentation in air will ensure a wider bandwidth in future studies.

Glycolaldehyde is a simple monosaccharide sugar linked to prebiotic chemistry and relevant to interstellar chemistry. It was first detected towards the molecular cloud Sagittarius B2(N), and then towards a star-forming hot molecular core G31.41+0.31 (Hollis et al. 2000; Beltrán et al. 2009, respectively). Very recently, early ALMA data showed the presence of glycolaldehyde in warm (200–300 K) gas close to the individual components of the binary system IRAS 16293-2422 (Jørgensen et al. 2012). Although several formation mechanisms of glycolaldehyde have been proposed and investigated by experimental and theoretical groups, the astrochemical origin of this molecule is still under debate (Woods et al. 2012, and references therein). It is, however, generally accepted that the formation of large organic molecules intimately involves surface chemistry on interstellar ice grains (e.g., Garrod et al. 2006). Therefore, laboratory THz spectra of prebiotic species have the potential to guide future astronomical observations that will allow the identification of complex species in both the gas and in the solid phase (e.g., Carroll et al. 2010).

In the experiments shown in the left-panel of Fig. 6, a solid sample of glycolaldehyde is prepared outside the vacuum system and, therefore, it is not directly deposited onto the cold Si substrate as described in Sect. 3.1. Here, glycolaldehyde ($\geq$98 %, Sigma-Aldrich) is first ground down to a fine powder and then mixed with polyethylene powder (15 % glycolaldehyde by mass). The mixture is further pressed into a pellet by means of a $\sim$1800 kg cm^{-2} oil press. The sample is placed into the substrate holder which is in thermal contact with the cold finger of the cryostat. Difference spectra with respect to a background spectrum of a second polyethylene pellet without glycolaldehyde are acquired at different temperatures.

Glycolaldehyde presents one low temperature absorption peak in the frequency range investigated here: 1.74 THz at 10 K. As the temperature increases, this absorption feature becomes broader and shifts. Above 60 K the feature becomes so broad that it is hard to distinguish it from the baseline. At THz frequencies, there are both intra- and inter-molecular degrees of freedom in the molecular crystal that can be excited. The peak shifting and narrowing are most likely due to overlapping fundamental and hot band features whose intensities are a strong function of temperature. Bands will either blue- or red-shift with decreasing temperature depending on the anharmonicity of the (intra- or inter-) molecular potential. 'Morse-like' or pseudo-diatomic stretch-like modes have an energy level spacing that decreases with increasing excitation, and so will blue shift with decreasing temperature. For either square well-like or semi-rigid bender potentials (such as might be expected for bending or torsional degrees of freedom) the anharmonicity is opposite in sign, and the bands should red shift with decreasing temperature.

Figure 6 shows also THz spectra of glutamic acid ($\geq$98 %, Sigma-Aldrich), a proteinogenic amino acid detected in solar-system small bodies like the martian meteorite Nakhla (Glavin et al. 1999). On Earth, amino acids are important both as nourishing substrate in the human body and as essential components of proteins. As for glycolaldehyde, 25 % glutamic acid is mixed with polyethylene and pressed in a pellet. Glutamic acid absorbs at 1.22 and 2.03 THz at 297 K. THz-TDS spectra of glutamic acid pellets at room temperature are available in literature and confirm our experimental results (Ueno et al. 2006). As the temperature decreases, the two aforementioned absorption features become stronger and sharper (see right-panel of Fig. 6). At 10 K, the higher-frequency feature presents a second peak at 1.93 THz and a new peak appears at 2.47 THz. As such we see that for glutamic acid, the number of features between 0.3–3 THz increases below 297 K. As noted above, THz spectra in particular provide a spectral fingerprint of intermolecular forces (or of the very lowest energy intramolecular forces). The increase in number of absorption peaks at low temperatures can be explained by an increase in the complexity of the intermolecular potential energy surface. Moreover, single peaks resolving to multiple peaks at low temperatures depend on the available energy state distribution. At higher temperatures there are more energy levels available to the molecules, generating additional absorption features that may sometimes be more intense than the fundamental vibrational mode. At lower temperatures, the lack of population in these excited states allows us to resolve the hidden, fundamental, vibrations.

3.3 Future Experiments

Molecular observations by astronomical flagship facilities such as the Herschel Space Telescope, SOFIA, and ALMA, are currently being used to probe the different evolutionary stages of the interstellar medium in our own Milky Way Galaxy as well as in external galaxies. The entire evolution of the universe, from the formation of the first stars in the early universe up to the delivery of prebiotic species to Earth-like planets, is strongly affected by the chemistry in space, a chemistry that is now open to investigation. To extract the maximum useful information from such hard-won astronomical spectra, laboratory experiments are necessary to unravel the molecular complexity in space.

Section 3.2 showed that the THz absorption peaks of complex molecules have different intensity and shape at different temperatures in the solid phase and they also increase in number as the complexity of the molecular ice (either due to a more complex monomer or to the hydrogen bonding environment of the material) increases. With an appropriate laboratory database in hand, THz spectroscopy with the flagship facilities outlined above can be used

to identify the presence and temperature of complex species in the ISM. Moreover, they can be used as critical experimental input to the simulation of intermolecular interactions in solids.

The long-term goal of the THz ice laboratory system at Caltech is to provide the scientific community with just such an extensive database of far-IR transmission spectra and optical constants for ices and materials that are relevant to the ISM and/or planetary astronomy. The laboratory work at Caltech will start with the THz spectral investigation of simple amorphous and crystalline pure ices over the full 10–300 K temperature range achievable by the cryostat. Subsequently, the project will shift to the THz study of interstellar relevant ice mixtures at different temperatures and mixture ratios in order to mimic the grain mantle compositions seen in the Spitzer spectroscopic surveys of star-forming clouds. Almost nothing is known about the THz behavior of such mixed ices, especially at the longer wavelengths accessible with Herschel, and so this work will be largely exploratory. Later on, the project will focus on a systematic investigation of first pure and then mixed samples of more complex species, such as polycyclic aromatic hydrocarbons (PAHs) and complex organics (e.g., amino acids and sugars), as well as silicate and carbon dust. This effort is in direct support of Herschel Space Telescope, SOFIA, and ALMA.

4 The Quartz-Crystal Microbalance Technique

Main contributors: authors in Virginia

4.1 Principle of Operation and Main Features

The use of quartz crystal microbalance (QCM) to study thin film growth, sublimation, and desorption is very popular in scientific research and industry due to the QCM's high accuracy, sensitivity, small size and compatibility with ultrahigh vacuum. The microbalance is based on the change of resonance frequency with mass of a piezoelectric quartz crystal, driven to oscillate mechanically by the application of an alternating voltage with frequency close to the crystal mechanical resonant frequency. Crystals are usually cut along crystallographic axes that minimize sensitivity to temperature or stress. Most common is the AT-cut (shown in Fig. 7) and the SC-cut. Crystals are in the form of thin disks with metal electrodes (typically Au or Ag) on their faces. The main oscillation is a shear-mode elastic stress propagating in the thickness direction with sound speed V_q. The resonant frequency $f = V_q/2\mathrm{d}$ occurs when the wavelength of the oscillation is twice the crystal thickness d. A deposit on an electrode behaves as if it were quartz, as long

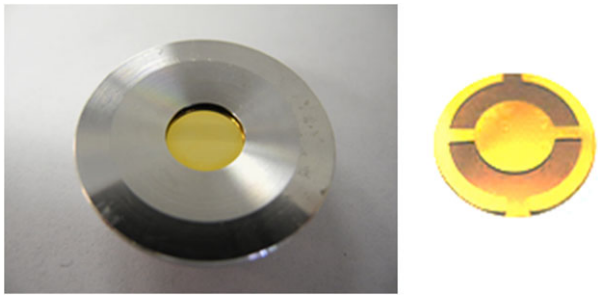

Fig. 7 (*Left*) Quartz-crystal, 12.7 mm in diameter, mounted. (*Right*) Back of the crystal with details of the Cr/Au electrodes. The *central circle* in the back view shows the active area of the crystal, which is ~28.5 mm^2 in this case

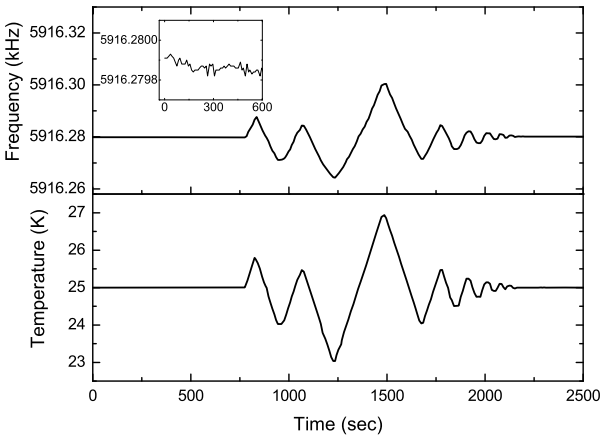

Fig. 8 QCM frequency stability vs. time in the presence of programmed temperature oscillations. The *inset* zooms in the first 600 sec, before introducing temperature instabilities

as its areal mass Δm is much smaller than $M_q = \mathrm{d} \times \rho_q$, the areal mass of the crystal, where ρ_q is the density of quartz. The deposit causes a change in the resonant frequency of a crystal Δf related to Δm by the equation $\Delta f/f = -\Delta m/M_q$ (Sauerbrey 1959; Lu 1975). The negative sign means that the frequency decreases when mass is added to the microbalance. For $\Delta f \ll f$:

$$\Delta m = -\Delta f \times \rho_q \times V_q / 2 f^2 = -s \times \Delta f$$

where $\rho_q \times V_q = 8.851 \times 10^6\ \mathrm{kg\,m^{-2}\,s^{-1}}$ for an AT-cut crystal. For a typical QCM, $f =$ 6 MHz, and

$$\Delta m = -1.23 \times 10^{-8} \Delta f\ \mathrm{g\,cm^{-2}\,Hz^{-1}}$$

The sensitivity factor $s = \Delta m/\Delta f$ is accurate to about 1 % for small masses (Lu 1984). In an experiment with water ice, a typical resolution $\Delta f = 0.1$ Hz corresponds to 4.1×10^{13} molecules $\mathrm{cm^{-2}}$, or about 0.04 monolayers. This very high sensitivity, coupled with the accuracy of s is the reason for the popularity of the QCM technique. However, to achieve those results one must be aware of a number of problems, most of them related to the dependence of the crystal frequency on other factors.

The frequency of the crystal depends on temperature. The popular AT crystals are designed to have a low temperature coefficient at room temperature. For use at cryogenic temperatures needed to study ices, it is essential to have a careful temperature control since a variation of 1 K causes a shift in frequency of the order of 10–50 Hz, depending on temperature within the range 5–120 K. An example is shown in Fig. 8 for a QCM operating at 25 K under management by a temperature controller with control of ∼0.01 K. With stable temperature, the QCM frequency stays within 0.1 Hz (see zoom in inset). After ∼750 sec we simulated temperature instabilities of different magnitude to illustrate problems with inconstant temperatures. The frequency stability is also affected by changes in capacitance due to, e.g., motion of cables, and by instabilities in the electronic oscillator circuit. Also, the resonance frequency of QCMs strongly depends on stress. This can be caused by a temperature gradient when a projectile beam impinges on the crystal (see Fig. 9), or by internal stresses in the film due to film radiation damage at very high fluences (Eernisse 1984), or formed during the growth of films of thickness of the order of microns.

Another aspect to consider is that the mass sensitive area of the QCM is situated in the central part of the crystal; the radial sensitivity distribution curve follows a bell-shaped curve

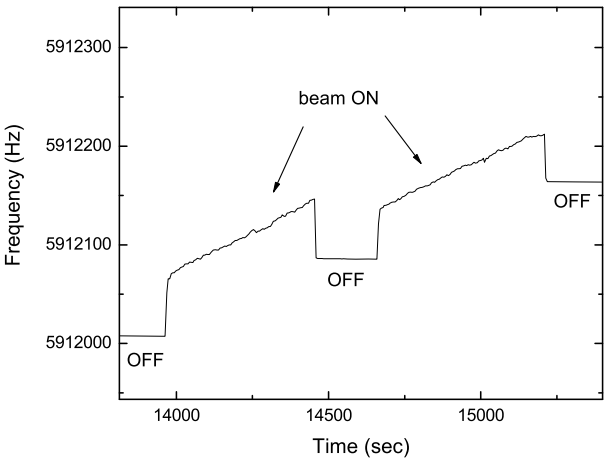

Fig. 9 QCM frequency shift under stress (seen as vertical jumps) when 100 keV H^+ ion beam is turned on and off. The target is a film of 5×10^{17} CO_2 cm^{-2} deposited at 50 K on the QCM and irradiated at 20 K. The ion current was 1 nA, for a power of 10 mW. The slope divided by the proton flux of 2.3×10^{12} ion cm^{-2} s^{-1} gives the sputtering yield

peaking at the center of the crystal (Oliva-Florio et al. 1987). The sensitivity is maximal at the center of the crystal and drops to zero at the edge. The given value of s holds as an average over the active area (of order 0.3 cm^2) and hence it is valid only if the mass change Δm is uniform over the QCM. For film deposition, this can be achieved using a microcapillary array (Winkler and Yates 1998), or condensation of background gas (although this latter method is prone to contamination by impurity molecules desorbing from walls). Studies of particle-induced desorption require a beam of projectiles that is uniform over the QCM.

4.2 Examples of the QCM Technique Applied to Experimental Astrophysics

Here we give several examples of different experiments on ices. All experiments were carried in a cryopumped, stainless steel, ultrahigh vacuum chambers with base pressure of 10^{-10} mbar, with dynamic temperature control to 0.01 K. The crystals typically have a polished gold electrode, which allows performing optical reflection spectroscopy on the film. Optical interference in the visible and UV is very accurate to obtain not only optical constants but also the thickness of the film. Then, the film density (which can be much smaller than intrinsic bulk values due to porosity) can be calculated directly. Film composition by reflection infrared absorption spectroscopy (RAIRS) is not straightforward, since neglect of optical interference can cause large errors in the derived optical constants, as demonstrated by Teolis et al. (2007b).

One can coat the gold electrode with a thin layer of another substance. Recently, we laid a 50 nm foil of Carbon-13 on the gold electrode of a QCM and grew ice films on top of the carbon. The use of a carbon substrate was to study the production of CO_2 in radiation-induced processes at the C-H_2O (Raut et al. 2012) and C-O_2 interfaces (Fulvio et al. 2012).

4.2.1 Deposition of Ice Films with Known Column Density

Figure 10 shows an example of a film of pure oxygen deposited at 21 K at a constant rate. Since the sensitivity of the microbalance is known to within 1 % (see above), the column density in the film is known very accurately, limited only by the purity of the gas and the deposition process.

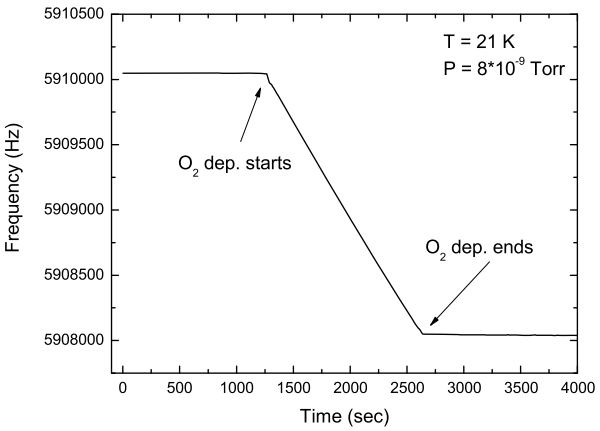

Fig. 10 Example of the frequency shift of the QCM during deposition of 4.6×10^{17} O_2 cm^{-2} at 21 K

The QCM is particularly adept at solving a typical need in studies of astrophysical ices: the growth of ice films composed of two or more species, with a precise composition. The straightforward method to deposit gas mixtures is problematic because of the difficulty in taking into account the mass and pressure dependence of the conductance of the gas manifold, leak valves and gas dozer and due to difference in the sticking coefficients of different species. These factors could modify the composition ratio in the condensed phase, making it different from the gas-phase mixing ratio in the gas manifold. This problem is circumvented with the use of a separate gas dozer for each gas and calibration of each flux by measuring the condensation in the QCM at the desired temperature. This method has been used, e.g. by Loeffler and Baragiola (2011) to grow H_2O_2:H_2O in the ratio 1:2 with high accuracy.

4.2.2 Sublimation and TPD of Radiation Products

The rate of sublimation of ices is a very important property that determines the lifetime of ice layers and matter balance in surface-bound exospheres. The rate of sublimation as a function of temperature can also be used to derive enthalpies of sublimation. Sack and Baragiola (1993) used the QCM to obtain sublimation rates for water ice and its change when it transforms from amorphous to the cubic crystalline phase. Moreover, coupling mass spectrometry to the QCM technique gives the ability to characterize the desorption products. Figure 11 shows the sublimation of a mixed O_2/O_3 film formed by ion irradiation of an initially pure solid oxygen film (the study of radiolyzed films is further discussed below). The desorption of O_2 at ∼33 K, leaves a porous ozone film on the substrate. The discovery of this low-density phase of O_3 is discussed in further detail in Teolis et al. (2007a). Further heating leads to compaction of porous O_3 film at ∼46 K, which is followed by its sublimation. In temperature programmed desorption (TPD), where the temperature is increased linearly with time, rates of desorption (sublimation) are obtained by differentiating the QCM data with respect to time. In general, the QCM technique can give information about the radiation-induced chemical processes in thin films from the temperature of desorption peaks of species that are possible end products of irradiation. In conjunction with mass spectrometry data, the QCM desorption data would also provide the masses of the new species present in the mixture, as discussed later in Sect. 5.7 (see Fig. 9 and description).

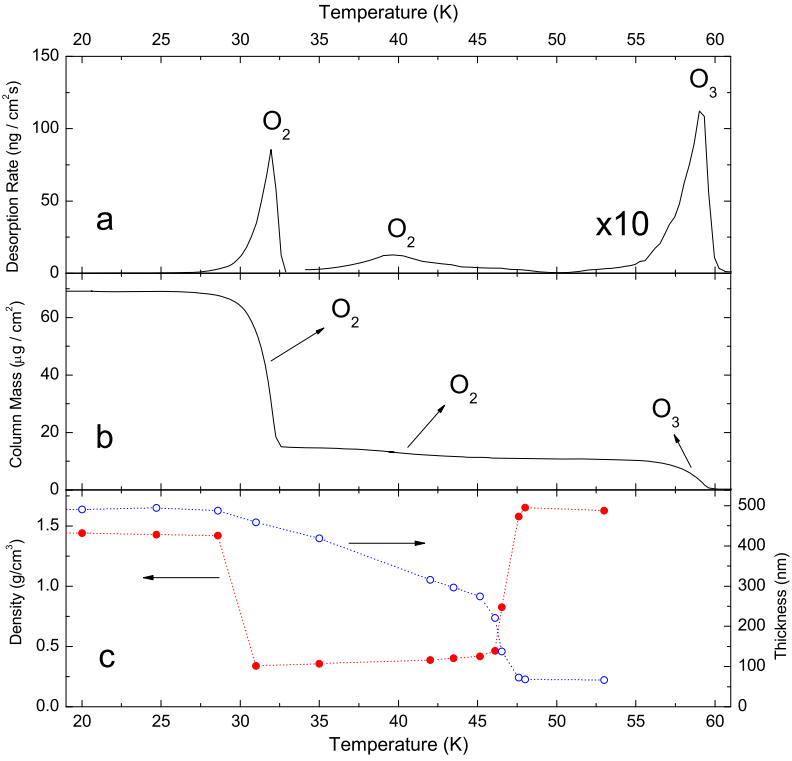

Fig. 11 TPD of an ion irradiated O_2 film showing the formation of low density ozone: (**a**) desorption rate; (**b**) mass per unit area; (**c**) thickness and mass density. From Teolis et al. (2007a)

4.2.3 Decomposition of Compounds

Loeffler and Baragiola (2011) combined QCM and IR absorption spectroscopy to study the decomposition of the metastable dihydrate of hydrogen peroxide at 151.6 K. This decomposition occurs by fractional distillation through the preferential sublimation of water, which leads to the formation of pure hydrogen peroxide, the less volatile phase. For this experiment, the films were prepared by co-deposition of water and hydrogen peroxide, measuring the individual deposition rates with the QCM just before and after growing the mixed ice.

4.2.4 Gas Uptake

Low temperatures enhance the absorption of gases on surfaces. After cleaning the QCM by light sputtering, we measure the evolution of frequency over extended periods of time. The time constant for adsorption of a monolayer of residual gases is typically of the order or larger than 3 hours, indicating pressures in the 10^{-11} Torr range at the QCM.

Raut et al. (2007) used a combination of QCM, UV-Vis interferometry and IR absorption spectroscopy to characterize the adsorption of methane on porous water ice. The attachment of CH_4 to the ice micropores was observed through the IR measurements of OH dangling bonds, CH_4 abundance and increase in film density, as voids were filled with methane. Crucial in these experiments was the absolute measurement of methane uptake that was possible with the QCM.

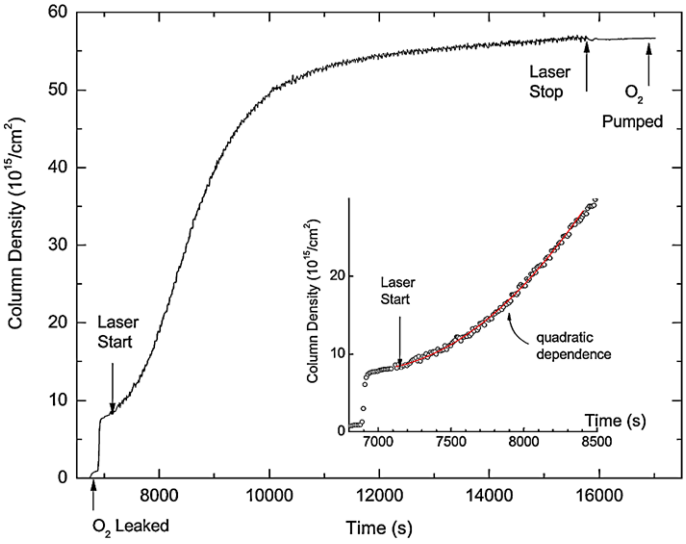

Fig. 12 Column density of O_2 adsorbed by a water ice film (1600 monolayers) at 50 K in the presence of ambient O_2, before, during and after UV irradiation of the film with 193 nm laser. *Inset*: magnified initial stage of laser irradiation to emphasize the initial quadratic dependence of O_2 uptake on time. The column density is obtained directly from the QCM by dividing the areal mass by the mass of an oxygen molecule. See Shi et al. (2011) for more details

In other experiments, we recently used a QCM to study the enhanced adsorption and trapping of oxygen in ice, induced by ions (Shi et al. 2009) and photons (Shi et al. 2011). Different mechanisms are responsible in both cases and these new phenomena are thought to occur in the outer solar system and in dense interstellar clouds. Figure 12 is an example of the QCM data during irradiation with 193 nm photons. The quadratic uptake of O_2 with photon fluence indicates that absorption of two photons is necessary for enhanced adsorption. Infrared spectroscopy shows that oxygen is adsorbed as part of new species, H_2O_2 and O_3.

4.2.5 Sputtering and Photodesorption

The sputtering yield is determined from the frequency change Δf due to mass removed by a fluence change ΔF (in projectiles cm^{-2}), after subtraction of the mass increase due to implanted projectiles, as discussed by Eernisse (1974a, 1974b), Andersen and Bay (1975), Schou et al. (1984), Oliva-Florio et al. (1987), Balaji et al. (1990):

$$\mathrm{SY} = s \times (\mathrm{d}f/\mathrm{d}F \times 1/M_2) + t \times M_1/M_2$$

where M_1 and M_2 are the masses of projectile and target atoms, respectively and t is the projectile trapping probability. For ices, where the sputtering yield is relatively large, projectile trapping is a small, usually negligible correction (Vidal et al. 2005; Fama et al. 2008).

The QCM has been used also to measure photodesorption yields at 10.2 eV (which are orders of magnitude smaller than sputtering yields) for pure ices of: H_2O (Westley et al. 1995), CO_2 and O_2 (Bahr and Baragiola, to be published) and at 6.4 eV for NH_3 (Loeffler and Baragiola 2010). We have also measured photodesorption cross sections for water on carbon at 6.4 eV (Mitchell et al. 2012, to be published).

4.3 Calibration of Mass Spectrometers Against the QCM

The flux of molecules coming off the film as the ice is sputtered or desorbed is often analyzed with mass spectrometers. In the same experiments, a QCM gives the total mass loss during sputtering/desorption but reveals no information about the molecules (or their fragments) responsible for the mass loss. Mass spectrometers (MS), which can identify the desorbing molecules, are especially useful when investigating sputtering or desorption of multi-component films. Once the species are identified, it is also possible to obtain the relative fraction of each component in the film from mass spectrometer readings. This is done with the aid of calibration experiments, where known quantities of each component are deposited on the QCM and desorbed. The area under the desorption peak measured by the MS is proportional to the mass of the film measured with the QCM. It is advisable to test the range of linearity between QCM and MS signal. The relative fraction of different component in a mixed film can then be estimated using this conversion factor.

4.4 Remarks

In summary, the QCM technique offers a unique capability for laboratory simulations of physical processes in astrophysical ices, allowing absolute measurements of mass with very high sensitivity, as a function of many variables, such as time, temperature, irradiation fluence, etc.

5 Mass Spectrometry of Desorbed or Sputtered Species

Main contributors: authors in Virginia

5.1 Quadrupole Mass Spectrometry

Mass spectrometry allows analyzing the composition of the flux of atoms and molecules ejected from the sample, with the aid of a mass spectrometer (MS) located inside the main vacuum chamber or in a differentially pumped arrangement through a small aperture and separate pumping. MS is a useful technique that is used to mainly identify neutrals and charged species coming off from the sample under study during thermal desorption or irradiation by energetic particles such as ions, electrons or photons. There are several MS in the marketplace that can provide the required mass spectra with sensitivity and resolution adequate for most laboratory astrophysics applications. Here we will discuss the most popular MS: the quadrupole mass spectrometer (QMS; see e.g. Dawson 1997). Another type, with advantages for the analysis of large molecules is the time-of-flight mass spectrometer (TOF-MS) that is discussed in Sect. 6.

Figure 13 shows a Hiden EQS300 spectrometer used in our laboratory which can analyze neutrals and ions, and is equipped with an electrostatic analyzer, useful for secondary ion mass spectrometry (SIMS). The QMS consists of an ionization chamber (ionizer or ion source), a selector of ions according to their mass to charge ratio (m/q), and a detector. The ionizer is needed because most species to be analyzed are neutral, but this stage is not necessary when analyzing species that are ejected as positive or negative ions from the sample. In the ionizer, a small chamber open to the incoming gas, electrons emitted from a hot filament are accelerated to tunable energies (10–150 eV) by a positively charged anode grid, and are confined in a small volume with the help of repelling lens. Since the ionization probability

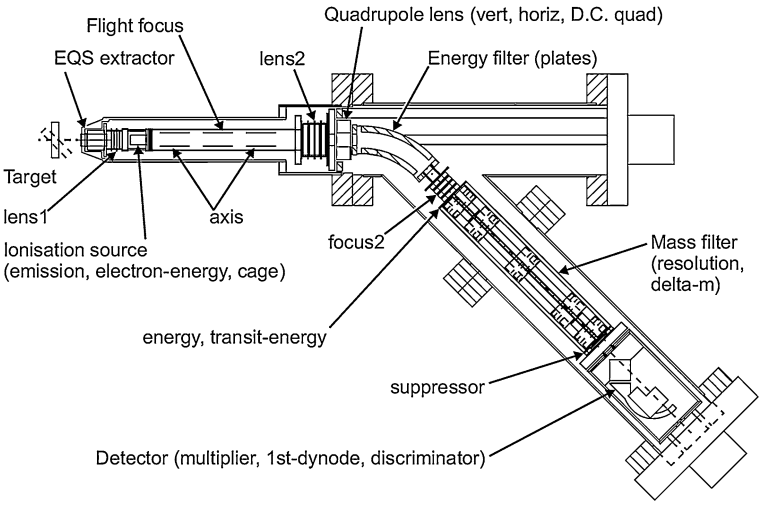

Fig. 13 Schematic drawing of the Hiden energy-filtered EQS quadrupole mass spectrometer used in the authors laboratory

of many molecules peak at ∼70 eV, QMS systems are typically operated at this electron energy, although one can tune the energy that maximizes the sensitivity for a particular species or maximizes the ability to distinguish species of similar m/q. In addition, one can adjust the electron emission current to maximize sensitivity. However, at high currents, linearity of the signal with electron current or with pressure is lost due to the buildup of space charge in the ionizer (Cowen et al. 1994). Different types of filament can be used, tungsten is most common but, for studies of reactive gases, such as oxygen, a thoria-coated type is preferred. Low-temperature electron emitters also minimize distortion of mass spectra by pyrolysis.

Collision processes in the ionizer (also called ion source) are complex. Molecules can be not only ionized but also dissociated. Thus, a mass spectrum of water contain peaks at masses (amu) 18: H_2O, 17:OH, 16:O and 1:H. Fast ion molecule reactions inside the chamber and at its walls give rise to additional peaks, such as 19:H_3O, and 2:H_2. The relative importance of these processes depends on electron energy, filament temperature, current density, pressure, and ionizer geometry.

Following the ionizer is an ion acceleration stage that limits the angular divergence of the ions entering the mass selection stage. In the QMS, m/q analysis is achieved by a combination of radiofrequency (RF) and DC voltages applied to four rods producing quadrupole electric fields. For a given ratio of RF-DC potentials, only ions with certain m/q ratio can exit the mass selector. Other ions undergo wide oscillations and end up hitting the rods or the walls surrounding the QMS.

At the exit of the mass selector is the ion detector. If the ion current is sufficient (>1 pA), one can use a Faraday cup, that collects the transmitted ions with ∼100 % efficiency (multiply charge ions produce currents that are higher by a factor q). In the more common case where the ion flux is small, the detection is assisted by a particle multiplier. In this device, an electron ejected from the front of the multiplier is accelerated and produces multiple electrons by secondary electron emission from the walls which are, in turn, accelerated and made strike the walls again. After several of those steps, one gets an avalanche of electrons which produces an output pulse for every incident ion with a current that is larger by a factor

of 10^3–10^9 (called the gain G). Since the multiplier pulses are 0.5–3 ns, much shorter than flight times, they can be used for time-of-flight studies of energy distributions.

The current I_m obtained at a particular m/q value is related to the partial pressure P_m of the species (or dissociation product) with mass m as:

$$P_m = I_m \times f_m/(S_m \times G)$$

where S_m is the sensitivity in Amps/Torr, f_m is the fragmentation fraction for the species m, and G is the detector gain, if the QMS is operated in multiplier mode. Sensitivity, an important parameter in measuring QMS performance, is defined as $S_m = (I_m - I_{mo})/(P_m - P_{mo})$, where $(I_m - I_{mo})$ is the change in ion current relative to the background current I_{mo}, when partial pressure of species m is increased from background P_{mo} to P_m. The fragmentation fraction f_m is 1 for the principal mass and between 0 and 1 for the secondary fragments.

5.2 Sensitivity of Mass Spectrometer

This is typically the important measure of the mass spectrometer's performance. Many MS parameters can be tuned to enhance the QMS sensitivity. The ionization in the ion source can be optimized by choosing the energy at which the ionization cross section peaks for the species of interest. The electron current, typically a few mA, is limited by the maximum temperature of the filament and by space-charge effects. At higher ion densities, ion-ion repulsion can defocus the ion beam and affect its path in the mass filter, lowering the ion count at the detector. The energy of the ions at the entry point of the mass filter can be increased such that the ions are subject to less filtering cycles in the mass filter, but this procedure diminishes the resolving power of the QMS.

5.3 Mass Range and Resolution

The mass range of typical QMS goes from 1 amu to a maximum in the range 100–500 amu. The maximum mass is proportional to $V_m/r_0^2 f^2$ where V_m is the maximum voltage that can be applied to the rods (typically, a few kilovolts) and r_0 the radius of a circle tangent to the rods. An important measure of MS performance is the ability to distinguish between ions of similar masses: the resolving power $R = m/\Delta m$, where Δm is the resolution. For a QMS, R is independent of mass, on first order, and one chooses the instrument (or operating conditions) that will provide the required Δm. This quantity depends on the dimensions of the quadrupole rods and their precision, the frequency f of the RF field (usually fixed), the ratio of the DC to RF voltages and the injection velocity of the ions at the entry point of the mass filter. The resolution improves with increasing DC/RF ratio as a greater fraction of the ions is lost from axial dispersion. However, the improvement of mass resolution is at the expense of the sensitivity, and the choice of DC/RF ratio is a compromise. Otherwise, the resolution Δm is proportional to $(v_i/fL)^2$ where v_i is the velocity component along the axis for an ion entering the mass filter of length L. The ion injection velocity is controlled by adjusting the anode grid voltage in the ionizer.

5.4 Combination of MS and Time-of-Flight with Pulsed Beams of Particles or Photons

If the ice target is bombarded with pulsed particle or photon beams, one can use time-of-flight (TOF) electronics to measure the velocity distribution of particular ejected species. An electronic clock is started with a signal driven from the beam pulse, suitably delayed to coincide in time with the moment the beam hits the target. The ejected species then traverses

a flight tube, tens of cm long and enters the MS where it is ionized and detected. The clock is stopped with a pulse from the electron multiplier detector in the MS. The velocity is then calculated from the flight distance divided by the TOF. Mounting the MS so that it can be moved closer or farther away from the target allows one to determine the time the detected ion spends in the mass spectrometer, which is hard to estimate accurately but may be significant compared to the total TOF.

5.5 The Problem of Mass Interference and Some Solutions

The most troublesome aspect of MS operation is the interference of mass peaks due to fragmentation and ion-molecule reactions, mentioned above, the presence of different isotopes and the accidental near-equality of masses (within Δm) of different species, the most common being mass 28 due to N_2 (28.013 amu) and CO (28.010 amu) which are closer in mass than the resolution of most QMS. We use this example to illustrate possible solutions to the interference problem, which can be used for other cases as well. Another technique for the analysis of interference in mass spectra is the use of Bayesian inference (e.g., Kang et al. 2002).

First is the examination of cracking patterns. One can measure the ratio of masses 14 to 28 (N/N_2) when using pure N_2 and masses 12 and 16 to 28 (C/CO, O/CO). Once the fragmentation ratios are known, one can set a simple algebraic equation to establish the proportion of CO and N_2 even if there is oxygen from a normal background source (H_2O).

A powerful technique is that of appearance potentials. It requires a MS with the ability to measure mass spectra as a function of bombarding electron energy, near the ionization threshold. Here, we discuss the case of N_2 and CO, illustrated in a classical article by Hagstrum (1951). For these molecules, thresholds are well separated, 14.1 eV (N_2) and 15.7 eV (CO). In addition, the products N^+, C^+ and O^+ have the dissociative ionization thresholds of 24.3, 20.9 and 23.3 eV, respectively. The use of energies below the dissociative ionization threshold will produce mass spectra without fragments but of low intensity, since cross sections can drop by one or two orders of magnitude compared to the maximum of sensitivity. Therefore, it is best to extrapolate curves of ionization vs. electron energy with procedures such as described by Hagstrum (1951) or by Singh et al. (2000).

5.6 Spurious Signals

The QMS ionizer has to be in line of sight with the target. Even then, it will accept molecules coming from other parts of the vacuum system (background) plus normal outgassing from the QMS. The best way to estimate the background in ion/photon beam experiments is to turn the beam on and off and use only the part of the signal that varied. However, if the beam hits other surface, it can produce a synchronous background which is hard to detect. Collimating the gas coming from the sample, as in a differentially pumped mass spectrometer, minimizes this problem.

Ion beams can backscatter from the surface and enter the mass spectrometer striking the rods and the detector, thus producing a signal that appears genuine (fluctuates with ion beam on and off). The best way to reduce this problem is by orientating the axis of spectrometer perpendicular to the line sample-ionizer. It is also a common practice to have off-axis detectors with a biased electrode in front that deflect low energy ions to the detector.

Common spurious signals originate from electron-stimulated ion desorption from surfaces in the ion source or impurity ions emitted from the filament. The most common are H, O and F (see, e.g. Adrados and de Segovia 1984). Another source of spurious signal is the

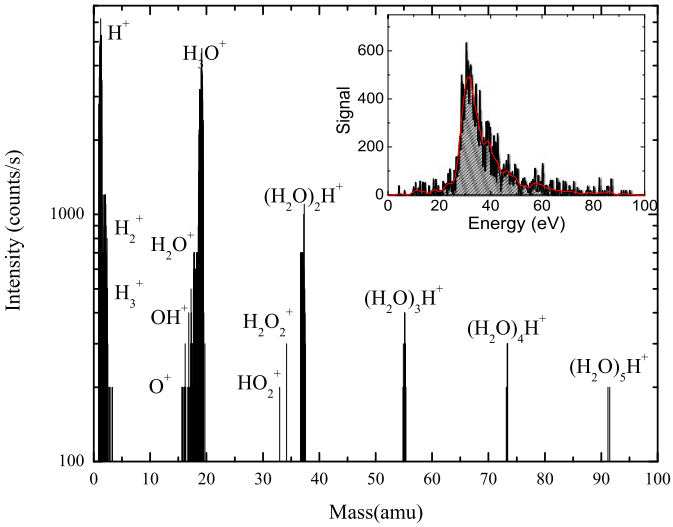

Fig. 14 Secondary ion mass spectrum from water ice at 80 K, irradiated with 100 keV Ar^+ with a flux of 7.8×10^{11} $cm^{-2}\,s^{-1}$. *Inset*: Energy scan of H_3O^+ (mass 19) showing that the ice has charged positively to about 20 V. The fluence used for the mass spectrum was 1.1×10^{14} cm^{-2}, and for the energy scan, 2.3×10^{14} cm^{-2}. For details, see Baragiola et al. (2008) and Shi et al. (2012)

replacement of an impurity molecule on a wall (either the vacuum system or the MS itself) by a molecule emitted from the sample. This can occur by replacement adsorption (e.g., O_2 desorbing CO from a wall) or the release of a previously pumped gas in ion or cryogenic pumps.

In summary, there are many possible sources of error in mass spectrometry. However, the technique is very valuable because it provides unique information of species released during particle bombardment of solids, and during the following thermal desorption of the irradiated region. Useful additional information about peculiarities of MS can be found in the articles published by metrological groups (Basford et al. 1983; Lieszkovsky et al. 1990).

5.7 Examples of MS Studies in Laboratory Astrophysics of Ices

Figure 14 shows a mass spectrum of ions emitted from an ice sample during impact with 100 keV Ar ions taken using a Hiden mass spectrometer. Ion spectra are more complex than that of neutrals due to the increased force that the ion charge induces in aggregating atoms and molecules. In particular, notice H_3^+ (neutral H_3 is not a stable molecule), and the protonated cluster ions $(H_2O)_nH^+$. The MS used for this study can analyze the energy of the incoming ions (see inset in Fig. 2 showing the energy distribution of $(H_2O)H^+$, the hydronium ion). In this particular case, the energy offset is useful to measure the surface potential of the ice sample during irradiation.

Mass spectrometers can be coupled with other techniques, such as the quartz-crystal microbalance (QCM; Sect. 4) or optical spectroscopy. The QCM provides an absolute measurement of the mass per unit area of the sample and enables a method for calibration of a MS, discussed below. Figure 15 demonstrates the QMS-QCM technique used in a typical temperature-programmed desorption (TPD) experiment conducted in Virginia laboratory. In the top panel, we show the QCM recorded rate of mass loss against temperature T during

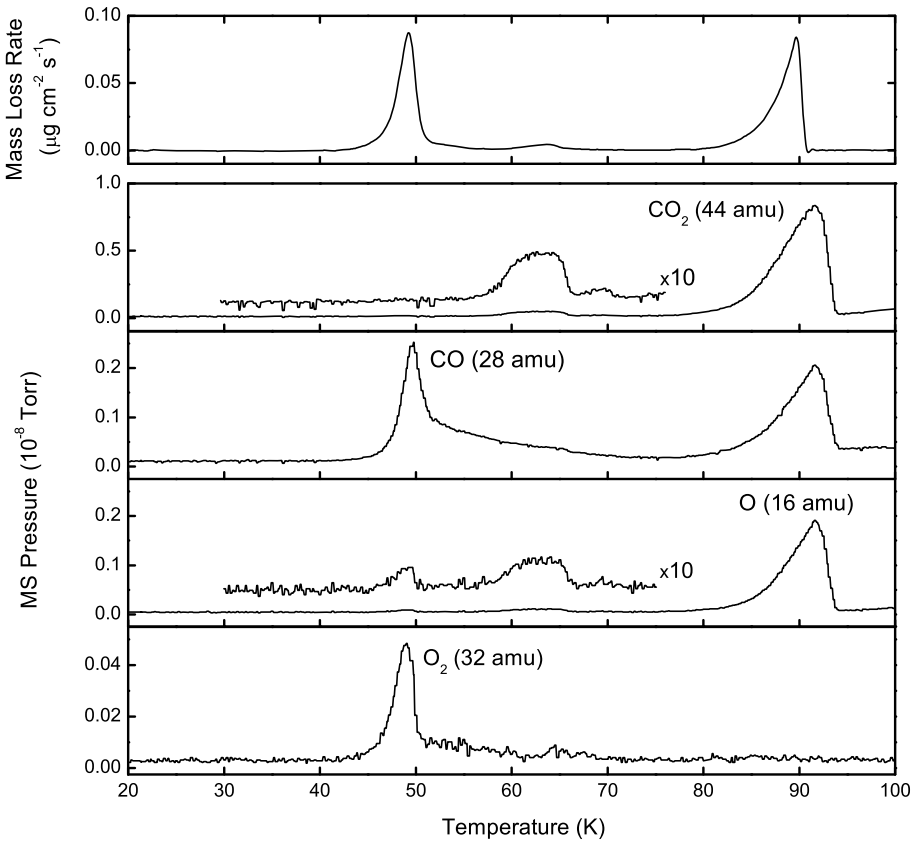

Fig. 15 *Top panel* shows the mass loss rate deduced from QCM vs. temperature during heating of an initially pure CO_2 film at 1 K min^{-1} following irradiation with 100 keV H^+ at 20 K. The *bottom panels* shows MS signals for 44, 28, 16 and 32 amu that correspond to CO_2, CO, O and O_2 respectively that desorb at different temperature during heating. Irradiation converts CO_2 into CO and O_2 that desorb at ∼50 K

desorption of an initially pure CO_2 film following irradiation with 100 keV protons at 20 K. In the bottom panels, we show partial pressures vs. T for different masses (16, 28, 32 and 44 amu) monitored using a quadrupole mass spectrometer. The mass spectrometer enables the identification of species that desorb at different temperatures causing mass loss as noted by the QCM. For instance, at 50 K, we observe pressure increase in mass 28 and 32 amu, which correspond to CO and O_2. CO_2 (44 amu) leaves at ∼90 K. Smaller amounts of CO_2 also leave at ∼63 K. This experiment shows that proton irradiation converts a fraction of the solid CO_2 mainly into CO and O_2. We note that, as expected from the O–C–O geometry the main dissociation fragments in the MS are CO + O at 70 eV electron impact, and not C +O_2, as noted by the absence of O_2 signal at 90 K. One can also study the dependence of the fragmentation channels on electron energies.

In the preceding example, we also quantify the amount of CO and O_2 in the irradiated films by direct calibration of the mass spectrometer against the QCM. Pure films CO and O_2, with same column densities (known to within ∼0.1 ML), can be deposited on the microbalance and desorbed while recording the flux with the QMS. The integrated area under

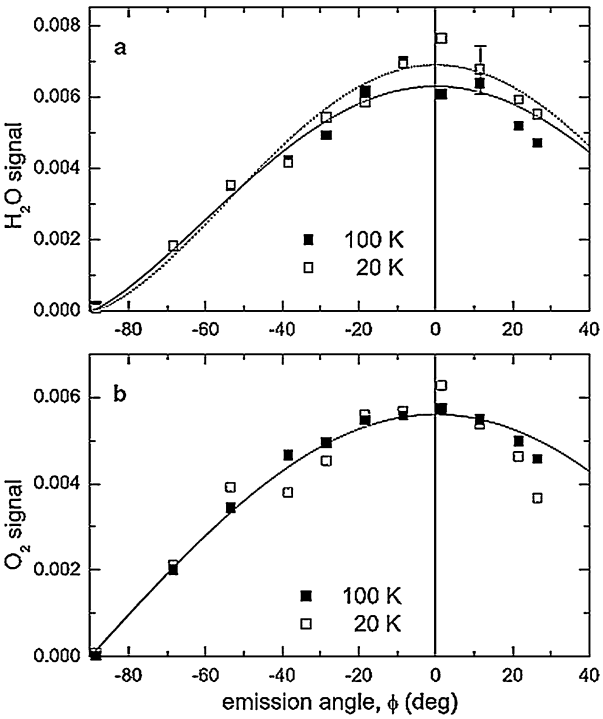

Fig. 16 Distribution of sputtered particles as a function of emission angle obtained using a mass spectrometer during irradiation of water ice film with 100 keV H^+ at 20 and 120 K. The signals have been normalized so that the integral over the emission solid angle is 1. The lines are fits to $\cos^f \theta$. For H_2O, $f = 1.3$(100 K)–1.5(20 K); for O_2, $f = 1$. From Vidal et al. (2005)

the desorption curve divided by the column density of the condensed films gives the conversion factor required to quantify the amount of CO and O_2 that desorb from the ice at ∼50 K in the experiment shown in Fig. 15. The implicit assumption in this calibration is that the angular distribution in irradiation-induced desorption is similar to that of evaporation.

An example of differences in these distributions occurs in the sputtering of ice, which we studied by rotating the target. In Fig. 16, we show the dependence of the sputtered flux of $H_2^{18}O$ and $^{18}O_2$ on emission angle measured with a QMS during irradiation of a isotopically labeled 1.8 μm thick ice film at 20 and 120 K with 100 keV H^+. The signals have been normalized so that the integral over the emission solid angle is 1. The lines are fits to $\cos^f \theta$ where θ is the ejection angle to the surface normal. For H_2O, $f = 1.5$; for O_2 $f = 1$; that is, the O_2 followed a cosine distribution, while the H_2O distribution was more forward-peaked along the normal. The cosine dependence of O_2 flux was attributed to the isotropic collision cascade and the O_2 transport to the surface by thermal diffusion. The sharper than a cosine outward H_2O peak was explained by the flux suppression at large angles by formation of transient craters. For the same experiment, the dependence of the total sputtering yield on the incidence angle of the projectile was also measured using the QCM at both temperatures. The sputtering yield increased with incidence angle; the dependence was fitted with $\cos^f \theta$, which yielded $f \sim -1.3$ at both temperatures. Additional details are available in Vidal et al. (2005). The angular dependence of the sputtered molecules, along with their energy distribution, is important to describe trajectories leading to molecular escape or return in different icy objects such as the satellites and rings of giant outer planets.

A final example is the observation of rich phenomena in an irradiated ammonia:water ice during temperature programmed desorption, shown in Fig. 17 (Loeffler and Baragiola

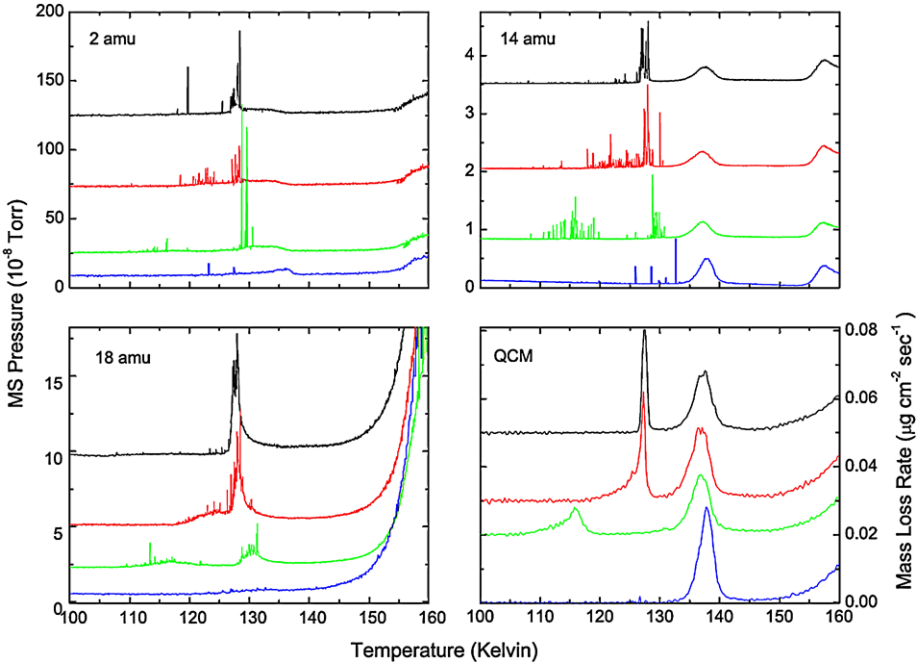

Fig. 17 Fluence dependence of thermal desorption measured by the mass spectrometer and the microbalance for a 1:2 ammonia-water mixture irradiated at 70 K with 100 keV protons, and warmed at 0.2 K min^{-1}. The fluence for each spectrum (*top to bottom* in all panels) is 3.7, 5.6, 7.1, and 9×10^{15} ions cm^{-2}. In each panel the spectra have been offset vertically for clarity. The spikes in the MS data between 110 and 135 K are due to the ejection of gas bubbles and blister covers. For details, see Loeffler and Baragiola (2012)

2012). In samples irradiated below 70 K, we observed fast gas outbursts that appear to indicate grain ejection and correlate well with the formation of micron-sized scattering centers detected by infrared reflection spectroscopy. Irradiation by 100 keV protons results in dissociation into radical species, with very efficient hydrogen loss and the recombination of the radicals into new stable molecules, predominantly H_2 and N_2, detectable in the ice by infrared spectroscopy due to lattice perturbations and during desorption with the QMS. H_2 has been in fact tentatively detected in interstellar ice (Sandford et al. 1993) and N_2 firmly detected in some objects in the outer solar system such as Pluto (Owen et al. 1993). Those molecules can trap at existing voids or at defect sites, such as vacancies, or diffuse through the lattice. At large fluences they may form high-pressure bubbles and blisters that exfoliate ejecting ice grains. We observe outgassing at temperatures below those where ice sublimates, which suggests that comets containing radiolyzed material may have outbursts farther from the Sun that those that are passive. In addition, the estimated size of the grains ejected from our sample is on the order of the size of E-ring particles, suggesting a plausible mechanism for how micron-sized grains could be formed from an icy surface (Loeffler et al. 2006).

5.8 Future Experiments

An astrophysical application where MS can play a unique role is when performing experiments on surface reactions. An ongoing project in the Virgina laboratory aims to understand

the mechanism of molecular desorption induced by surface recombination, under conditions of astrophysical interest. Indeed, a key question in astrochemistry is how molecules can be maintained in the gas phase in cold interstellar regions at temperatures well below their thermal desorption values. Surface recombination with energy release and subsequent molecules desorption could be one of the underlying mechanisms and the MS technique give us unique information on the desorbed molecules or their fragments. Examples will be pure ices (such as O_2, N_2, CO or CO_2) exposed to a flux of O, C or H atoms coming from an atom source. If the pure ice molecules do not contain the incoming atomic species, the MS will provide information on the surface reactions and the fragmentation mechanisms, particularly as a function of surface temperature.

6 TOF-SIMS of Ion Irradiated Materials

Main contributors: authors in Caen

6.1 The Technique

Impact of ionizing radiation on surfaces may lead to a variety of physico-chemical processes. Changes of surface topography such as smoothing or roughening, phase changes, appearance of hillocks or craters have been observed. Under ion irradiation, implantation of projectiles occurs with possible changes in physical and chemical properties, as well as desorption or sputtering of atoms, molecules and clusters. Several physical mechanisms may lead to sputtering (see e.g. Baragiola 2004; Behrisch and Eckstein 2007, and references therein). Elastic interaction of projectile and target nuclei sets target atoms in motion and in turn a cascade of recoiling atoms develops, some of which may be energetic enough to be ejected. This process is dominant at low projectile velocities and often referred to as "knock-on" sputtering. With increasing velocity, energy deposition on target electrons becomes dominant and "electronic sputtering" occurs. Possible Mechanisms include "Coulomb explosion", "thermal spike" due to electron-phonon coupling and short-time transient "heating" in a zone of typically some nm around the ion trajectory. Other processes are related to formation and self-trapped excitons ("defect mediated sputtering") and the potential energy of highly charged ions (which leads to electron capture), referred to as "potential sputtering". The ejected, sputtered particles may be used as a tool to analyze the composition of the target. A certain number of techniques has been developed for this purpose (for a recent review see Wucher et al. 2007). Indeed, in particular "Secondary Ion Mass Spectroscopy" (SIMS) is a widely used surface and materials analysis technique. Often quadrupole mass spectrometers (QMS) are used to record mass spectra of sputtered ions. Another experimental technique is the measurement of the "time of flight" (TOF) of ejected particles with pulsed beams.

The majority of particles are ejected as neutrals, some may undergo charge exchange (ionization) upon emission from the surface. Typically, the reported ratios of charged particles to neutrals are of the order of 10^{-1} to 10^{-6} depending on projectile-target combination, impact energy, surface structure and so on. However, in some cases relevant to astrophysics, ionized particle yields of the same magnitude as that of neutrals have been reported, demonstrating the usefulness of ionic particles as information about surface stoichiometry (Dukes et al. 2011). Therefore, if an experimental technique relying on electromagnetic manipulation of the ejecta is to be applied for detection of sputtered neutrals, a post-ionization by electrons or laser beams must be used. These techniques allow measuring mass resolved partial sputter yields and in specific cases that of energy distributions.

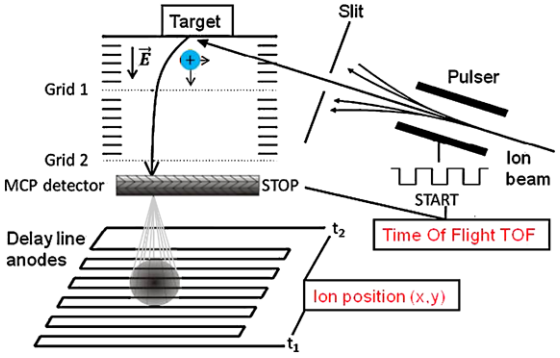

Fig. 18 Principle of XY-TOF-SIMS (see text)

An alternative for detection of neutrals is the "catcher technique", where sputtered particles are collected on a suitable support such as e.g. ultrapure aluminum (Assmann et al. 2007). The amount of deposited sputtered particles is measured with different techniques such as Rutherford Backscattering Spectroscopy (RBS), and Elastic recoil Detection Analysis (ERDA); in some cases, tracks induced by neutron activation of fissionable sputtered atoms on the catcher were counted. Also, Auger electron spectroscopy may be applied. Such techniques allow measuring total yields and angular distributions, but analysis of the size of sputtered particles or measurement of energy distributions have been possible only in a few selected cases.

Conventional TOF-SIMS is optimized for Mass resolution (SIMS) and/or detection of large molecular fragments for analytical applications in chemistry, biology, often using laser induced desorption. We can distinguish between "static SIMS" where measurements are made with low intensity beams which do not significantly alter the surface during measurement, and "dynamic SIMS", where measurements are made during irradiation with rather high currents and the evolution with fluence is recorded for selected masses (QMS). The imaging XY-TOF-SIMS measurements described below belong to the former, "static SIMS" type. However, we can also apply a procedure, which allows monitoring the evolution of surface stoichiometry as a function of fluence, by alternating a "static" low beam intensity measurement (which does not change the surface composition or structure), with a high beam intensity irradiation. Such a cycle can be repeated as often as necessary to simulate exposure of surfaces to solar wind or cosmic rays during a certain period of time.

The specific advantage of adding an imaging XY detection to conventional TOF-SIMS is that now three quantities (the TOF and the two positions X and Y) are measured. Thus, the three components of the complete velocity vector can be calculated. This feature allows in turn to determine, in addition to mass distributions, differential yields such as angular distributions $N(\theta)$, also for the polar angle $N(\phi)$, or energy spectra $N(E)$ (Jalowy et al. 2002, 2004; Hijazi et al. 2011, 2012). A sketch of a typical experimental set-up is shown in Fig. 18. An ion beam impinges on a target inside a vacuum irradiation chamber. The sputtered secondary ions are extracted by means of an electrostatic field and the directed onto a position-sensitive Micro-Channel-Plate (MCP) detector. The induced electron avalanche at the position of the secondary ion impact yields a fast "STOP" signal. From the time difference between the "STOP" and a suitable "START" signal, the TOF of the secondary ions can be determined. The electron avalanche is collected by an XY-delay-line anode. From the four time signals X1, X2, Y1, Y2 of the two delay lines X and Y, the position (X, Y) can be calculated.

It is possible to collect all secondary ions emitted within the solid angle half sphere of $\Delta\Omega = 2\pi$. It is also important to note that the detected ions are a "direct" probe of the

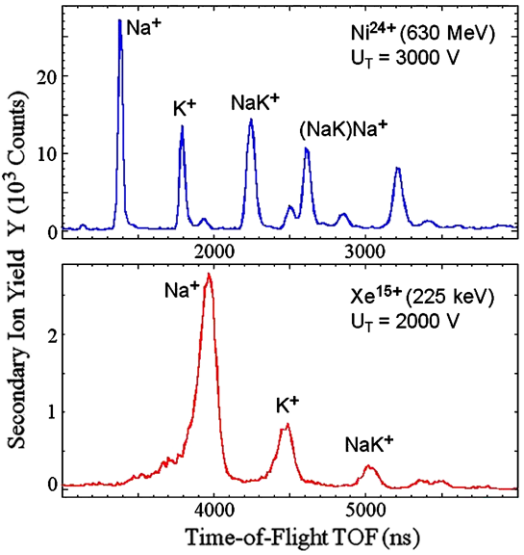

Fig. 19 TOF spectra from nepheline by low energy Xe ion beams at 225 keV (*bottom*) and high energy Ni ion beams at 630 MeV (*top*). Note the different extraction voltages of 2000 V (*bottom*) and 3000 V (*top*)

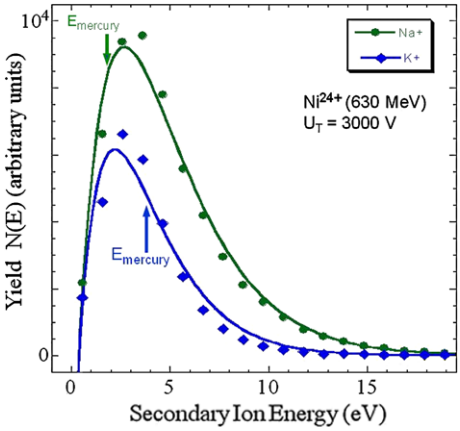

Fig. 20 Energy distributions of Na and K ions induced by high energy Ni ion beams at 630 MeV. The escape velocity from mercury is indicated for the two species Na and K by *arrows*. The *line* is a best fit of a Maxwell-Boltzmann distribution $N(E) = A \times E \exp(-\alpha E)$ to the data

species emitted from the surface. No destruction ("cracking") of molecules and clusters occurs as in QMS using post-ionization. However, fragmentation may occur during the moment of emission and arrival at the detector, since particles may be emitted in an excited state with sufficient energy in inner degrees of freedom to allow in-flight dissociation. QMS without post-ionization generally has a small detection solid angle $\Delta\Omega$. The three numbers (X, Y, TOF) allow to calculate the velocity vector of each secondary ion and to deduce differential yields such as $N(\theta)$ and $N(E)$, in ejection angle theta or secondary ion energy E. Correctly, with a total sputtering yield for a given species Y, these quantities should be written as $\mathrm{d}Y/\mathrm{d}E$ and $\mathrm{d}Y/\mathrm{d}\theta$. Multiply differential spectra such as $\mathrm{d}2Y(\theta)/\mathrm{d}E\mathrm{d}\Omega$ can be calculated, and it becomes even possible to construct numerically a "virtual catcher" to perform a direct straight-forward comparison to measurements of neutral sputtering by the catcher method (Hijazi et al. 2012). Examples for TOF spectra and energy distributions $N(E)$ are shown in Figs. 19 and 20.

With a continuous low energy beam as delivered by e.g. Electron Cyclotron Resonance (ECR) sources at GANIL's highly charged ion beam facility ARIBE, the beam is pulsed with deflection plates and a fast pulse generator which triggers a fast high voltage supply and also delivers the projectile "START" pulse for the TOF measurement (Fig. 18). Here, pulse widths of the order of some 10 ns can be reached. At the medium energy line SME of Ganil (typically 10 MeV/u), the beam is accelerated by a cyclotron and is already pulsed (pulse width about 2 ns). Thus, no beam pulser is necessary. Instead, a single ion detector made of a thin Al foil is placed in the beam (Hijazi et al. 2011). Secondary electrons emitted upon projectile impact on the foil are accelerated towards a MCP detector by an electrostatic potential and deliver the projectile "START" pulse.

Ordinary TOF spectrometers use a high extraction field (grid 1 close to the target surface and high, typically >10 kV extraction voltage applied). Choosing a larger distance between grid 1 and the target, and using a smaller extraction voltage serves to obtain a broader TOF peak with increased resolution of the axial velocity (Jalowy et al. 2004). This can be combined with a field free TOF region between grid 1 and 2. In a simple configuration, which works well at high enough projectile energies (MeV), one of the grids can be completely discarded, the remaining grid 2 serves just to post-accelerate the ions before hitting the MCP thus increasing the detection efficiency. Other configurations are possible, such as keeping the target at ground potential, and applying an extraction voltage to grid 1, and the same to grid 2 leading to a field free flight region. The voltage on grid 2 serves also to increase the final energy of secondary ions and thus increase the detection efficiency of the MCP. A precise calibration of the secondary ion mass and t_0 (time of ejection from the surface) is obtained from the photon peak and from the so-called "gas line". The recoil ions due to the ionization of the residual gas or a specific added gas such as He form a line in the Y-position versus TOF distributions (for a detailed description see Jalowy et al. 2004).

6.2 Preliminary Results Obtained So Far

As an example, Fig. 19 shows TOF spectra from nepheline evaporated on a Si substrate, irradiated by low energy Xe ion beams at 225 keV and by high energy Ni ion beams at 630 MeV. Nepheline is an alumino-silicate containing Na and K, and is believed to be a good analogue of the surfaces of Mercury and the Earth's moon. Experiments with beams of H, He, C, O, S etc. in the low energy range would be a laboratory simulation of solar wind impact on planetary or lunar surfaces. The experiments with the nickel beam with an atomic number close to that of iron are a good simulation of effects induced by the heavy ion fraction (a few percent) of cosmic rays (Seperuelo Duarte et al. 2010). Strong peaks are observed for Na^+, K^+ and NaK^+ in both spectra. Note that the time difference between the peaks is enhanced in the bottom spectrum (Xe 225 keV) compared to the top spectrum (Ni 630 keV) due to a lower extraction voltage of 2000 V instead of 3000 V. In the latter case, also the cluster $(NaK)Na^+$ and others are visible.

From the energy distributions $N(E)$ it is possible to estimate the fraction of particles that can escape from the gravitational field, and those that fall back to the surface and contribute to the atmosphere of the planet or moon (Baragiola et al. 2002). Of course, this is strictly valid only for neutrals, since charged particles may interact with electromagnetic fields. As an example, the energy distributions of Na and K ions induced by high energy Ni ion beams at 630 MeV are shown in Fig. 20. The maximum of $N(E)$ is at $E_{max} \approx 3$ eV for Na, and at $E_{max} \approx 2$ eV for K. The shape of the distributions is similar and follows a Maxwell-Boltzmann law $N(E) = A \times E \exp(-\alpha E)$. The "temperatures" which can be deduced from the parameter α from fitting the function to the data are of the order of $T \approx 24 \times 10^3$ K for Na

and $T \approx 19 \times 10^3$ K for K. These values are in reasonable agreement with track temperature values in the electronic stopping regime measured for other crystalline materials or by high resolution Auger spectroscopy (Hijazi et al. 2013). In Fig. 20, the escape velocity from Mercury is indicated for the two species Na and K by arrows. About 85 % of Na and 45 % of K would escape from Mercury, and 95 % of Na and 80 % of K from the Earth's Moon. Thus, sputtering may contribute to composition of the lunar or mercury exosphere (Dukes et al. 2011; Meyer et al. 2011).

6.3 Future Experiments

In the future, since secondary ions yield information about surface stoichiometry (Dukes et al. 2011), XY-TOF-SIMS measurements as a function of projectile fluence will allow to monitor changes in surface stoichiometry of e.g. silicates such as nepheline. In particular, laboratory modeling of the evolution of the surface of mercury (or the moon) exposed to solar wind will be performed by alternating cycles of a static low ion beam intensity measurement and high ion beam intensity irradiation. Modification of specific partial sputtering yields of different species and changes of the energy distribution may both lead to a time dependent contribution of sputtering to the composition of the lunar or mercury exosphere. Such an irradiation time dependence is due to changes in surface structure and stochiometry, which may also alter emission patterns and thus the energy distributions $N(E)$, which in turn determine the fraction of particles that can escape from the body's gravitational field (Baragiola et al. 2002).

Solar wind is an expanding flux of fully ionized plasma that reaches at distances greater than a few solar radii an expansion speed of about 400 km s^{-1} corresponding to an energy of ≈1 keV/u (slow solar wind, see e.g. Gosling 2007). As known 1 keV H^+ are the most abundant of the solar wind ions although the "integrated" effects of all of the heavy ions might be even more important. For this reason it will be essential to do experiments with a variety of ions and energies in order to establish the dependence of the sputtering yield on the parameters of the irradiating ions (energy, mass) and extend the results to different ion populations.

Another class of astrophysical materials are ices, which may e.g. be present on dust grains, comets, planets and moons. Most studies concerning the interaction of ionizing radiation with simple ices or ice mixtures were conducted with UV photons and proton or helium ion beams using infrared (IR) absorption spectroscopy as analyzing tool. This yields important information about radiolysis (destruction of molecules, formation of new species) and also changes in the structure (compactation, amorphization). TOF-SIMS measurements can complete such studies (Andrade et al. 2013). For example, information about species which cannot be directly observed by IR spectroscopy (symmetrical molecules such as N_2 and O_2) can be obtained. IR spectroscopy probes the bulk of the samples, whereas TOF-SIMS is sensitive to the surface. Furthermore, the observed ejected particles are instantaneous messengers of the induced processes. Several studies by PDMS-TOF-SIMS (PDMS = "Plasma Desorption Mass Spectroscopy", sputtering induced by ^{252}Cf fission fragments) have been performed, see Farenzena et al. (2005) for a review. XY-TOF-SIMS studies have been conducted in some select cases only such as distributions of H^+ and H^- sputtered from water ices (Iza et al. 2007). In the near future, our existing UHV XY-TOF-SIMS set-up will be upgraded and equipped with a closed helium cycle cold head. The field is open for investigations by XY-TOF-SIMS of angular- and velocity distributions of positive and negative secondary ions emitted from simple ices and mixtures. Also, the temperature dependence of

emission can be investigated (see also Fig. 15). With slow projectile ions, effects of implantation of e.g. C or S in water ice as occurring on ice-covered Jovian moons can be investigated. As mentioned in Sect. 5, study of surface reactions (ices on carbonaceous materials or silicates as models for dust grains) will also become an important topic.

Important information, possibly also on emission of neutrals, can be obtained from comparison of emission patterns of positive and negative secondary ions. Emission patterns may show a material dependent sensitivity to ion induced track potential (e.g. acceleration or deceleration). Also, physical processes behind the emission process may be different. For example, the yield of Li^+ emitted from lithium fluoride LiF scales with the electronic energy loss, whereas F^- scales with the "nuclear" energy loss (Pereira and da Silveira 1997). LiF and other alkalihalogenides seem to be "special" compared to most other materials, since they also show peculiar angular distributions, see Hijazi et al. (2012) and references therein. On the other hand, if similar mass spectra with similar scaling laws for e.g. distributions of negative and positive clusters were found, one could expect neutrals to behave in the same way as secondary ions with probably similar emission patterns (energy and angular distributions).

We finally mention the possibility of combining SIMS and beam focusing techniques. Such techniques include electromagnetically focused ion beams FIB, which are already widely applied, or possibly in the future, nano-beams obtained by guiding in capillaries. This allows to obtain spatially resolved analysis of inhomogeneous surfaces.

7 Luminescence Spectroscopy of Electron Irradiated Ices

Main contributors: authors in Kharkov

A diversity of luminescence methods (Vij 1998) seem to be particularly attractive to study astrophysical ices because of their extremely high sensitivity, several orders of magnitude higher than that of absorption spectroscopy. Moreover the measurements of transmission or absorption spectra require transparent samples but ices are often of snow-like structure that may be a problem for transmission spectra but does not give particular problem for luminescence detection. The merits of luminescence methods are also the wide dynamic range (5–6 orders of magnitude) and a weak background signal especially with the use of cooled detectors. The special convenience of luminescence spectroscopy is the possibility to access forbidden electronic states which are difficult to populate using conventional absorption spectroscopy. In luminescence experiments these states may be accessed indirectly, via nonradiative relaxation cascades from higher electronic states, directly accessible by allowed optical transitions or may be populated by inelastic electron collision in the case of excitation by charged particles.

Luminescence spectra provide a plenty of information on composition of ices, its transformation under ionizing radiation (molecule fragmentation or association, accumulation of radiation-induced species), diffusion, modification of structure, desorption of excited particles, radiation-induced chemical reactions and cascades of relaxation processes involving both electronic and atomic processes. It is conventional to classify luminescence types according to the excitation method (Vij 1998).

Here we present our recent findings in the field of the spectroscopy of simple ices with a focus on the interaction of electron beam with model systems of astrophysical interest and relaxation processes. Many remote-operated methods in use are here presented: cathodo- and photoluminescence (CL and PL) spectroscopy, nonstationary luminescence (NsCL), and activation spectroscopy–thermally and optically stimulated luminescence (TSL, OSL) and electron emission (TSEE, OSEE), desorption control through the pressure detection.

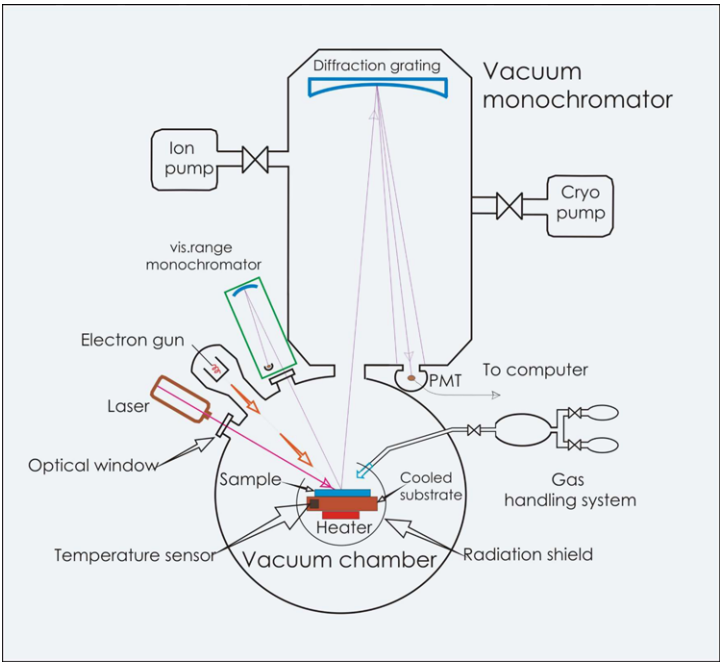

Fig. 21 Scheme of the experimental setup for luminescence study of ices combined with activation spectroscopy

7.1 The Techniques in Use

7.1.1 Cathodo- and Photoluminescence

Icy objects in outer Solar System are exposed to irradiation by fast ions, electrons and vacuum ultraviolet photons. Excitation by charge particles, in particular electrons, results in heavy ice ionization because the ionization cross section is an order of magnitude higher than that for photoionization. Due to different secondary processes, excitation by electrons may result in electrostatic charging while after photoionization positive and negative charges are formed in equal amounts. The special convenience of excitation with an electron beam is the possibility to probe an ice "layer-by layer" varying electron energy and thus changing the penetration depth. This allows to distinguish surface and bulk emitting centers as well as the desorbtion of excited species. Essential point is the choice of the bombarding electron energy. Bombardment by fast charged particles inevitably causes an appearance of relatively energetic electrons ($\sim$100 eV) capable to ionize ices. The energies needed to produce electron-hole pair in Ar, N_2 and H_2O ices are 26.6, 37.0 and 30.0 eV respectively (Johnson and Schou 1993) and maxima of the ionization cross-section are about 100 eV. In view of that we used electrons having energies from 200 eV up to 2 keV to produce excitations.

The experimental setup is shown in Fig. 21. Icy samples are formed by deposition of pure gases or their mixtures onto a cold metal substrate mounted in a high-vacuum chamber with a base pressure of 10^{-8} mbar. An advantage of the sample growth from the gas phase is the ability to easily obtain samples of required thickness with an open surface, which allows to study the luminescence in a wide spectral range. The sample growth from the gas phase has

also the advantage that it is easy to grow films of required thickness to optimize the luminescence signal as a function of the wavelength. The substrate is cooled by a closed cycle refrigerator or a liquid He cryostat. The substrate temperature, controlled by a Si diode, can be set as needed. Changes in deposition temperature and rate allow to modify grain size and number of defects in the deposited films. An important point is the influence of defects and grain size on the accumulation of charge. Nanostructured films with a number of defects are able to accumulate much greater charge. The samples are irradiated with an electron beam of a given energy. The beam is focused in such a way to provide irradiation of an area of 1 cm^2. Two modes of irradiation are used: irradiation of ices after deposition or deposition under the electron beam bombardment. The first mode permits to probe the sample by depth while second mode of deposition enables us to form charged species throughout the entire sample. The current density can be set from 7 $\mu A/cm^2$ up to 7 mA/cm^2. The luminescence spectra are recorded simultaneously in VUV and visible range using two ports of the experimental chamber (Fig. 21). Spectra were recorded repetitively to monitor the dose dependence of excited species formation and accumulation. In addition, the spectra ensured control over the presence of impurities in the films.

Another port of the same setup can be used for experiments on photoluminescence of electron irradiated ices. Different lamps are available as a source of VUV light: hydrogen and deuterium lamps, xenon and mercury lamps. Xenon and mercury lamps provide a continuous emission from 220 nm up to infrared while a deuterium lamp produces a continuous spectrum at shorter wavelength (below 350 nm). All these lamps operate at high pressure, so a protective window is used to introduce the VUV light into the experimental chamber. The protective window limits the wavelength range available for study. In view of that an original VUV source is used which produces VUV light "*in situ*". The source is based on emissions of solid rare gases and their mixtures. In detail the experimental procedure is: first the ice under study is deposited onto the substrate; then a thin film of Ar or another rare gas is deposited onto the ice surface. Irradiation of the cover layer by an electron beam results in excitation of VUV emission which, in turn, irradiates the investigated ice. Because of the wide band gap energy of rare gas solids (up to 21.56 eV in Ne) these cover layers are transparent to emission spectra of many molecular ices. The wavelength distribution of the source spectrum can be tuned by changing the composition of the cover layer. Solid Ne exhibits intense emission near 74 nm, the most intense bands of solid Ar, Kr and Xe are at 126, 149 and 174 nm correspondingly with a halfwidth of about 8 nm.

7.1.2 Nonstationary Luminescence

An additional opportunity to reveal connection of emissions observed with ionic species is provided by the method of nonstationary luminescence NsCL. The method calls for the generation of charged species with an intense electron beam. This is followed by probe of species with a low density beam of electrons at gradual linear heating of the sample. This allows to release electrons from progressively deeper traps so to enhance their recombination with positively charged ions. The NsCL method in combination with Thermally Stimulated Exoelectron Emission (TSEE) was used e.g. to ascertain the part of neutralization reaction in formation of $(Xe_2H)^*$ (Savchenko et al. 2010a). The ionic species of interest $(Xe_2H)^+$ were first generated with an intense electron beam of a high current density of 0.1 mA/cm^2 during 20 min. The time interval was large enough to create and to fill the shallow electron traps. The ionic species produced were then probed by the nonstationary luminescence (in the emission band of $(Xe_2H)^*$ at 252 nm) using a low-density electron beam (about 10 $\mu A/cm^2$) to minimize the production of new ions. The NsCL spectrum of Xe doped with hydrogen

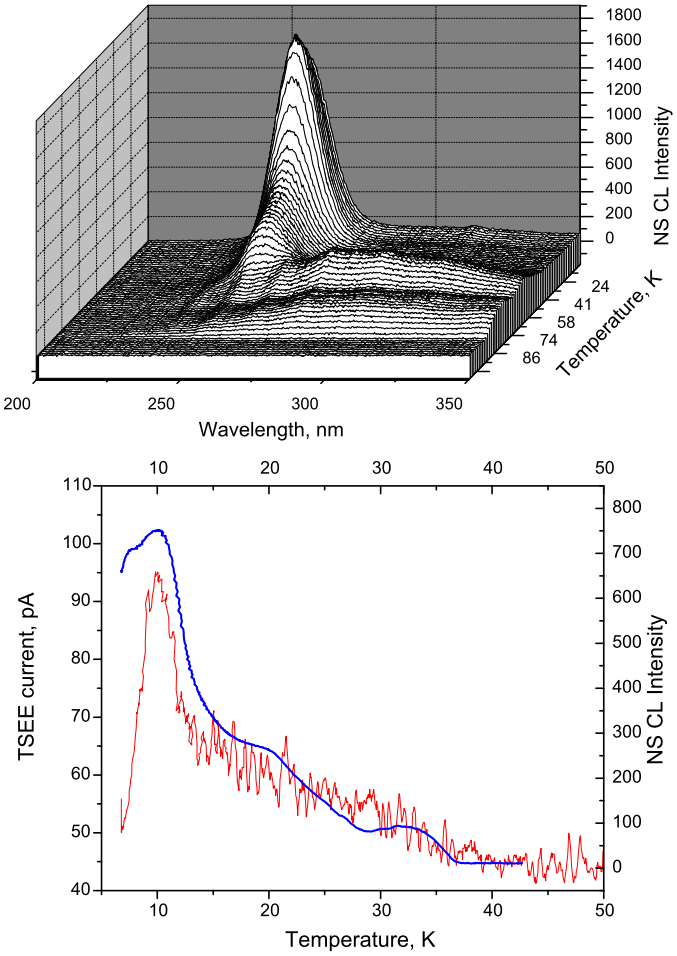

Fig. 22 Nonstationary luminescence of hydrogen doped Xe measured in the range of $(Xe_2H)^*$ emission at the sample heating rate of 3.2 K/min; (*top*) spectra, (*bottom*) comparison of the $(Xe_2H)^*$ emission temperature behavior (*blue line*) with TSEE yield from pre-irradiated sample (*red line*)

is shown in the top panel of Fig. 22. The measurement of $(Xe_2H)^*$ luminescence upon heating revealed nonmonotonic temperature dependence of the NsCL. Correlation of the NsCL intensity with the behavior of the TSEE yield (top panel in Fig. 22) measured after identical pre-irradiation of the sample implied the neutralization reaction $(Xe_2H)^+ + e^- \rightarrow (Xe_2H)^* \rightarrow h\nu(4.92\ \text{eV})\ Xe + Xe + H + \Delta E$ is being a process responsible for the $(Xe_2H)^*$ excimer formation. This technique of nonstationary luminescence based on stimulation of "internal electron emission" demonstrated its considerable promise in study of ionic species.

7.1.3 Activation Spectroscopy

The basis behind activation spectroscopy techniques consists in the stimulation of the absorbed species under irradiation and the release of stored energy by a controlled heating of the sample or via optical stimulation (Chen and McKeever 1997). There are several acti-

vation spectroscopy techniques: optical (thermally stimulated luminescence TSL), and current (thermally stimulated conductivity TSC and thermally stimulated exoelectron emission TSEE). The use of these techniques provide information on dose of irradiation, defects in irradiated materials (trap-level analysis), stability and relaxation of radiation-induced species. The technique of most frequent use is TSL. It is worthy of note that TSL arises from both—recombination of charged particles (neutralization reaction) and recombination of neutral species. For volatile materials such as ices with their small sublimation energy, mass diffusion is essential at T close to sublimation temperature. The first particles to be mobilized are electrons, which radiatively react with positively charged species. At higher temperature atoms and other reactive intermediates start to diffuse, and their reactions also may give rise to a photon emission. In order to discriminate between these processes it is reasonable to combine optical and current activation spectroscopy techniques. The mechanism underlying TSEE involves release of electrons from trap promoting them to the conduction band. Then electrons could either recombine with positively charged ions yielding TSL or escape from the surface. In ices with negative electron affinity E_a (e.g. Ne, Ar) an electron in the conduction band will experience an increase of kinetic energy when it exits from the sample surface. In ices with positive E_a (e.g. O_2, N_2O) electron should get enough energy to overcome the potential barrier at the surface and leave the ice to be detected with an electrode of positive potential fixed near the sample. If an electron has a large escape depth one can expect to get information about both kind of traps—surface traps and the bulk ones. For example the TSEE active layer estimated for Ar film (Savchenko et al. 2007) appeared to be ~1000 nm in agreement with a large electron escape depth (500 nm) found by Gullikson (1988). Analysis of TSEE provides also the information on electrostatic charging of irradiated ice, distribution of electron traps (Frankowski et al. 2004; Savchenko et al. 2011) and phase transitions (Khyzhniy et al. 2010). In view of the competition of relaxation channels terminating in TSEE and TSL it is clear that the contemporary use of both technique is preferable.

7.2 Selected Results Obtained

Luminescence spectra monitoring under electron beam combined with analysis of TSL and TSEE enabled us to reveal radiation-induced defect production in rare gas ices, to propose the mechanisms of their formation via electronic excitations and ascertain their atomic configuration (Savchenko et al. 2009).

Interesting results on relaxation processes in electron-irradiated Ar ices doped with O_2 were obtained using spectrally resolved TSL technique (Savchenko et al. 2006, 2011). Two heating modes were used: linear heating at a constant rate of 3.2 K/min and step-wise heating of the samples with a step of 2 K and a 20 min interval between successive steps. Figure 23 shows the yield of TSL in the VUV M-band stemmed from Ar_2^+ neutralization.

The reported results evidence a nonmonotonic background between 17 and 25 K. After each temperature step the intensity of VUV TSL does not reach its zero level. This because of the chemiluminescence (often also called TSL) of oxygen as reported in the inset of the same figure. The chemiluminescence was detected at the wavelength of the (0–10) band of the vibrational progression $C_3\Delta u \rightarrow X^3\Sigma_g^-$ of O_2^*. The background maximum and the maximum of O_2^* chemiluminescence are in close agreement. Note that in the experiments performed with nominally pure Ar samples such an effect was absent (Ponomaryov et al. 2007). These experiments explained a puzzling origin of the broad 22 K peak in thermally stimulated yields of photons and electrons which was under discussion over 15 years. Recently obtained new data (Gumenchuk et al. 2009; Savchenko et al. 2010b, 2011) provide support to the long-range radiation mechanism of relaxation triggering in pre-irradiated ices.

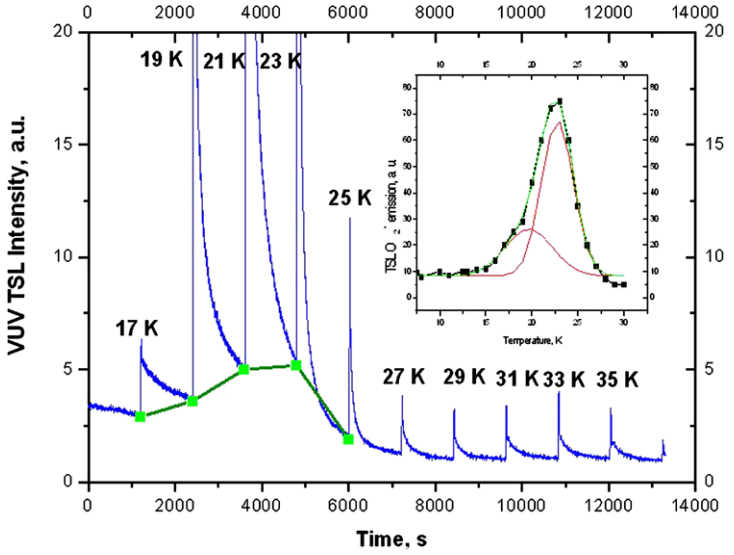

Fig. 23 The VUV TSL glow curve was taken from the oxygen-containing Ar film (0.1 % O_2) deposited at 17 K to "clean" the curve by removing the low-temperature peaks and thereafter irradiated with 500 eV electrons. Thermally stimulated chemiluminescence of oxygen is shown in the *inset*

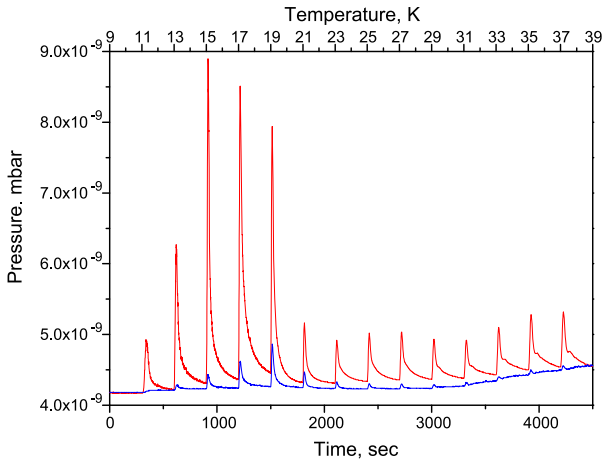

Fig. 24 Pressure curves taken from unirradiated Kr (*blue curve*) and from Kr film pre-irradiated with a 500 eV electron beam of 30 μA/cm^2 current density during 30 min (*red curve*). Temperature was changed by steps of 2 K

Synchronous detection of three relaxation emissions: TSL, TSEE and P revealed a new phenomenon in atomic ices—anomalous low temperature post-irradiation desorption ALTpD (Savchenko et al. 2005, 2010c, 2012; Ponomaryov et al. 2007). ALTpD was observed upon warming-up of the pre-irradiated samples at $T \ll T_{sb}$ (T_{sb} is the sublimation temperature). The radiative origin of the ALTpD was demonstrated by comparison of pressure behavior detected from irradiated and unirradiated films as exemplified for Kr in Fig. 24. It is found that the ALTpD correlates with the yield of TSEE and TSL stemmed from the intrinsic charge recombination reaction pointing to a common primary process triggering the relaxation cascades—thermally stimulated electron detrapping (Fig. 24).

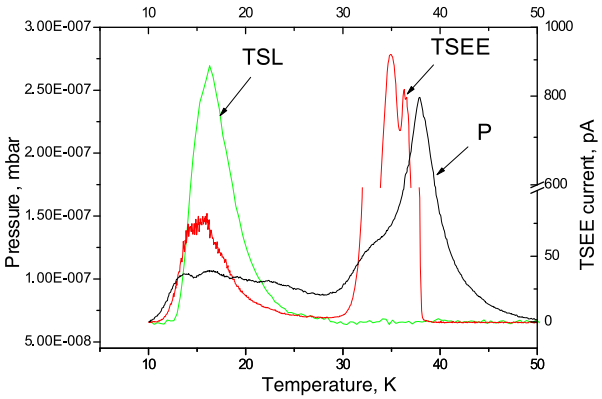

Fig. 25 Yields of the TSL, TSEE current and pressure curve P taken from pre-irradiated nitrogen ice

The ALTpD proceeds in two steps: (i) the release of electrons from their traps and (ii) a subsequent recombination of electrons with self-trapped holes (molecular ions Kr_2^+) terminated in the excimer Kr_2^* states. After radiative transition to a repulsive part of the ground state potential the excess energy (0.87 eV) is shared between two excimer atoms. It causes a creation of the two "hot" Kr atoms near the surface with a 0.43 eV kinetic energy available for desorption. The second stage of the scenario coincides with the suggested one for the case of desorption induced by electronic transition DIET under excitation (Johnson and Schou 1993).

7.3 Future Study

We plan to extend the study of relaxation processes on molecular ices irradiated by electron beams. First preliminary results on "post-desorption" from pre-irradiated α-phase nitrogen ices are obtained. They show existence of ALTpD at temperature of about 15 K. The "post-desorption" increases in the temperature range, where yields of TSEE and TSL exhibit maxima (Fig. 25).

We intend to elucidate which reactions stimulate the ALTpD from nitrogen ices. Closely related topic of interest is the formation of ionic species in solid nitrogen under ionizing radiation. Results of our current study of luminescence and TSL of α-phase nitrogen in VUV range suggest formation of tetranitrogen cation N_4^+. In other words self-trapping of holes. Investigation of possible reactions involving charged species is the next task of our experiments. The study directed to elucidation of electronic and atomic processes in molecular ices (CO, CO_2, NO, N_2O etc.) and their mixtures is also scheduled. We plan to perform experiments on photoluminescence using the original VUV source based on rare-gas solid films as described in Sect. 7.1.

8 Laser Induced Fluorescence on PAHs/Ice Mixtures

Main contributors: authors at JPL

Laboratory fluorescence/phosphorescence spectroscopy of ices date back several decades (Prince et al. 1976), where the authors observed fluorescence of OH radicals produced by electron bombardment in ice at 77 K. While terrestrial applications also took early developments (Bolshov et al. 1989) using laser-induced-fluorescence (LIF) of atomic (Pb

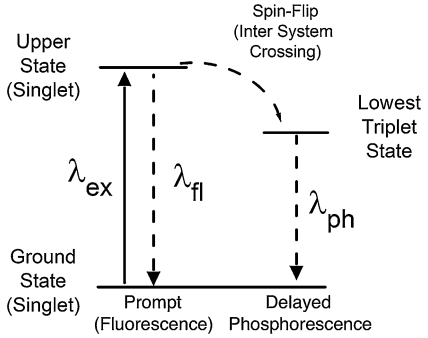

Fig. 26 Fundamentals of fluorescence and phosphorescence of an atom or molecule. When the excitation source is a monochromatic laser, the technique is called Laser Induced Fluorescence (LIF). The spin multiplicity of most of the closed-shell molecules is singlet in the ground state, while open-shell atoms and radicals possess spin multiplicity of doublet, triplet or higher multiplets. Fluorescence occurs between the states of same spin multiplicity whereas phosphorescence involves change of spin multiplicity. Fluorescence and phosphorescence are also generally called a luminescence (emission of light)

and other anthropogenic contaminants) species in Antarctic ice, application of LIF to astrophysical ices containing organic materials had only gained momentum in early 2000s, subsequent to the work by Gudipati and Allamandola of polycyclic aromatic hydrocarbons (PAHs) quantifying the spectroscopic properties and matrix-effect (Gudipati 2004; Gudipati and Allamandola 2003). Earlier reports on LIF of PAHs involve excited-state-proton-transfer (ESPT) between 2-Naphthol hydrogen bonding with ice matrix in H_2O and D_2O ices (Akiyama et al. 1997).

Mid-infrared region is strongly dominated by ice and silicate features, leaving room only for species with significant absorption or concentration. For this reason, early 2000s efforts were put in utilizing "transparent" spectral regions in the UV-VIS of ice to study and understand the chemical evolution of organic molecules in astrophysical ices. Using PAHs as probes, "optical spectroscopy of astrophysical ice analogs" lead to the discovery of ionization and stabilization of PAH radical cations in ices (Gudipati 2004; Gudipati and Allamandola 2003, 2004, 2006a), followed by detailed kinetics and identification of new species (Bouwman et al. 2009, 2010, 2011a, 2011b; Cuylle et al. 2012a).

8.1 The Technique

Laser induced fluorescence is a commonly used technique to study the fluorescence and the lifetime of molecules of interest, whether in the gas-phase, liquid, or solid-state. Typically, a UV laser pulse (nanoseconods to picoseconds pulsewidth) is fired on to the sample, causing resonant electronic absorption in an atom or a molecule (Fig. 26), which promptly emits photons (fluorescence) or after intersystem crossing results in change of spin, followed by delayed emission of photons (phosphorescence). Fluorescence is typically in picoseconds (ps) to nanoseconds (ns) lifetime, whereas phosphorescence lives for several microseconds to seconds. It would be necessary to focus the laser for non-linear processes such as multi-photon excitations.

At the Ice Spectroscopy Laboratory (ISL) of JPL, nanosecond pulsed (about 5 ns) lasers at 10 to 20 Hz repetition rate are used as excitation sources. These include a compact Optical Parametric Oscillator (OPO) that can be tuned between 210 nm and 700 nm as well as the higher harmonics of Nd-YAG laser (532 nm, 355 nm, 266 nm, and 213 nm). Ices are

prepared at a wide variety of temperatures (5 K–160 K) and impurity composition (PAHs, CO_2, O_2, etc.). Fluorescence is collected at 45–90 degrees rom the excitation laser using a 25 mm biconvex lens placed at about 50 mm from the ice probe. Focused fluorescence is transported through an optical fiber to a spectrometer. Fluorescence can be measured in steady state or time-resolved modes ranging from nanoseconds to several milliseconds time-resolution.

8.2 Results

Water-ice is one of the most fascinating system, everywhere in the Universe, where temperatures are low and molecular number density is high—from interstellar medium (Smith et al. 1994) to the surface and interior of Earth under pressure at several km depths of arctic ice sheets (Price et al. 2002) spanning from ∼10 K to several hundred K (273–220 K). Similarly, water-ice exists in over 10 different phases (Malenkov 2009; Bartels-Rausch et al. 2012).

However, in astrophysical context, interstellar medium, circumstellar matter, or outer rims of protoplanetary discs—all these regions are known to be dominated by amorphous water-ice containing other impurities (Tielens et al. 1983). Thus, studying LIF properties of various impurity molecules in astrophysical ices such as CO, CO_2, NH_3, CH_3OH, PAHs, and their radiation products such as H, OH, O, NH, CH, C, etc., will be important to improve our understanding of chemical evolution of these ices. So far we have only tentative understanding on OH radicals in ice.

Earlier work on luminescence from radiation processes of pure water-ices were reported by Quickenden and coworkers (Langford et al. 2000; Quickenden et al. 1982; Selby et al. 2006), whereby identification of luminescent species were tentatively identified as OH radicals, strongly bonded with surrounding water molecules, due to which the spectral bands are considerably shifted. Recently, similar emission was observed when ice was bombarded with charged particles (Lee et al. 2009), or gamma rays (Yada et al. 2002).

One of the main issues in understanding the luminescence of the photoproducts of water ice (OH in particular) was the severe perturbation of its excited state behavior by the ice matrix. In fact, this was the general understanding about the optical properties of impurities embedded in ice matrix—that their spectra will be severely distorted. Further, due to the fact that amorphous ice is optically opaque and strongly scattering, optical or LIF spectroscopic studies were not common until recently, when Gudipati and Allamandola (Gudipati and Allamandola 2003; Gudipati et al. 2003) showed that thin ice films can be utilized to quantitatively study both optical absorption as well as LIF spectroscopic properties of embedded organic molecules such as PAHs. Surprising finding was that the spectroscopic signatures of PAHs such as naphthalene ($C_{10}H_8$), pyrene ($C_{16}H_{10}$), etc., in amorphous ice matrices were very similar to those observed when these PAHs were trapped in rare-gas matrices such as Ar (Gudipati 2004). Water-ice behaving like rare-gas matrices at astrophysical temperatures has a tremendous advantage in terms of identifying molecular species both in optical absorption spectroscopy as well as LIF spectroscopy. In fact, utilizing these properties, UV induced photoionization of naphthalene in water ice has been quantified and the formation mechanism of hydroxylated naphthalene (1-naphthol), whose LIF spectra were in excellent agreement with those observed in supersonic expansion LIF studies, has been deduced (Gudipati 2004).

Amorphous water-ice at very low temperatures behaves like Ar in terms of its static dielectric constant (ϵ close to 1) on the embedded molecules such as PAHs, except when strong electronic interactions dominate solute-solvent interactions as in the case of OH in

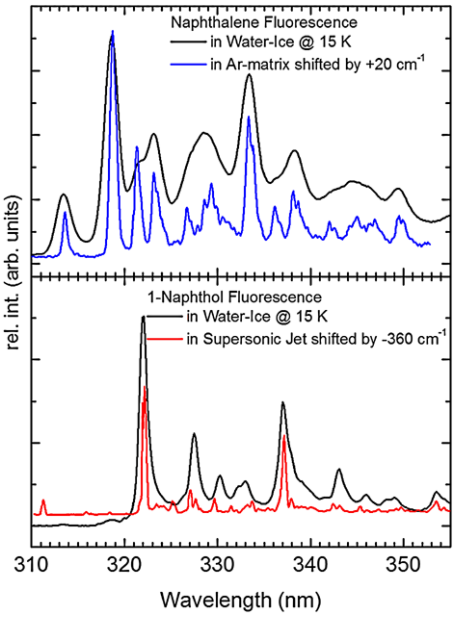

Fig. 27 (*Top*) Fluorescence from naphthalene ($C_{10}H_8$) trapped in ice (*black*) and in Ar matrix (*blue*) shifted by 20 cm^{-1}. (*Bottom*) Fluorescence from 1-naphthol that is formed subsequent to UV-irradiation of naphthalene trapped in ice (*black*) and measured in a supersonic jet expansion (*red*) shifted by -360 cm^{-1}. A general broadening of fluorescence bands in water-ice can be noticed compared to Ar matrix or supersonic jet. This behavior is due to inhomogeneous nature of amorphous ice matrix, which may get narrower in crystalline ice (to be studied systematically)

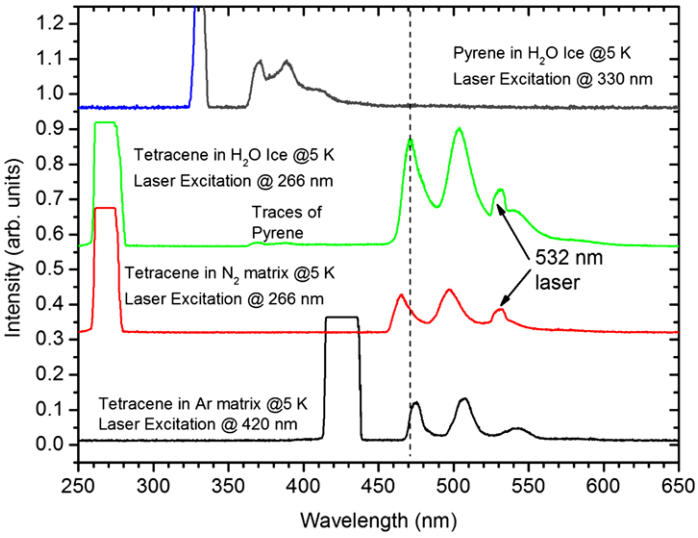

Fig. 28 Laser induced fluorescence (LIF) spectra of pyrene ($C_{16}H_{10}$) and tetracene ($C_{18}H_{12}$) trapped in H_2O ice as well as in N_2 and Ar matrices at 5 K. Matrix-shift of ice is minimal when compared to nitrogen and argon matrices, falling between these two. Scattering due to excitation laser as well as 532 nm laser in studies using 266 nm excitation are also seen in the spectra

ice. For this reason, matrix-shifts are observed to be very small for PAHs, as can be seen in Fig. 27. Recently we conducted LIF studies of tetracene ($C_{18}H_{12}$) in nitrogen, argon, and ice matrices at 5 K. As can be seen in Fig. 28, the spectral shifts in the LIF spectra of tetracene are very small, with water ice falling between N_2 and Ar matrix-shifts. For example, the 0–0

line of fluorescence has maximum in H_2O-ice at 471 nm, whereas in N_2 matrix at 465 nm, and in Ar matrix at 475 nm. On the other hand, pyrene 0–0 fluorescence occurs at 371 nm both in Ar matrix (Gudipati et al. 1993) as well as in H_2O ice, as seen in the top spectrum of Fig. 28. In the gas-phase absorption for the $S_1S_0(0–0)$ transition in tetracene occurs at 446.5 nm, which shifts steadily to longer wavelengths when surrounded by Ne, H_2, and Ar clusters (at ∼462 nm) (Kuma et al. 2011). Based on these observations, H_2O matrix behaves very similar to Ar or N_2 matrices in influencing the LIF spectral properties of PAH molecules trapped in amorphous ices—analogs of interstellar ices.

Ice being in solid-state for a wide-range of temperatures in vacuum (<160 K), this unique property could be taken into advantage to study fluorescence and phosphorescence of organics through LIF. Such a study has recently been conducted by Johnson et al. (2011) using NeCu laser at 248.6 nm excitation. These studies on substituted benzenes showed that fluorescence remains unaffected and phosphorescence decreases with increasing temperature from 20 K to 140 K, which is in agreement with similar observations in rare-gas or Spolski matrices (Gudipati 1992, 1994).

8.3 Future Work

LIF is a very sensitive technique to probe the chemical processes occurring in astrophysical ice analogs in the laboratory. While LIF of PAHs behaves very similar in ice, Ar, and N_2 matrices, significant changes in fluorescence spectra are seen for small molecules such as OH. However, we do not have significantly large data set of small oxygen, nitrogen, and carbon containing molecules such as O, NH, CH, etc. In the future it would be important to conduct these studies systematically in the laboratory. Another important aspect that also needs systematic study is the effect of amorphous vs. crystalline ice on the LIF spectral properties of embedded species in astrophysical ice analogs.

Luminescence (fluorescence and phosphorescence) of atoms and molecules embedded in ice is an emerging filed of laboratory astrophysics that is yet to be fully explored. This technique, using modern high-power and compact lasers, will become a complementary technique to other methods such as Raman spectroscopy for in-situ detection of organics (in particular aromatic species) for future solar system exploration missions. For interstellar and circumstellar ices, LIF would be a powerful complementary laboratory technique to other methods such as infrared, ultraviolet, and mass spectroscopic techniques to obtain information on the processes that occur in ices. For example, IR does not detect atoms or diatomics such as O_2, N_2, etc., whereas, vacuum UV is necessary to see these species in electronic spectra. Only mass spectroscopy could detect these molecules, but with appropriate excitation light source, luminescence spectroscopy could complement mass spectroscopy to detect these molecules.

9 Raman Spectroscopy of Ion Bombarded Solid Phase Molecules

Main contributors: authors at Catania Observatory

9.1 Experimental Apparatus

The Raman effect is an inelastic scattering of light first discovered in liquids by Sir Chandrasekhara Venkata Raman and Kariamanickam Srinivasa Krishnan (Raman and Krishnan 1928). Examples of Raman spectra of sulfur at different temperatures, are given in Fig. 29.

In situ Raman spectroscopy of ion irradiated frozen ices is carried out at the Laboratorio di Astrofisica Sperimentale (LASp) of the INAF-Osservatorio Astrofisico di Catania. A schematic view of the experimental apparatus is reported in Fig. 30. The in situ analysis are performed within an UHV chamber where the pressure is kept below 10^{-8} mbar, a substrate (crystalline silicon) is placed in thermal contact with a cold finger whose temperature can be varied between 10 K and 300 K. The vacuum chamber is interfaced with an ion implanter (200 kV; Danfysik) from which ions with energy up to 200 keV (400 keV for double ionizations) can be obtained. The ion beam produces a 2×2 cm^2 spot on the target and currents in the range of 100 nA/cm^2 to a few μA/cm^2 to avoid macroscopic heating of the sample. In order to prepare icy samples, a needle valve is used to admit pre-prepared gases (or mixtures) into the chamber, where they freeze on the substrate. A He–Ne laser can be used to measure the refractive index and to monitor the thickness of the ice film during accretion; this is achieved by looking at the interference pattern (intensity versus time) given by the laser beam reflected at an angle of 45° by the vacuum-film and film-substrate interfaces (see Westley et al. 1998; Baratta and Palumbo 1998, for further details). In situ Raman spectra can be acquired by using two different set-up that use visible (514.5 nm) and near infrared (785 nm) laser excitation. In the first set up, a Triplemate spectrometer by SPEX equipped with a Peltier cooled CCD detector is used. A continuous Ar-ion laser beam ($\lambda = 514$ nm) enters a confocal illuminator by DILOR, perpendicularly to its optical axis, into which it is deflected by a microprism. The confocal optical system is arranged in such a way that any parallel beam incident along the optical axis in the opposite direction of the laser is focused onto the entrance slit of the spectrometer. By means of two flat mirrors, the laser beam is reflected towards the vacuum chamber and focused by an objective lens into a 40 μm spot on the sample. The back-scattered Raman light is collimated by the same objective into a parallel beam that, according to the setup geometry, goes back along the same path of the laser beam and reaches the confocal illuminator where it is focused onto the entrance slit of the spectrometer. Since the incoming laser and the Raman collected light are collimated into parallel beams, this configuration allows to acquire Raman spectra up to several meters far from the spectrometer, with negligible performance loss.

The second, near infrared, set up uses an optical fiber based compact monocromator HE785 by HORIBA. The fast spectrometer has a fixed objective grating and is equipped with a Peltier cooled CCD detector. The probe head has a confocal optical configuration and is oriented directly toward the objective lens of the chamber. The optical path of the incoming laser beam that emerges from the head, and the collected Raman beam is analogous to that already described for the "visible" system. A solid state CW (continuous wave) 785 nm laser diode is used as exciting source. The near infrared excitation allows to significantly decrease the strong fluorescence continuum usually observed in carbon containing molecular ices irradiated at low doses, when using visible laser excitation (see Ferini et al. 2004). Although the Raman features are relatively $(785\ \text{nm}/514.5\ \text{nm})^4 = 5.4$ times less intense with respect to the 514.5 nm excitation, this set-up is particularly useful when searching for weak features of species formed by ion bombardment. A strong fluorescence continuum can indeed totally mask weak features.

A critical parameter to consider while performing simulation experiments on molecular ices, is the temperature of the ice sample. Many physical processes like condensation, sublimation, crystallization etc. strongly depend on temperature. Hence the application of the experimental results to astrophysical environments need a reliable measurement of the sample temperature. Raman spectroscopy gives a valid tool for measuring the temperature of the ice sample remotely. As an example Fig. 29 shows the Raman spectra of a Sulphur pellet acquired at different temperatures and Fig. 31 shows the anti-Stokes to Stokes ra-

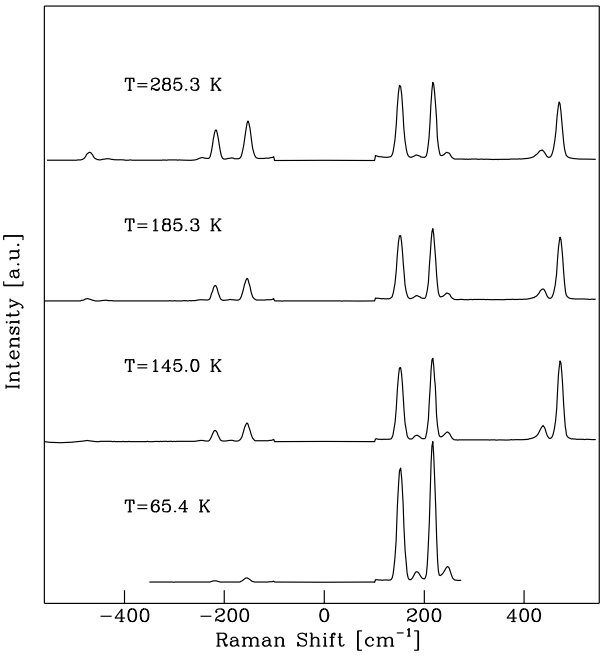

Fig. 29 Raman spectra ($\lambda_L = 514.5$ nm) of a sulfur pellet acquired at different temperatures under vacuum

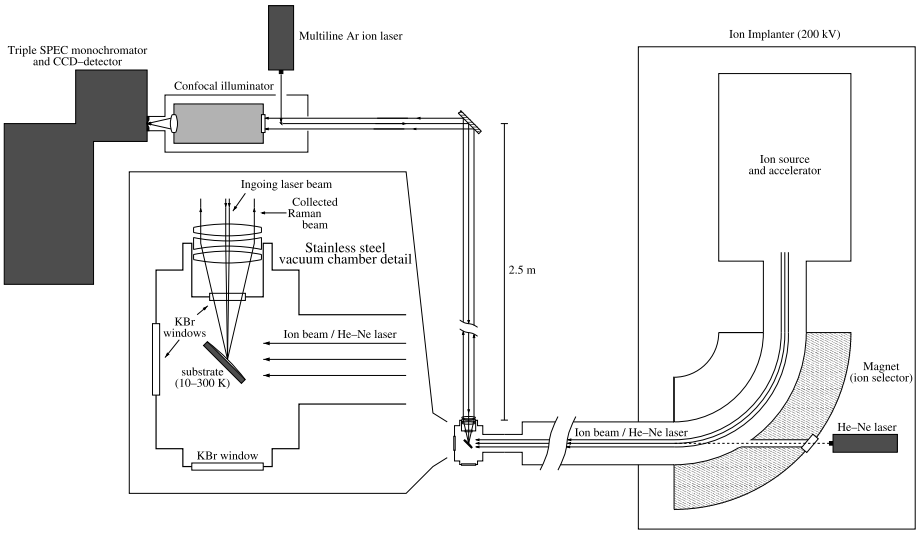

Fig. 30 Schematic view of the experimental apparatus used to acquire in situ Raman spectra of ion irradiated frozen ices at INAF-Catania

tios measured from the spectra together with the best fit temperatures obtained by using Eq. (1).

$$\frac{I_{AS}}{I_S} = \frac{(\nu_0 + \nu_v)^4}{(\nu_0 - \nu_v)^4} e^{-\frac{h\nu_v}{kT}} \tag{1}$$

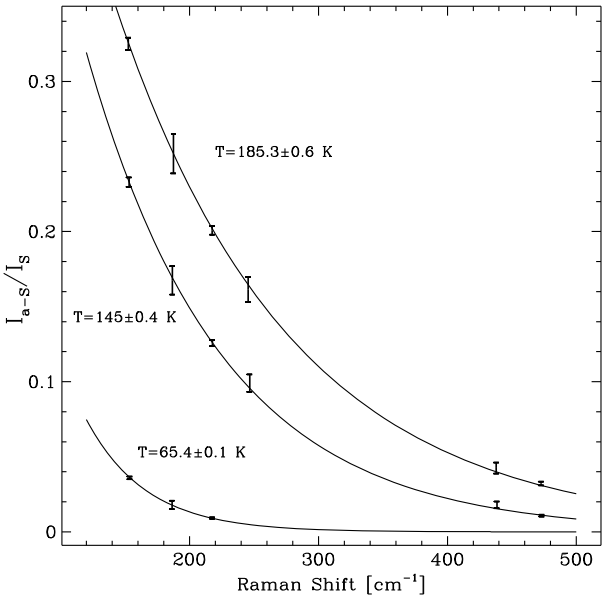

Fig. 31 Theoretical best fit of the anti-Stokes to Stokes ratio measured for the spectra reported in Fig. 29

We have checked that the temperatures given by the diode sensor on the cryostat controller are within 1 K with respect to that computed trough Eq. (1).

9.2 Results

Infrared and Raman spectroscopies are two powerful and complementary tools to study the physical and chemical properties of icy samples. In particular, it is possible to identify molecular groups and specific molecules by infrared (IR) spectroscopy. Raman spectroscopy gives further information on the structural properties of the sample and is often used to study the effects of ion induced lattice damage in carbonaceous solids (e.g., Elman et al. 1981; Strazzulla and Baratta 1992; Baratta et al. 1996; Kalish et al. 1999; Strazzulla et al. 2001; Costantini et al. 2002).

Figure 32 shows the infrared and Raman spectra of a H_2O:CH_4:N_2 mixture at 12 K. Since a molecule can have infrared active transitions which are not Raman-active (or extremely weak) and vice versa (because of the different selection rules), some features present in the IR spectrum are absent in the Raman spectrum. For example, water bands, very intense in the IR spectrum of thin icy films, cannot be easily observed in the Raman spectrum (because of the small cross-section), while the opposite is the case for the symmetric modes of mono- and poly-nuclear molecules such as N_2 and CH_4 (which are IR-inactive).

It is well known that when fast ions impinge on an icy sample, many molecular bonds are broken, and fragments are formed along the ion track which recombine giving rise to molecular species not present in the original sample. Beyond the chemical modifications, ion irradiation drives a gradual alteration of the sample structure, causing a rearrangement of the atoms in their lattice sites and a thorough modification of the optical properties of the ice. Raman spectroscopy is a powerful tool for monitoring structural changes.

Table 1 gives a list of ion bombarded solid samples analyzed by “in situ” Raman spectroscopy. Ion bombardment of simple C-bearing ice mixtures causes the formation of volatile species and of a refractory residue (e.g., Strazzulla et al. 2001; Sicilia et al. 2012).

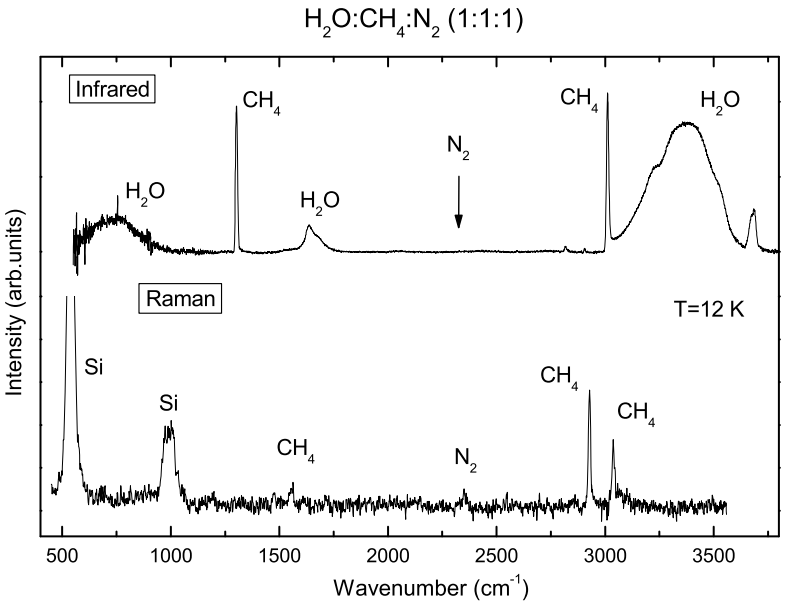

Fig. 32 Infrared and Raman spectra ($\lambda_L = 514.5$ nm) of a H_2O:CH_4:N_2 mixture at 12 K. The arrow in the IR spectrum indicates the position of the N≡N symmetric stretching mode, which is IR inactive

Table 1 Ion bombarded solid samples analyzed by "in situ" Raman spectroscopy

Sample	T (K)	Ion (energy)	λ (nm)	Reference
C_6H_6	77	He^+ (3 keV)	514.5	Strazzulla and Baratta (1992)
C_4H_{10}	10	He^+ (3 keV)	514.5	Strazzulla and Baratta (1992)
$C_{22}H_{14}$ (pentacene)	300	He^+ (3 keV)	514.5	Cannia et al. (1994)
C_{60} (fullerene)	300	He^+ (30 keV)	514.5	Cataldo et al. (2002)
C_{70} (fullerene)	300	He^+ (30 keV)	514.5	Cataldo et al. (2003)
CH_4	12	He^+ (30 keV)	514.5	Ferini et al. (2004)
CH_3OH:N_2 = 1:2	12	He^+ (30 keV)	514.5	Ferini et al. (2004)
CH_3OH:N_2 = 1:2	12	Ar^{++} (60 keV)	514.5	Ferini et al. (2004)
H_2O:CH_4:N_2 = 1:6:3	12	He^+ (30 keV)	514.5	Ferini et al. (2004)
C_2H_2	16	H^+ (200 keV)	785	Compagnini et al. (2009)
C_2H_4	16	H^+ (200 keV)	785	Compagnini et al. (2009)
C_2H_6	16	H^+ (200 keV)	785	Compagnini et al. (2009)

Figure 33 shows the Raman spectra of C_2H_2 (acetylene) as deposited at 16 K, after ion bombardment at 16 K with 200 keV H^+ ions and after annealing at 110 K. Spectra are acquired using a 785 nm excitation wavelength.

After ion bombardment, the Raman spectrum shows new bands which indicate the formation of molecular species not present in the original sample and an intense fluorescence continuum appears, typical of disordered polymer-like carbons containing a relatively large quantity of hydrogen, and due to radiative recombination of electron-hole pairs. When high bombardment doses are reached, a broad band appears near 1560 cm^{-1} which is attributed

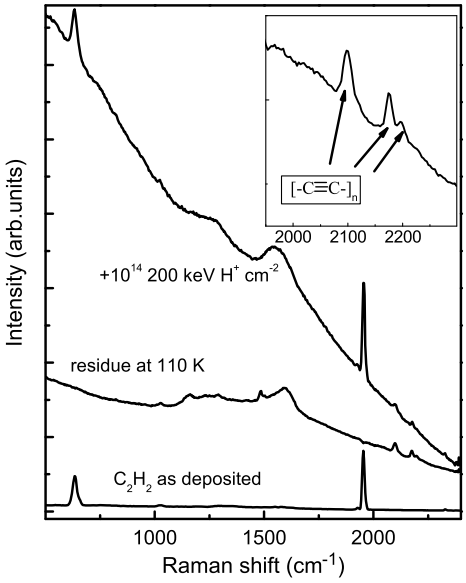

Fig. 33 Raman spectra ($\lambda_L = 785$ nm) of C_2H_2 before and after bombardment with 200 keV H^+ at 16 K. The spectrum of the sample after in situ annealing at 110 K is also shown. In the *inset* the annealed spectrum in the 2000–2200 cm^{-1} spectral region is shown

to the C=C stretching vibration of amorphous carbon (G line). Furthermore new bands are present at 2100, 2170 and 2190 cm^{-1} which are attributed to the formation of linear carbon chains (8–10 carbon atoms). The line width of these features is small, indicating that the chains are of well-defined lengths and that they are probably isolated into the rest of the ice matrix. The carbon chains features are even more evident when the sample is annealed at 110 K because of the reduction of the fluorescence background and the disappearance of the acetylene signals because of sublimation (Compagnini et al. 2009). It is worth mentioning that the detection of these species would not be straightforward by infrared spectroscopy.

9.3 Future Experiments

Compagnini et al. (2009) have shown for the first time that ion irradiation of solid hydrocarbons (namely C_2H_2, C_2H_4, and C_2H_6) leads to the formation of sp-hybridized carbon nanowires (polyynes) with well definite lengths. The physics and chemistry of carbon nanowires is actually a challenging topic in carbon science. They are linear chains of carbon atom pairs with alternating single and triple bonds and represent unique, truly one-dimensional molecular systems with intriguing optical and electronic properties. Polyynes are also molecules of interest in astrochemistry. Polyynes (as well as cyanopolyynes) have been detected in different astrophysical environments such as the atmosphere of Titan, the atmospheres of Uranus and Saturn, in dense molecular clouds, and along the line of sight of late type stars. These detections refer to species in the gas phase. However it is largely accepted, that many complex molecules are formed after energetic processing in the solid phase and are released to the gas phase after desorption of frozen species. In order to investigate the role of energetic processing in the formation of complex species in space, we plan to further study the formation of polyynes (and cyanopolyynes) by ion irradiation of relevant hydrocarbons and mixtures.

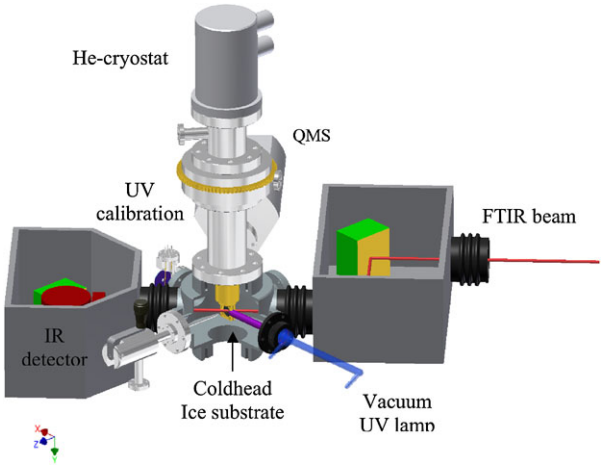

Fig. 34 A 3D schematic representation of CRYOPAD in FT-IR transmission modus

10 CRYOPAD and OASIS—Shining Light on Interstellar Ice Analogues

Main contributors: authors in Leiden Observatory

In this paragraph the focus is on processes taking place upon UV irradiation of interstellar ice analogues: photo-desorption, photo-dissociation, and photo-chemistry, and both smaller (CRYOPAD) and larger (OASIS) precursor species are considered. The experiments mimic the interstellar radiation field (ISRF) that results in a background UV field of about 10^8 photons $cm^{-2}\,s^{-1}$. This UV field is enhanced by orders of magnitude close to young stellar objects and even in environments protected from external UV light (e.g., in cloud cores and disk midplanes) cosmic rays can interact with hydrogen inducing Ly-α emission at 10.2 eV (121.6 nm). Laboratory studies of UV irradiated interstellar ice analogues are astronomically important. UV excitation of ice constituents provides a non-thermal desorption mechanism that may explain gas phase observations of species at temperatures below their accretion value. Molecules can also dissociate upon irradiation and recombination of radical fragments will lead to the formation of more complex species, providing pathways towards molecular complexity in space. These processes depend on many different parameters (ice composition, and morphology, temperature, flux, etc.) that can be studied under fully controlled conditions in the laboratory. Moreover the underlying molecular processes may be wavelength dependent.

10.1 CRYOPAD (CRYOgenic Photoproduct Analysis Device)

10.1.1 Experimental Details

CRYOPAD is an ultra-high vacuum (UHV) setup operating at the laboratory in Leiden and comprising one central vacuum chamber with typical base pressures lower than 10^{-10} mbar. The setup has been described in detail before (Fuchs et al. 2006; Öberg et al. 2009d) and here only the main characteristics are summarized. A schematic is shown in Fig. 34. CRYOPAD has been constructed to study the interaction of UV light with interstellar ice analogues. These are grown with monolayer (ML) precision at thicknesses between a few up to a few hundred MLs by exposing a cold gold substrate at the center of a central vacuum chamber to a steady flow of gas, directed along the surface normal. The used gases have very

high purity levels and in order to exclude the influence of possible background pollution isotopes can be used. The substrate is mounted on top of a closed cycle He cryostat generating temperatures that are controlled between 12 and 200 K, using a Lakeshore temperature controller and a set of thermo-couples mounted on top and close to the sample holder. Light of a special microwave powered H_2 discharge lamp is directed towards the ice (Muñoz Caro and Schutte 2003). The lamp consists of a flow tube clamped in a McCarroll cavity and emits mainly Ly-α radiation around 121.6 nm and, with less intensity ($\sim$20 %), a band centered around 160 nm. The cavity is excited by a Sairem or Opthos Instruments MW power supply (100 W, 2450 MHz). The H_2 pressure in the lamp is maintained at about 0.4 mbar. This results in a vacuum UV photon flux of 10^{14}–10^{15} photons/cm^2 s at the ice sample. This system is used in several laboratories around the world to simulate spectral distribution of the UV interstellar radiation field (Muñoz Caro et al. 2010; Bernstein et al. 2002; Ciesla and Sandford 2012). In the remaining of this chapter the lamp will be described as a Ly-α source though this is formally not fully correct. The flux is calibrated against a NIST silicate photodiode. The UV induced ice processes are studied in two complementary ways. The light of a Fourier transform infrared spectrometer (600–4000 cm^{-1}, 0.5 cm^{-1} band width) is guided through the ice in a reflection-absorption mode (FT-RAIRS) onto a liquid nitrogen cooled InSb/MCT infrared detector. Alternatively, also transmission spectroscopy can be used, replacing the gold surface by an infrared transparent window. Absorption signals are used to identify (new) species in the ice and to quantify changing ice compositions during irradiation, as signal strengths can be translated into absolute number densities. TPD (Temperature Programmed Desorption) is a complementary analytical tool to identify ice photoproducts. In a TPD experiment, ice evaporation is induced by linear heating (i.e., 0.5 to 4 K min^{-1}) of the ice and evaporated gas phase molecules are detected by a quadrupole mass spectrometer (QMS). TPD curves depend on the evaporation energy of the ice and this parameter is known for most investigated ice species. In more complex ices other effects such as mixing and segregation are also at play (Öberg et al. 2009a). The QMS software allows for the simultaneous detection of up to 60 different mass/charge (m/z) values. TPD and RAIRS experiments are performed at the same time in order to facilitate mass or spectral assignment. The ice thickness is determined (approximately) by choosing the appropriate deposition pressure and deposition time and is confirmed with 1 ML precision or better via an iso-thermal desorption experiment (Fuchs et al. 2009). Also, for ice thicknesses up to $\sim$20 ML the integrated RAIRS area is linearly correlated with the ice layer thickness and can be used as an additional tool. The latter method, however, is not accurate for thicker ices and does not work for infrared inactive species.

CRYOPAD has been extensively used to study the photo-desorption and photo-chemistry of interstellar ices upon vacuum UV irradiation (Linnartz et al. 2011). A few highlights are summarized in the results section.

10.1.2 Results

Upon Ly-α irradiation CO ice photodesorbs non-dissociatively (Öberg et al. 2007, 2009d). This process is illustrated in Fig. 35A. Here the decreasing CO RAIRS signal is shown as a function of irradiation time. The RAIRS signal can be translated into a number density, and the loss of CO absorption signal, therefore can be converted into a photodesorption yield, as the UV flux at the ice surface is known. For pure CO ice this yields a value of about 3×10^{-3} desorbed molecules per incident UV photon. Experiments on pure CO_2, H_2O and CH_3OH ice show that these molecules not only photo-desorb, but also dissociate upon UV irradiation (Öberg et al. 2009b, 2009c, 2009d). If the resulting fragments are in the surface

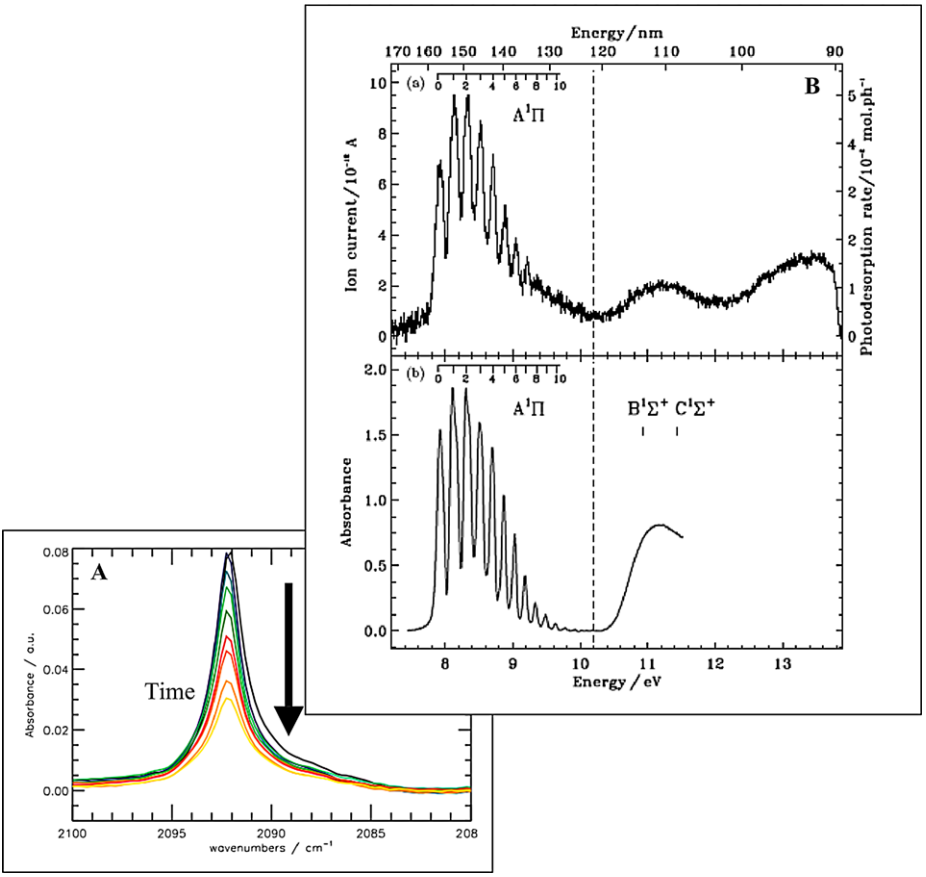

Fig. 35 *Panel A* shows the decreasing strength of the ^{13}CO fundamental as function of UV irradiation time (i.e., fluence), using a H_2 microwave discharge lamp that emits around Ly-α. *Panel B* shows the photo-desorption rate measured for different wavelengths (using the Synchrotron facility DESIRS/SOLEIL). The desorption efficiency follows the CO rovibronic absorption profile. See Öberg et al. (2007) and Fayolle et al. (2011)

layers, they either desorb directly from the excess energy provided by the photon or react with other radicals, which may still result in indirect photodesorption due to the release of energy. If the dissociated fragments remain in the ice mantle, the radicals can either become frozen in the ice matrix, diffuse through the ice to react with other radicals or recombine reforming the parent molecule. To constrain the photodesorption of the ice and thus determine the loss of precursor molecules into the gas phase rather than into photoproducts in the ice, a special method has to be used, described in detail by Öberg et al. (2009b). Photodesorption from a multilayer ice is a zeroth order process with respect to photon fluence, since it only depends on the amount of molecules in the surface layers. The photodesorption yield will not change with fluence as long as the original ice is sufficiently thick. Ice photolysis, however, is a first order process, since it depends on the total amount of ice. Through simultaneous modeling of the ice loss with an exponential decay and a linear function, the two physically different processes can be mathematically separated. This yields again effective photodesorption yields. For CO_2 and H_2O values of the order of 10^{-3} photon^{-1} are found,

and for CH_3OH the photodesorption yield is about twice as large. It should be noted that not only the UV field, but also the ice thickness, ice temperature, and temperature dependent mean-free-path of the excited molecule play a role. The photodesorption of N_2 ice has a yield that is at least an order of magnitude lower; N_2 is likely only to co-desorb with other molecules since it has no dipole-allowed transition within the energy range of the lamp. In order to investigate the wavelength dependent photo-desorption behavior of CO ice, similar experiments have been performed using SPICES (a sister-setup of CRYOPAD) at DESIRS, a tunable vacuum UV beamline at the synchrotron facility SOLEIL (Fayolle et al. 2011; Bertin et al. 2012). The wavelength dependent photo-desorption rate (also including the Ly-α value derived previously) is shown in Fig. 35B. Here, PSD (photon stimulated desorption) mass spectrometry is used to record ejected molecules. Depending on wavelength the value varies from about 4×10^{-3} molecules/photon (around 121 nm) to 5×10^{-2} molecules/photon. The value recorded at 10.2 eV is within the error margins in agreement with the value derived at CRYOPAD for the Ly-α lamp. This means that on average about 250 Ly-α photons are required to kick-out one CO-molecule, whereas for lower energies, around 8.5 eV, this efficiency increases to about 50 photons. In the ISM an icy dust grain is hit by roughly one photon/day, i.e., these rates yield ejection values of about 1 to 7 CO-molecules per year. The lower diagram shows the CO absorption curve and the similarity with the recorded photodesorption spectrum is striking. Obviously, the desorption follows a so-called DIET mechanism: desorption induced by electronic transition. This means that depending on the vacuum UV absorption cross section, more or less energy is available for the actual desorption process. As CO is known to be the precursor of methanol upon H-atom addition reactions (Watanabe and Kouchi 2002; Fuchs et al. 2009), and methanol has been found to be a good precursor in the formation of complex species upon vacuum UV irradiation (Öberg et al. 2009b), this directly affects the efficiency with which organic compounds may be formed. Using layered ices, with ^{12}CO on top of ^{13}CO ice and vice versa, it was also shown that the CO photo-desorption mechanism is mainly restricted to the upper few ice layers (Bertin et al. 2012). As a consequence, the presence of other molecules in the ice will affect the outcome of the present findings, e.g., it is found that for CO hiding in the pores of a water matrix, the overall efficiency is much smaller (Bertin et al., in preparation).

The astronomically relevant consequence of this work and studies performed in other groups (Westley et al. 1995; Muñoz Caro et al. 2010) is that the UV photodesorption of ice provides a non-thermal process that explains why some species in space can be observed in the gas phase for temperatures below their accretion value (Bergin and Snell 2002).

UV light also triggers photo-chemical processes. In the past, but also more recently this was studied in a top-down approach (Muñoz Caro et al. 2002; Bernstein et al. 2002; Ciesla and Sandford 2012): an ice mixture comprising different components is irradiated and the residue is shown to comprise organic compounds. Nowadays, with laboratory astrophysicists having at their disposal UHV techniques, also bottom-up approaches have been realized. These have the advantage that individual reaction schemes can be studied in much more detail. In Öberg et al. (2009b) the UV induced photochemistry of pure CH_3OH ice has been studied. Upon irradiation several fragments form—CH_3, CH_3O, CH_2OH, OH—which can react to form larger molecules such as ethanol that recombines from CH_3 and CH_2OH. A full reaction scheme, composed along the observed radical fragments and end products, and based on gas phase data as well as chemical intuition is shown in Fig. 36. The striking outcome of this experiment is that many of the larger complex species identified in space, particularly hot cores, using radio-astronomy, are actually formed in the ice. Just very recently glycolaldehyde was observed in the neighborhood of a solar-like star

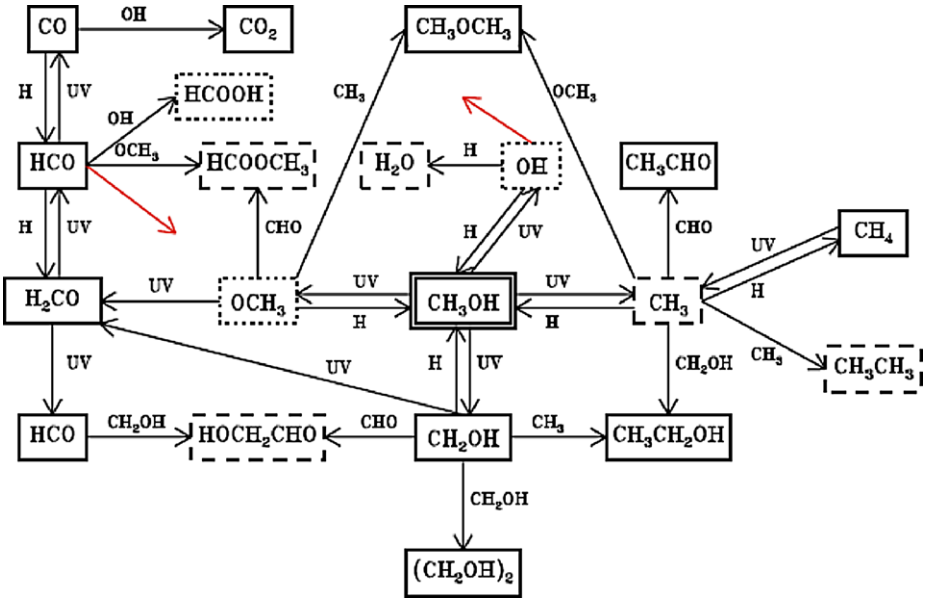

Fig. 36 The overall reaction scheme describing pathways upon UV irradiation of CH_3OH ice. The majority of the reaction products meanwhile has been identified in space. Taken from Öberg et al. (2009b)

(Jørgensen et al. 2012), using ALMA. Complementary TPD experiments further support identifications, since each product has a unique combination of mass signal and desorption temperature. The formation yields typically depend on ice temperature and ice composition as well as the UV flux and fluence. The role of the H_2O concentration on the photochemistry of more volatile species also has been studied (Öberg et al. 2009d). It was found, among others, that increasing the water concentration also increases the destruction efficiency of the volatile mixture constituent resulting in a substantially higher trapping efficiency of the formed radicals in the ice.

The formation of more complex species in this way is interesting since solid methanol has been observed towards a range of young stellar objects, including solar-type protostars. A UV driven methanol-ice chemistry may thus be a common pathway to chemical complexity in space. Complex molecule formation starting from methanol formation through CO hydrogenation and subsequent UV irradiation of methanol containing ices seems to provide a consistent reaction pathway for molecular complexity in space up to species with about 10 atoms. The presence of H_2O may be essential as a catalyst, although a recent study showed astronomical CH_3OH to be embedded in CO-rich (and H_2O-poor) ice, following a combined observational and laboratory study (Cuppen et al. 2011).

At this stage, it should also be noted that H-atom bombardment and UV irradiation are not the only possibilities to trigger chemical reactions in an ice for astronomical conditions. This is also discussed in other contributions of this manuscript. Many experimental efforts have been made to characterize surface reactions upon impacting H-atoms, e.g., in the formation of methanol (Watanabe and Kouchi 2002; Fuchs et al. 2009), water (Ioppolo et al. 2008, 2010, 2011; Miyauchi et al. 2008; Oba et al. 2009; Cuppen et al. 2010; Dulieu et al. 2010; Romanzin et al. 2011) and hydroxylamine (Congiu et al. 2012a, 2012b; Fedoseev et al. 2012) as well as low energy ions on interstellar ice analogues (Ioppolo et al. 2009; Palumbo 2006; Mennella et al. 2004; Strazzulla et al. 2001). Also thermal processing (Danger et al. 2012;

Duvernay et al. 2010) and the influence of electron and cosmic-ray impact on interstellar ice analogues has been investigated (see e.g. Bennett et al. 2010; Zheng and Kaiser 2010). In recent years much progress has also been made in simulating the dynamical processes that take place in the ice (see e.g. Arasa et al. 2010, 2011). This provides valuable and necessary information to interpret laboratory observations in terms of interacting surface species.

10.1.3 Outlook

With the experimental findings obtained at CRYOPAD (and SPICES) much has been learned about the molecular physics involved in the photo-processing of interstellar ice analogues. In the nearby future, these studies will be extended. It is likely that co-desorption is at play in interstellar ice analogues, i.e., if an ice can act as Newtons's cradle the excitation of one molecule may cause the ejection of another and possibly different chemical species. It is also likely that the efficiency of at least some of the UV induced processes that take place in interstellar ices will be depending on mass, and therefore it will be useful to study possible isotope effects upon UV irradiation. How do H_2O, HDO and D_2O compare? Not only the photo-desorption, but also the UV photo-chemistry of an ice may be wavelength dependent. For CO for specific energies higher reaction rates may be found, e.g., when these coincide with molecular absorptions. Moreover, different energies may trigger different dissociation channels, and also this will affect the overall chemical process in the ice. The consequence for astronomy would be that in inter- and circumstellar environments with different radiation fields, different chemical processes, or chemical processes with different efficiencies will take place. The interstellar radiation field is dominant in diffuse and translucent, lovering clouds or at the edge of dark clouds or disks and does not vary strongly with wavelength in the 90 to 200 nm regime. A significant variation with wavelength is found for cool stars, depending on the effective temperature of the star, e.g., in disks with low accretion rates. Many narrow lines between 90 and 160 nm are found in regions that are dominated by cosmic ray induced photons and that comprise Ly-α and Werner bands. This is the case inside dark clouds and protostellar envelopes, i.e., also those regions where ices are found. Purely Ly-α dominated radiation fields are mainly found in certain regions of disks with high accretion rates. See also van Dishoeck et al. (2006), Schindhelm et al. (2012), van Dishoeck and Visser (2013).

This will be particularly interesting for methanol ice, given its potential to form larger organic compounds, such as dimethylether and glycolaldehyde. As stated before, the latter was detected in a solar-like protostar (Jørgensen et al. 2012). Also other precursor molecules should be considered. For example methylcyanide, CH_3CN as the nitrogen containing equivalent of methanol, is likely a good starting point in the formation of N-bearing species such as glycine and pyrimidine. Finally, the Greenberg experiments should be fully reproduced, showing to which extent molecular complexity can be realized in an interstellar ice analogue, but the focus should be on a bottom-up approach, and data should be taken in situ.

10.2 OASIS (Optical Absorption Spectrometer for Ice Spectroscopy)

10.2.1 Experimental Details

Most laboratory techniques that are used to study interstellar ice constituents spectroscopically, operate in the infrared and characterize *vibrational* parameters; band position, band-

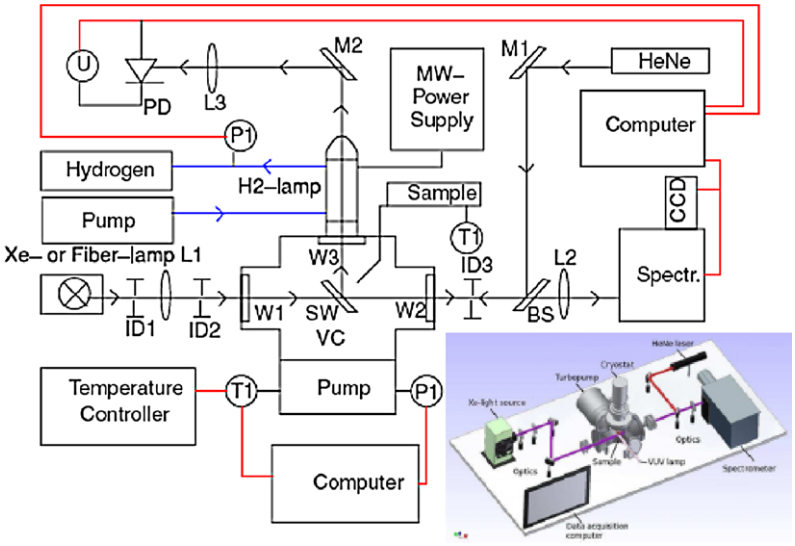

Fig. 37 A schematic drawing of OASIS. BS = Beam splitter, IDX = Iris Diaphragm X, LX = Lens X, MX = Mirror X, PD = Photo Diode to monitor interference fringes, PI = Pressure Indicator, SW = MgF_2 Cold Sample Window, TI = Temperature Indicator, U = Voltage meter, VC = Vacuum Chamber and WX = MgF_2 Window X. The *light paths* are indicated by *arrows*, the data wiring is indicated in *red dotted lines* and the hydrogen flow is indicated by *blue lines*. Taken from Bouwman et al. (2010)

width, and band intensity. An extension to the UV/VIS and near-IR allows to monitor *electronic* properties of interstellar ice analogues (Gudipati and Allamandola 2004, 2006a; Bouwman et al. 2009, 2010, 2011a). OASIS is based on incoherent, broadband, direct absorption spectroscopy. Response times are fast and photochemical processes can be studied for astronomically relevant temperatures at subsecond time scales. The performance of the apparatus has been demonstrated on the example of complex species embedded in water ice (e.g. Bouwman et al. 2011a).

The full experimental details of OASIS have not been summarized before and are listed in detail below. A schematic view of the experimental setup is shown in Fig. 37. OASIS consists of three units: a high vacuum chamber in which the ice is grown, an UV irradiation source similar to the one used in CRYOPAD (see Sect. 10.1.1) and a spectrograph equipped with a sensitive CCD camera that disperses broadband visible-UV light from an intense Xe arc lamp after crossing the (photoprocessed) ice. The vacuum chamber consists of an ISO-160 6-cross-piece. Differential pumping is used to guarantee an operating pressure of 10^{-7} mbar or lower. A catalytic trap is mounted on the pre-vacuum pump to prevent pump oil from entering the vacuum chamber. The top flange of the cross piece holds a HV rotary flange on which a closed cycle helium refrigerator (ARS type DE202NE) is mounted. A MgF_2 sample window, clamped into an oxygen free copper holder between indium gaskets, is mounted on a cold finger and centered along the rotation axis. The rotary flange allows a full rotation of the sample window through 360° while maintaining vacuum. The sample window temperature is thermally controlled between 12 and 325 K through resistive heating using a Lakeshore temperature controller. A Chromel-Au/Fe (0.07 %) thermocouple is used to determine the absolute temperature value with an accuracy of 0.1 K. The interstellar ice analogues are grown onto the cold sample window by vapor deposition. For this, a gas bulb containing the matrix material is connected to a stainless steel tube (1 mm inner diam-

eter at the tip) ending perpendicular to the sample window with a distance of about 15 mm. Solid precursor material is deposited together with the matrix material using small ovens. For evaporation temperatures below 50 °C, an external glass oven is used, and for higher temperatures, a resistively heated steel oven attached to the deposition tube inside the chamber is taken. The flow rate of the matrix material is accurately set by a high precision dosing valve, while the evaporation rate of the solid precursor can be roughly chosen by changing the power of the heater. Condensation at any place inside the tube is prohibited by additional resistive heating along the full length of the deposition tube. The resulting ice film thickness is accurately measured by recording the number of interference fringe maxima (m) of a HeNe laser beam ($\lambda_{HeNe} = 632.8$ nm) that hits the sample window at an angle of $\theta = 45°$. For monitoring film growth and thickness, the intensity of the reflected laser light is measured with a sensitive photodiode and the signal is digitized with a 16 bit analogue to digital converter board. The ice thickness is determined through $d = (m\lambda_{HeNe})/(2n_{ice}\cos\theta)$, with the refractive index of the predominantly H_2O ice being ∼1.3 (see also Bossa et al. 2012, and refs. therein). In a typical experiment, ice thicknesses of the order of 0.4 to 2.4 μm are grown. This can be directly related to the number of H_2O molecules in the sample ice by using the value for the density of amorphous solid water ice ($\rho = 0.94$ g/cm^3). Also the column density of the embedded species (e.g., PAHs and fullerenes) can be monitored during deposition by correlating the absorption signal strength to an absolute molecule number. This yields typical concentrations of embedded (complex) species of 1:5000 to 1:10000 w.r.t. water. The absorption spectrometer consists of a 150 W Xe arc lamp (LOT-Oriel) that serves as a broad band white light source. The lamp has a spectral energy distribution that covers the full detector range (200 nm $< \lambda <$ 2400 nm). An optical system consisting of lenses and diaphragms guides the light beam through a MgF_2 window along the optical axis—coinciding with the HeNe beam that is also used for pre-alignment—and crossing the ice sample at a 45° angle. Light that is not absorbed exits the vacuum chamber through a second MgF_2 window, after which it is focused onto the entrance slit of a spectrometer (Shamrock 303i). The spectrometer is equipped with two interchangeable turrets which hold four gratings in total (2400, 1200, 600 and 150 l/mm), allowing for a trade-off between wavelength coverage and spectral resolution, depending on experimental needs.

Typical electronic ice absorption bands exhibit a FWHM of 4 to 20 nm, and therefore the 150 l/mm grating is normally used. This grating provides a wavelength coverage of ∼140 nm. The light is subsequently dispersed onto a very sensitive 1024 × 256 pixel CCD camera with 16 bit digitization (ANDOR iDus DV-420 OE). The resulting signal is read out in vertical binning mode by a data acquisition computer. Spectra are taken in absorbance mode ($\tau = \log(I/I_0)$) with respect to a reference spectrum (I_0) taken directly after sample deposition. The recording of a single spectrum takes about 10 s and typically consists of 100 spectra co-added to improve S/N ratios. In a regular experiment more than 1000 individual spectra are recorded and reduced using LabView routines.

To trigger reactions in the ice, it is irradiated by UV radiation from a microwave powered hydrogen discharge lamp as discussed in the previous section. The lamp is centered on the front flange and the UV radiation enters the setup through a MgF_2 window that also serves as a vacuum seal. A shutter in between window and ice substrate is used to block the UV light until the ice processing is started. In addition, eliminating the need to switch the H_2 lamp on and off for (non)irradiation allows the lamp to stabilize. This is particularly useful when tracking the photochemical behavior during extended periods of photolysis. Spectra are subsequently subtracted from the unprocessed ice spectrum, yielding a difference spectrum in which negative signals indicate that a precursor species is consumed, and positive signals correspond to the formation of new species. For the data reduction local linear baseline corrections and multiple Gaussian fitting of the band profiles is applied. As the HeNe laser

and visible absorption spectrum are monitored simultaneously, these measurements can be performed with full characterization of the ice composition. Hence, the setup allows high quality, sub-second time resolution spectroscopic experiments in which the photoprocessing of well-defined interstellar ice analogues can be carefully monitored.

10.2.2 Results

The performance of the setup is demonstrated discussing the UV irradiation of a commercially available PAH, Pyrene (Py, $C_{16}H_{10}$) embedded in water ice (see also Bouwman et al. 2009, 2011a for cross-references). The presence of polycyclic aromatic hydrocarbons (PAHs) in many phases of the interstellar medium is evidenced by their strong and ubiquitous mid-infrared (mid-IR) emission features (Tielens 2008). Mid-IR features are efficiently emitted by a PAH after excitation by an energetic photon. Towards dense clouds, however, these mid-IR features are strongly quenched. Here, most volatile molecules are frozen out on grains forming layers of ice (e.g. Boogert et al. 2008; Öberg et al. 2011). Under such conditions, less volatile molecules such as PAHs condense on interstellar grains as well, where they will influence or contribute to the solid state chemical network.

The PAH:H_2O sample is prepared by vapor depositing (Py, $C_{16}H_{10}$, 99 %) with milli-Q water vapor from a purified liquid sample. The thickness of the ice sample is monitored as described above. Typical final ice thicknesses are ∼1.7 μm and reproducible to within 5 % or lower. In parallel, the number of pyrene (or other PAH) molecules in the ice sample (N_{Py}) is monitored by measuring the integrated absorbance of its strongest transition ($S_2 \leftarrow S_0$). The number of pyrene molecules per cm^2 can be calculated via $N = \int \tau d\nu / 8.88 \times 10^{-13} f$ where $f = 0.33$ is the well known oscillator strength of the ($S_2 \leftarrow S_0$) transition of pyrene, and τ is optical depth. Typical pyrene concentrations range from 1:5000 to 1:10000 pyrene:H_2O mixture. The concentration can be roughly varied by changing the H_2O flow rate or the PAH sample temperature. These mixing ratios are close to the predicted values for the ISM, where overall PAH abundances of the order of a few percent are taken. The neutral Py bands cover mainly the high energy range below 350 nm. The individual bands are readily assigned using available data from rare gas matrix isolation spectroscopy, e.g., for Py Kjaergaard et al. (2000), Wang et al. (2003). The water ice environment causes bands to shift and broaden compared to rare gas matrix experiments, because of the stronger molecular interactions in the polar water environment. Similar findings are derived for other PAHs, such as anthracene, coronene and benzo[ghi]pyrelene (Bouwman et al. 2011a).

Since PAH electronic transition strengths are some 100 to 1000 times stronger than IR band strengths, photochemical processes of PAHs in ice can be followed with OASIS, even at highly dilute concentrations. This pushes the threshold for PAH detection and monitoring one to two orders of magnitude beyond the IR detection threshold. In the IR, indeed, PAH:H_2O ∼1:100 mixtures are needed to discriminate PAH bands, particularly as common interstellar ice constituents such as H_2O, CO, CO_2, etc. have very strong bands in the IR, making it very difficult if not impossible to disentangle weak PAH IR absorptions in an ice. These species, however, do not exhibit strong transitions in the optical range. Furthermore, electronic transitions are more unique than infrared vibrations that can be rather similar, also for very different PAHs.

The UV photolysis of Py:H_2O mixtures has been described in detail by Bouwman et al. (2011a). The negative bands that appear between 290 and 345 nm (Fig. 38) are assigned to the $^1B_{2u} \leftarrow {}^1A_g$ electronic transition of neutral pyrene ($S_2 \leftarrow S_0$) (Halasinski et al. 2005). Most of the positive bands that form upon UV photolysis of the Py containing H_2O ice can

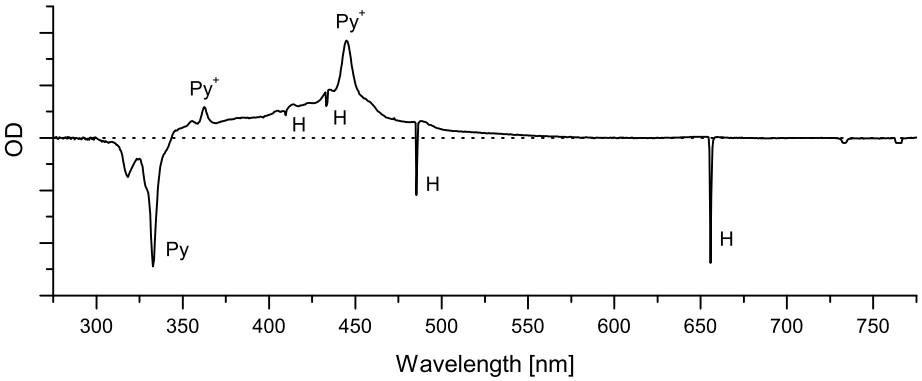

Fig. 38 The 280 to 800 nm spectrum of the PAH pyrene in H_2O ice, photolyzed at 25 K. Negative features indicate that the corresponding band carrier is destroyed, positive bands indicate that a species is formed. Hydrogen emission lines (sharp negative signals) originating from the VUV lamp are labeled with an H. Taken from Bouwman et al. (2011a)

be ascribed to the Py^+ species. The system ranging from ~411–470 nm is the strongest Py^+ transition and assigned as $^2A_u \leftarrow {}^2B_{3g}$. The weaker absorption bands between 350 and 370 nm are assigned to the $^2B_{1u} \leftarrow {}^2B_{3g}$ Py^+ vibronic transition. The band on the red-wing of the strongest Py^+ transition, situated around 490.1 nm, is due to the $^2B_{1u} \leftarrow {}^2B_{3g}$ transition. The Py^+ bands are broader in solid H_2O than in rare gas matrices, in accordance with the stronger interactions within the H_2O matrix network. Similarly, larger shifts in peak position are expected. For the studied conditions, the direct ionization channel is found to be dominant. This observation is also confirmed for other PAHs embedded in water ice (Bouwman et al. 2011a) and was concluded earlier by Gudipati and Allamandola (2003), Gudipati (2004). Besides the rather strong Py cation absorptions, two weak bands which do not correlate with the cation features are detected around 400 and 405 nm. The band at 400 nm has been previously found to originate from an electronic transition in PyH· and the band at 405 nm has been tentatively assigned to an electronic transition of ^{3}Py (Bouwman et al. 2010).

OASIS also allows to derive temperature dependent kinetic information, simply by recording the integrated absorbances as function of time. Spectra are taken every 10 seconds during photolysis. For pyrene it is found that Py^+ vibronic bands quickly build up to a maximum after about 1000 s and then slowly fall off over the course of the experiment. In a similar way it is interesting to note that charged species remain in the ice, also when the UV light is switched off. This is relevant for solid state astrochemical processes as charge induced interactions may play a key role.

In a recent study the effect of the ice matrix was studied by exchanging water by ammonia (Cuylle et al. 2012a). Whereas all investigated PAHs convert to cationic species upon UV irradiation, this is clearly different in an ammonia environment, where PAH-anion signatures are found. The cause of the different behavior observed in water and ammonia PAH-containing ices lies in the energetics of charged molecule chemistry. The closeness between the electron affinities of PAHs and NH_3 reaction products—NH and NH_2—means that PAHs in photolyzed NH_3 ice are near equal competitors for free electrons with the other ice components. This is not the case in water ice, where the photoproduct OH has an electron affinity of 5 eV (Gudipati and Allamandola 2006a, 2006b), making it a more favored electron acceptor than PAH molecules. Interesting is the case of a mixed ice. For NH_3:H_2O 1:10 ice

mixtures, a ratio as found around young stellar objects (Bottinelli et al. 2010), PAH cations are more likely to form than anions. In planetary atmospheres, e.g., on Jupiter, this situation can be different and the results found by Cuylle et al. (2012b) indicate that here anion chemistry may be relevant.

10.2.3 Outlook

Infrared emission features assigned to PAH vibrational modes are visible along many lines of sight, with exception of those regions in space where ices are known to exist. Indeed, Geers et al. (2009) concluded that these non-detections are most probably due to PAHs being frozen in ice layers, or condensed in coagulated form, quenching the typical IR emission signatures. The work described in the previous section therefore offers an alternative, i.e., solid state approach to search for PAHs (or other large complex species) in space, providing laboratory based spectra of PAHs and PAH photoproducts embedded in water ice. Moreover, the work shows that also complex species may be involved in solid state astrochemical processes. The unique properties of OASIS hold the potential to extend these measurements to other large species. In a recent study it has been possible to record the electronic spectrum of C_{60} in water ice (Cuylle et al. 2012b). With the recent detection of C_{60} in space in a variety of astronomical sources (Cami et al. 2010; Sellgren et al. 2010), again, it becomes interesting to have spectra at hand of C_{60} embedded in water ice. The spectra presented in Cuylle et al. (2012b) largely follow previous rage gas matrix studies on C_{60} (see e.g. Leach et al. 1992; Sassara et al. 2001) and exhibit a rather characteristic pattern with two strong and broad bands around 258 and 327 nm as well as many weaker bands in the 350–420 nm region. Similarly interesting is the possibility to include organic compounds in UV irradiated interstellar ice analogues. Greenberg and others showed mass spectrometrically that amino acids can be formed upon long term UV irradiation of an astronomical mixture of ice constituents (Muñoz Caro et al. 2002). In recent years similar experiments have been performed for different ice mixtures by a number of groups. Very recently Ciesla and Sandford (2012) published new findings illustrating the possible synthesis of organic material via irradiation and warming of ice grains in the solar nebula. OASIS allows to approach this type of studies from a different point of view, i.e., by studying the UV photo-stability of organic compounds embedded in an interstellar ice analogue, or the parameters (i.e., temperature, ice constituents) for which stable conditions can be reached. This will add to existing studies as available from e.g. Ehrenfreund et al. (2001). First experiments on alanine in water ice have been performed and more work is to follow. The main advantage, however, of this new setup is, that it delivers complementary data to existing infrared work and offers spectroscopic information in a wavelength domain in which observational astronomy has been historically strong, providing the tools for ice research using ground based telescopes.

11 Final remarks

We have described in details some of the techniques that, in addition to the here not considered infrared spectroscopy, are being used in some “astrochemical laboratories” worldwide that have shown, in particular, that photolysis and radiolysis of ices produce a number of relevant and observable effects such as sputtering or photo-sputtering, the modification of the structure and a number of non-thermal, “hot” chemical reactions that can lead to the formation of a large number of molecules and also organic refractory residues. The paper follows the outcome of a 3-day workshop of the authors in November 2012 at the Observatoire de Meudon in France. The purpose of the workshop and of this paper was to present

the techniques, in order to give to the authors and to the readers an overview of the efforts done to develop novel techniques but also the opportunity to use available techniques but in a complementary way for a more in depth characterization of irradiated targets.

All of the information we have about the chemical, physical and structural composition of materials in the interstellar medium are obtained by remote detection of electromagnetic radiation and need an in depth comparison with the results of laboratory "simulation" experiments. The simulations can be limited to the measurement of relevant parameters (e.g. atomic or molecular parameters) or extended to the study of significant processes such as photolysis and radiolysis.

We believe that the present paper can also be useful in the context of the scientific programs of Solar System space exploration that require the availability of efficient and selective analytical tools to analyze the nature of space environments where ices are abundant. To reach the scientific goals a multi-scale approach is necessary according to the spatial range of analyses: macroscopic global scale (km, m) is analyzed by orbiters; local scale (cm, mm) requires in-situ instruments. The microscopic scale (μm, nm) is still out of the technological achievements ready to be flown in next future and can be reached only by laboratory analyses of returned samples.

It is obvious that the experiences acquired in the laboratory, among which those described in the present paper, are essential to understand past and present observations and to prepare future enterprises. The global characterization of a planetary surface (e.g.: size, shape, roughness, composition, etc.) is the basic information by which it is possible to infer hints on the origin and evolution of the object and spectroscopic techniques, from the UV to the terahertz, play a fundamental role in the global characterization.

In-situ analyses require characterization of the object obtained by payload instruments on board of lander that will perform local measurements, possibly at several surface locations. Any local surface scale is a complex mixture of various icy components with different compositions and morphologies intimately mixed with solid refractory component (dust). They would have suffered an intense processing that could have modified their chemical and mineralogical properties or have formed micro-structures that require to be analyzed in-situ. Because an accurate knowledge of the local context is fundamental to describe the distinctive nature of samples, a detailed microscopic study with very high levels of analytical precision (ppm levels) of the material at the surface or sub-surface is, therefore, needed.

Among the techniques here discussed some are "mature" to be used in space instruments. As an example, luminescence offers the possibility of high sensitivity and, in the case of complex samples, improved selectivity. However, this mode of detection requires that the compound exhibit native fluorescence or contain a group to which a fluorophore can be attached chemically. The number of compounds that fall into the former category is small, and while many compounds contain derivatizable groups (e.g., amino, carboxyl, hydroxyl), most derivatization chemistries are limited by one or more disadvantages difficult to be obtainedovercome in a space designed instrument (slow reaction kinetics, complicated reaction or cleanup conditions, interference by matrix components). In order to obtain acceptable sensitivity, it is necessary to focus sufficient excitation light on the sample. This is difficult to achieve with a conventional light source, but is easily accomplished using a laser. As discussed above the most appropriate techniques are laser-induced fluorescence (LIF) detection. Lasers are in fact stable and relatively inexpensive for space application and produce emission lines close to the excitation wavelengths for several common fluorophores. This technique, using modern high-power and compact lasers, could become a complementary technique to other methods such as Raman spectroscopy for in-situ detection of organics in future solar system exploration missions. LIF would be a powerful

complementary technique to other methods such as infrared, ultraviolet, and mass spectroscopic techniques to obtain information on the processes that occur in ices. For example, IR does not detect atoms or diatomics such as O_2, N_2, etc., whereas, vacuum UV is necessary to see these species in electronic spectra. Mass spectroscopy detect these molecules, but with appropriate excitation light source, luminescence spectroscopy could complement mass spectroscopy detecting those species directly in the solid phase.

Acknowledgements Authors acknowledge several grants and persons as follows:
H. Linnartz: Grants within NWO, NOVA and Marie Curie programs. The setups and conclusions presented here have been the outcome of dedicated work by several PhD students, postdocs, and scientific collaborators. Special thanks go to Karin Oberg, Jordy Bouwman, Edith Fayolle, Steven Cuylle, Lou Allamandola, Jean-Hugues Fillion and Mathieu Bertin.
S. Ioppolo: NASA SARA and Exobiology/Astrobiology programs, Niels Stensen Foundation (NSS) through a bursary and a Marie Curie Fellowship (FP7-PEOPLE-2011-IOF-300957).
G.A. Blake: NASA SARA and Exobiology/Astrobiology programs.
M. A. Allodi: Department of Defense (DoD) through the National Defense Science & Engineering Graduate Fellowship (NDSEG) Program.
G. Strazzulla: European COST Action CM 0805: The Chemical Cosmos: Understanding Chemistry in Astronomical Environments.
Z. Kaňuchová: VEGA—The Slovak Agency for Science, grant no. 2/0022/10 and the European COST Action CM 0805: The Chemical Cosmos: Understanding Chemistry in Astronomical Environments.
M. Gudipati and A. Lignell: NASA Astrobiology Institute (NAI) through Icy Worlds (JPL) and Early Habitable Environments (NASA Ames) nodes, NASA Spitzer Science Center (Cycle 5), NASA funding through Rosetta US Science Team. Research was carried out at the Jet Propulsion Laboratory, California Institute of Technology, under a contract with the National Aeronautics and Space Administration.
R.A. Baragiola, U. Raut and D. Fulvio: NASA program: Origins of the Solar System and Outer Planet Research, and programs NSF.
F. Salama: The Astrophysics Research and Analysis program (APRA) of NASA SMD, The technical support provided at NASA-Ames by R. Walker is gratefully acknowledged.
C. Contreras and E. Sciamma-O'Brien: NASA Postdoctoral Program (NPP).
Ph. Boduch and H. Rothard: CAPES-COFECUB French-Brazilian exchange program; European COST Action CM 0805: The Chemical Cosmos: Understanding Chemistry in Astronomical Environments; T. Langlinay and H. Hijazi, and Region "Basse Normandie".

References

J.P. Adrados, J.L. de Segovia, Anomalous mass numbers in quadrupole mass spectrometers (QMS) at very low pressures. Vacuum **34**, 741–747 (1984). doi:10.1016/0042-207X(84)90319-1

T. Akiyama, M. Sakamaki, K. Abe, T. Shigenari, Proton motions on the fluorescence from 2-naphthol-doped ice ih and the proton ordering transition. J. Phys. Chem. B **101**, 6205–66207 (1997). doi:10.1021/jp963177h

L.J. Allamandola, D.M. Hudgins, S.A. Sandford, Modeling the unidentified infrared emission with combinations of polycyclic aromatic hydrocarbons. Astrophys. J. Lett. **511**, 115–119 (1999). doi:10.1086/311843

H.H. Andersen, H.L. Bay, Heavy-ion sputtering yields of gold: further evidence of nonlinear effects. J. Appl. Phys. **46**, 2416–2422 (1975). doi:10.1063/1.321910

D. Andrade, A. de Barros, S. Pilling, A. Domaracka, H. Rothard, P. Boduch, E. da Silveira, Chemical reactions induced in frozen formic acid by heavy ion cosmic rays. Mon. Not. R. Astron. Soc. **430**, 787–796 (2013)

C. Arasa, S. Andersson, H.M. Cuppen, E.F. van Dishoeck, G.-J. Kroes, Molecular dynamics simulations of the ice temperature dependence of water ice photodesorption. J. Chem. Phys. **132**(18), 184510 (2010). doi:10.1063/1.3422213

C. Arasa, S. Andersson, H.M. Cuppen, E.F. van Dishoeck, G.J. Kroes, Molecular dynamics simulations of D_2O ice photodesorption. J. Chem. Phys. **134**(16), 164503 (2011). doi:10.1063/1.3582910

W. Assmann, M. Toulemonde, C. Trautmann, Electronic sputtering with swift heavy ions, in *Sputtering by Particle Bombardment*, eds. by I.R. Behrisch, W. Eckstein. Topics in Applied Physics, vol. 110 (Springer, Berlin, 2007), pp. 401–450.

V. Balaji, D.R. David, T.F. Magnera, J. Michl, H.M. Urbassek, Sputtering yields of condensed rare-gasses. Nucl. Instrum. Methods Phys. Res., Sect. B, Beam Interact. Mater. Atoms **46**, 435–440 (1990). doi:10.1364/JOSAA.15.003076

R.A. Baragiola, Sputtering: survey of observations and derived principles. Philos. Trans. R. Soc. Lond. **362**(1814), 29–53 (2004)

R.A. Baragiola, C.L. Atteberry, C.A. Dukes, M. Fama, B.D. Teolis, Atomic collisions in solids: astronomical applications. Nucl. Instrum. Methods Phys. Res., Sect. B, Beam Interact. Mater. Atoms **193**(1), 720–726 (2002)

R.A. Baragiola, M. Fama, J. Loeffler, U. Raut, J. Shi, Radiation effects in ice: new results. Nucl. Instrum. Methods Phys. Res., Sect. B, Beam Interact. Mater. Atoms **266**, 3057 (2008). doi:10.1016/j.nimb.2008.03.186

G.A. Baratta, M.M. Arena, G. Strazzulla, L. Colangeli, V. Mennella, E. Bussoletti, Raman spectroscopy of ion irradiated amorphous carbons. Nucl. Instrum. Methods Phys. Res., Sect. B, Beam Interact. Mater Atoms **116**, 195–199 (1996). doi:10.1016/0168-583X(96)00124-3

G.A. Baratta, M.E. Palumbo, Infrared optical constants of CO and CO_2 thin icy films. J. Opt. Soc. Am. A **15**, 3076–3085 (1998) doi:10.1364/JOSAA.15.003076

T. Bartels-Rausch, V. Bergeron, J.H.E. Cartwright, R. Escribano, J.L. Finney, H. Grothe, P.J. Gutierrez, J. Haapala, W.F. Kuhs, J.B.C. Pettersson, S.D. Price, C.I. Sainz-Diaz, D.J. Stokes, G. Strazzulla, E. Thomson, H. Trinks, N. Uras-Nevin, Ice structures, patterns, and processes: a view across the icefields. Rev. Mod. Phys. **84**, 885–944 (2012). doi:10.1103/RevModPhys.84.885

J.A. Basford, et al., J. Vac. Sci. Technol., A, Vac. Surf. Films **11**, A22 (1983)

M. Batchelor, D. Adler, W. Trogus, New plans for first far infrared and sub-millimetre space astronomy mission for 2007. Adv. Space Res. **18**, 185–188 (1996)

R. Behrisch, W. Eckstein, *Sputtering by Particle Bombardment, Experiments and Computer Calculations from Threshold to MeV Energies*. Topics in Applied Physics, vol. 110 (2007), pp. 1–20

M.T. Beltrán, C. Codella, S. Viti, R. Neri, R. Cesaroni, First detection of glycolaldehyde outside the galactic center. Astrophys. J. Lett. **690**, 93–96 (2009). doi:10.1088/0004-637X/690/2/L93

C.J. Bennett, C.S. Jamieson, R.I. Kaiser, Mechanistical studies on the formation and destruction of carbon monoxide (CO), carbon dioxide (CO_2), and carbon trioxide (CO_3) in interstellar ice analog samples. Phys. Chem. Chem. Phys. **12**, 4032–4050 (2010)

P.P. Bera, M. Head-Gordon, T.J. Lee, Initiating molecular growth in the interstellar medium via dimeric complexes of observed ions and molecules. Astron. Astrophys. **535**, 74 (2011). doi:10.1051/0004-6361/201117103

E.A. Bergin, R.L. Snell, Sensitive limits on the water abundance in cold low-mass molecular cores. Astrophys. J. Lett. **581**, 105–108 (2002). doi:10.1086/346014

M.P. Bernstein, J.P. Dworkin, S.A. Sandford, G.W. Cooper, L.J. Allamandola, Racemic amino acids from the ultraviolet photolysis of interstellar ice analogues. Nature **416**, 401–403 (2002)

M. Bertin, E.C. Fayolle, C. Romanzin, K.I. Öberg, X. Michaut, A. Moudens, L. Philippe, P. Jeseck, H. Linartz, J.H. Fillion, UV photodesorption of interstellar CO ice analogues: from subsurface excitation to surface desorption. Phys. Chem. Chem. Phys. **14**, 9929–9935 (2012)

L. Biennier, F. Salama, L. Allamandola, J. Scherer, Pulsed discharge nozzle cavity ringdown spectroscopy of cold polycyclic aromatic hydrocarbon ions. J. Chem. Phys. **118**, 7863–7872 (2003). doi:10.1063/1.1564044

L. Biennier, M. Hammond, J. Elsila, R. Zare, F. Salama, From organic molecules to carbon particles: implications for the formation of interstellar dust, in *IAU Symposium*, vol. 235 (2005), p. 214

L. Biennier, A. Benidar, F. Salama, Flow dynamics of a pulsed planar expansion. Chem. Phys. **326**(2–3), 445–457 (2006). doi:10.1016/j.chemphys.2006.03.016

V.M. Bierbaum, V. Le Page, T.P. Snow, PAHs and the chemistry of the Ism, in *EAS Publications Series*, ed. by C. Joblin. A.G.G.M. Tielens EAS Publications Series, vol. 46 (2011), pp. 427–440. doi:10.1051/eas/1146044

G.A. Blake, Microwave and terahertz spectroscopy. Encyclopedia of Chem. Phys. Phys. Chem. **2**, 1063–1088 (2001).

G.A. Blake, Terahertz spectroscopy in the lab and at telescopes, in *Submillimeter Astrophysics and Technology: A Symposium Honoring Thomas G. Phillips*, ed. by D.C. Lis, J.E. Vaillancourt, P.F. Goldsmith, T.A. Bell, N.Z. Scoville, J. Zmuidzinas Astronomical Society of the Pacific Conference Series, vol. 417 (2009), p. 231

M.A. Bol'shov, C.F. Boutron, A.V. Zybin, Determination of lead in antarctic ice at the picogram-per-gram level by laser atomic fluorescence spectrometry. Anal. Chem. **61**, 1758–1762 (1989)

A.C.A. Boogert, K.M. Pontoppidan, C. Knez, F. Lahuis, J. Kessler-Silacci, E.F. van Dishoeck, G.A. Blake, J.-C. Augereau, S.E. Bisschop, S. Bottinelli, T.Y. Brooke, J. Brown, A. Crapsi, N.J. Evans II, H.J. Fraser, V. Geers, T.L. Huard, J.K. Jørgensen, K.I. Öberg, L.E. Allen, P.M. Harvey, D.W. Koerner, L.G.

Mundy, D.L. Padgett, A.I. Sargent, K.R. Stapelfeldt, The c2d spitzer spectroscopic survey of ices around low-mass young stellar objects. I. H_2O and the 5–8 μm bands. Astrophys. J. **678**, 985–1004 (2008). doi:10.1086/533425

J.-B. Bossa, K. Isokoski, M.S. de Valois, H. Linnartz, Thermal collapse of porous interstellar ice. Astron. Astrophys. **545**, 82 (2012). doi:10.1051/0004-6361/201219340

S. Bottinelli, A.C.A. Boogert, J. Bouwman, M. Beckwith, E.F. van Dishoeck, K.I. Öberg, K.M. Pontoppidan, H. Linnartz, G.A. Blake, N.J. Evans II, F. Lahuis, The c2d Spitzer spectroscopic survey of ices around low-mass young stellar objects. IV. NH_3 and CH_3OH. Astrophys. J. **718**, 1100–1117 (2010). doi:10.1088/0004-637X/718/2/1100

J. Bouwman, D.M. Paardekooper, H.M. Cuppen, H. Linnartz, L.J. Allamandola, Real-time optical spectroscopy of vacuum ultraviolet irradiated pyrene:H_2O interstellar ice. Astrophys. J. **700**, 56–62 (2009). doi:10.1088/0004-637X/700/1/56

J. Bouwman, H.M. Cuppen, A. Bakker, L.J. Allamandola, H. Linnartz, Photochemistry of the PAH pyrene in water ice: the case for ion-mediated solid-state astrochemistry. Astron. Astrophys. **511**, 33 (2010). doi:10.1051/0004-6361/200913291

J. Bouwman, H.M. Cuppen, M. Steglich, L.J. Allamandola, H. Linnartz, Photochemistry of polycyclic aromatic hydrocarbons in cosmic water ice. II. Near UV/VIS spectroscopy and ionization rates. Astron. Astrophys. **529**, 46 (2011a). doi:10.1051/0004-6361/201015762

J. Bouwman, A.L. Mattioda, H. Linnartz, L.J. Allamandola, Photochemistry of polycyclic aromatic hydrocarbons in cosmic water ice. I. Mid-IR spectroscopy and photoproducts. Astron. Astrophys. **525**, 93 (2011b). doi:10.1051/0004-6361/201015059

B. Broks, W. Brok, J. Remy, J. van der Mullen, J. Benidar, L. Biennier, F. Salama, Numerical investigation of the discharge characteristics of the pulsed discharge nozzle. Phys. Rev. E **71(3)**, 36409 (2005a). doi:10.1103/PhysRevE.71.036409

B. Broks, W. Brok, J. Remy, J. van der Mullen, J. Benidar, L. Biennier, F. Salama, Modeling the influence of anode-cathode spacing in a pulsed discharge nozzle. Spectrochim. Acta B **60**, 1442–1449 (2005b). doi:10.1016/j.sab.2005.08.012

J. Cami, J. Bernard-Salas, E. Peeters, S.E. Malek, Detection of C_{60} and C_{70} in a young planetary nebula. Science **329**, 1180 (2010). doi:10.1126/science.1192035

R. Cannia, G. Strazzulla, G. Compagnini, G.A. Baratta, Vibrational spectroscopy of ion-irradiated pentacene. Infrared Phys. Technol. **35**, 791–800 (1994). doi:10.1016/1350-4495(94)90007-8

P.B. Carroll, B.J. Drouin, S.L. Widicus Weaver, The submillimeter spectrum of glycolaldehyde. Astrophys. J. **723**, 845–849 (2010). doi:10.1088/0004-637X/723/1/845

F. Cataldo, G.A. Baratta, G. Strazzulla, He^+ ion bombardment of C_{60} fullerene: an FT-IR and Raman study. Nanotub. Carbon Nanostruct. **10**(3), 197–206 (2002). doi:10.1081/FST-120014734

F. Cataldo, G.A. Baratta, G. Ferini, G. Strazzulla, He^+ ion bombardment of C_{70} fullerene: an FT-IR and Raman study. Nanotub. Carbon Nanostruct. **11**(3), 191–199 (2003). doi:10.1081/FST-120024038

F.J. Ciesla, S.A. Sandford, Organic synthesis via irradiation and warming of ice grains in the solar nebula. Science **336**, 452 (2012). doi:10.1126/science.1217291

R. Chen, S.W.S. McKeever, *Theory of Thermoluminescence and Related Phenomena* (World Scientific, Singapore, 1997)

I. Cherchneff, The formation of polycyclic aromatic hydrocarbons in evolved circumstellar environments, in *EAS Publications Series*, ed. by C. Joblin. A.G.G.M. Tielens EAS Publications Series, vol. 46 (2011), pp. 177–189. doi:10.1051/eas/1146019

G. Compagnini, L. D'Urso, O. Puglisi, G.A. Baratta, G. Strazzulla, On the irradiation of solid hydrocarbons and the formation of linear carbon chain. Carbon **47**, 1605 (2009).

E. Congiu, H. Chaabouni, C. Laffon, P. Parent, S. Baouche, F. Dulieu, Efficient surface formation route of interstellar hydroxylamine through NO hydrogenation. I. The submonolayer regime on interstellar relevant substrates. J. Chem. Phys. **137**, 054713 (2012a)

E. Congiu, G. Fedoseev, S. Ioppolo, F. Dulieu, H. Chaabouni, S. Baouche, J.L. Lemaire, C. Laffon, P. Parent, T. Lamberts, H.M. Cuppen, H. Linnartz, No ice hydrogenation: a solid pathway to NH_2OH formation in space. Astrophys. J. Lett. **750**, 12 (2012b). doi:10.1088/2041-8205/750/1/L12

C.S. Contreras, C.L. Ricketts, F. Salama, Formation and evolution of circumstellar and interstellar PATHs: a laboratory study, in *EAS Publications Series*, ed. by C. Joblin. A.G.G.M. Tielens EAS Publications Series, vol. 46 (2011), pp. 201–207. doi:10.1051/eas/1146021

C.S. Contreras, F. Salama, Astrophys. J. (submitted) (2013)

J.M. Costantini, F. Couvreur, J.P. Salvetat, S. Bouffard, Micro-Raman study of the carbonization of polyimide induced by swift heavy ion irradiations. Nucl. Instrum. Methods Phys. Res., Sect. B, Beam Interact. Mater. Atoms **194**, 132–140 (2002). doi:10.1016/S0168-583X(02)00669-9

M.C. Cowen, W. Allison, J.H. Batey, Nonlinearities in sensitivity of quadrupole partial-pressure analyzers operating at higher gas-pressures. J. Vac. Sci. Technol., A, Vac. Surf. Films **12**, 228–234 (1994)

H.M. Cuppen, S. Ioppolo, C. Romanzin, H. Linnartz, Water formation at low temperatures by surface O2 hydrogenation. II. The reaction network. Phys. Chem. Chem. Phys. **12**, 12077 (2010)
H.M. Cuppen, E.M. Penteado, K. Isokoski, N. van der Marel, H. Linnartz, CO ice mixed with CH_3OH: the answer to the non-detection of the 2152 cm^{-1} band? Mon. Not. R. Astron. Soc. **417**, 2809–2816 (2011). doi:10.1111/j.1365-2966.2011.19443.x
S.H. Cuylle, H. Linnartz, UV/VIS spectroscopy of C60 embedded in water ice. Chem. Phys. Lett. **550**, 79–82 (2012a)
S.H. Cuylle, E.D. Tenenbaum, J. Bouwman, H. Linnartz, L.J. Allamandola, Lyα-induced charge effects of polycyclic aromatic hydrocarbons embedded in ammonia and ammonia:water ice. Mon. Not. R. Astron. Soc. **423**, 1825–1830 (2012b). doi:10.1111/j.1365-2966.2012.21006.x
J.B. Dalton, D.P. Cruikshank, K. Stephan, T. McCord, A. Coustenis, R.W. Carlson, A. Coradini, Chemical composition of icy satellite surfaces. Space Sci. Rev. **153**, 113–154 (2010). doi:10.1007/s11214-010-9665-8
G. Danger, F. Duvernay, P. Theulé, F. Borget, T. Chiavassa, Hydroxyacetonitrile ($HOCH_2CN$) formation in astrophysical conditions. competition with the aminomethanol, a glycine precursor. Astrophys. J. **756**, 11 (2012). doi:10.1088/0004-637X/756/1/11
P.H. Dawson, *Quadrupole Mass Spectrometry and Its Applications* (American Inst. of Physics, New York, 1997), 376 pp.
C.A. Dukes, W.-Y. Chang, M. Famá, R.A. Baragiola, Laboratory studies on the sputtering contribution to the sodium atmospheres of mercury and the moon. Icarus **212**, 463–469 (2011). doi:10.1016/j.icarus.2011.01.027
F. Dulieu, L. Amiaud, E. Congiu, J.-H. Fillion, E. Matar, A. Momeni, V. Pirronello, J.L. Lemaire, Experimental evidence for water formation on interstellar dust grains by hydrogen and oxygen atoms. Astron. Astrophys. **512**, 30 (2010). doi:10.1051/0004-6361/200912079
F. Duvernay, V. Dufauret, G. Danger, P. Theulé, F. Borget, T. Chiavassa, Chiral molecule formation in interstellar ice analogs: alpha-aminoethanol $NH_2CH(CH_3)OH$. Astron. Astrophys. **523**, 79 (2010). doi:10.1051/0004-6361/201015342
E.P. Eernisse, Light ion bombardment sputtering, stress buildup, and enhanced surface contamination. J. Nucl. Mater. **53**, 226–230 (1974a)
E.P. Eernisse, Sputtering measurements with the double resonator technique. J. Vac. Sci. Technol. **11**, 408 (1974b)
E.P. Eernisse, *Applications of Piezoelectric Quartz Crystal Microbalances* (Elsevier, Amsterdam, 1984). Chap. 4
P. Ehrenfreund, M.P. Bernstein, J.P. Dworkin, S.A. Sandford, L.J. Allamandola, The photostability of amino acids in space. Astrophys. J. Lett. **550**, 95–99 (2001). doi:10.1086/319491
B.S. Elman, M.S. Dresselhaus, G. Dresselhaus, E.W. Maby, H. Mazurek, Raman scattering from ion-implanted graphite. Phys. Rev. B. **24**, 1027–1034 (1981). doi:10.1103/PhysRevB.24.1027
E.F. Erickson, SOFIA: the next generation airborne observatory. Space Sci. Rev. **74**, 91–100 (1995). doi:10.1007/BF00751257
M. Fama, J. Shi, R.A. Baragiola, Sputtering of ice by low-energy ions. Appl. Surf. Sci. **602**, 156–161 (2008). doi:10.1016/j.susc.2007.10.002
L.S. Farenzena, P. Iza, R. Martinez, F.A. Fernandez-Lima, E.S. Duarte, G.S. Faraudo, C.R. Ponciano, M.G.P. Homem, A.N. de Brito, K. Wien, E.F. da Silveira, Electronic sputtering analysis of astrophysical ices. Earth Moon Planets **97**, 311–329 (2005). doi:10.1007/s11038-006-9081-y
E.C. Fayolle, M. Bertin, C. Romanzin, X. Michaut, K.I. Öberg, H. Linnartz, J.-H. Fillion, CO ice photodesorption: a wavelength-dependent study. Astrophys. J. Lett. **739**, 36 (2011). doi:10.1088/2041-8205/739/2/L36
G. Fedoseev, S. Ioppolo, T. Lamberts, J. Zhen, H.M. Cuppen, H. Linnartz, Efficient surface formation route of interstellar hydroxylamine through NO hydrogenation. II. The multilayer regime in interstellar relevant ices. J. Chem. Phys. **137**, 054713 (2012)
B. Ferguson, X.-C. Zhang, Materials for terahertz science and technology. Nat. Mater. **1**, 26–33 (2002). doi:10.1038/nmat708
G. Ferini, G.A. Baratta, M.E. Palumbo, A Raman study of ion irradiated icy mixtures. Astron. Astrophys. **414**, 757–766 (2004). doi:10.1051/0004-6361:20031641
M. Frankowski, E.V. Savchenko, A.M. Smith-Gicklhorn, O.N. Grigorashchenko, G.B. Gumenchuk, V.E. Bondybey, Thermally stimulated exoelectron emission from solid neon. J. Chem. Phys. **121**, 1479–1974 (2004). doi:10.1063/1.1763568
M. Frenklach, C.S. Carmer, E.D. Feigelson, Silicon carbide and the origin of interstellar carbon grains. Nature **339**, 196–198 (1989). doi:10.1038/339196a0
G.W. Fuchs, K. Acharyya, S.E. Bisschop, K.I. Öberg, H. Linnartz, F.A. van Broekhuizen, H.J. Fraser, S. Schlemmer, E.F. van Dishoeck, H. Linnartz, Comparative studies of O_2 and N_2 in pure, mixed and layered CO ices. Faraday Discuss. **133**, 331–345 (2006). doi:10.1039/B517262B

G.W. Fuchs, H.M. Cuppen, S. Ioppolo, C. Romanzin, S.E. Bisschop, S. Andersson, E.F. van Dishoeck, H. Linnartz, Hydrogenation reactions in interstellar CO ice analogues. A combined experimental/theoretical approach. Astron. Astrophys. **505**, 629–639 (2009). doi:10.1051/0004-6361/200810784

D. Fulvio, U. Raut, R.A. Baragiola, Photosynthesis of carbon dioxide from carbon surfaces coated with oxygen: implications for interstellar molecular clouds and the outer solar system. Astrophys. J. Lett. **752**, 33 (2012). doi:10.1088/2041-8205/752/2/L33

R. Garrod, I.H. Park, P. Caselli, E. Herbst, Are gas-phase models of interstellar chemistry tenable? The case of methanol. Faraday Discuss. **133**, 51 (2006). doi:10.1039/b516202e

V.C. Geers, E.F. van Dishoeck, K.M. Pontoppidan, F. Lahuis, A. Crapsi, C.P. Dullemond, G.A. Blake, Lack of PAH emission toward low-mass embedded young stellar objects. Astron. Astrophys. **495**, 837–846 (2009). doi:10.1051/0004-6361:200811001

E.L. Gibb, D.C.B. Whittet, W.A. Schutte, A.C.A. Boogert, J.E. Chiar, P. Ehrenfreund, P.A. Gerakines, J.V. Keane, A.G.G.M. Tielens, E.F. van Dishoeck, O. Kerkhof, An inventory of interstellar ices toward the embedded protostar W33A. Astrophys. J. **536**, 347–356 (2000). doi:10.1086/308940

E.L. Gibb, D.C.B. Whittet, A.C.A. Boogert, A.G.G.M. Tielens, Interstellar ice: the infrared space observatory legacy. Astrophys. J. Supp. Ser. **151**, 35–73 (2004). doi:10.1086/381182

D.P. Glavin, J.L. Bada, K.L.F. Brinton, G.D. McDonald, Amino acids in the martian meteorite Nakhla. Proc. Natl. Acad. Sci. USA **96**, 8835–8838 (1999). doi:10.1073/pnas.96.16.8835

J.T. Gosling, The solar wind, in *Encyclopedia of the Solar System*, 2nd edn., ed. by L. McFadden, P.R. Weissman, T.V. Johnson (Academic Press, San Diego, 2007), pp. 99–116

J.M. Greenberg, A. Li, C.X. Mendoza-Gomez, W.A. Schutte, P.A. Gerakines, M. de Groot, Approaching the interstellar grain organic refractory component. Astrophys. J. Lett. **455**, 177 (1995). doi:10.1086/309834

M.S. Gudipati, UV absorption and luminescence spectroscopy of tetrabenzo[B,H,N,T]tetraphenylene. Chem. Phys. Lett. **196**, 481–485 (1992)

M.S. Gudipati, Exciton, exchange, and through-bond interactions in multichromophoric molecules—an analysis of the electronic excited-states. J. Phys. Chem. **98**, 9750–9763 (1994)

M.S. Gudipati, Matrix-isolation in cryogenic water-ices: facile generation, storage, and optical spectroscopy of aromatic radical cations. J. Phys. Chem. A **108**, 4412–4419 (2004)

M.S. Gudipati, L.J. Allamandola, Facile generation and storage of polycyclic aromatic hydrocarbon ions in astrophysical ices. Astrophys. J. Lett. **596**, 195–198 (2003). doi:10.1086/379595

M.S. Gudipati, L.J. Allamandola, Polycyclic aromatic hydrocarbon ionization energy lowering in water ices. Astrophys. J. Lett. **615**, 177–180 (2004). doi:10.1086/426392

M.S. Gudipati, L.J. Allamandola, Unusual stability of polycyclic aromatic hydrocarbon radical cations in amorphous water ices up to 120 K: astronomical implications. Astrophys. J. **638**, 286–292 (2006a). doi:10.1086/498816

M.S. Gudipati, L.J. Allamandola, Double ionization of quaterrylene (C_4OH_2O) in water-ice at 20 K with Ly_α (121.6 nm) radiation. J. Phys. Chem. **110**, 9020 (2006b). doi:10.1021/jp061416n

M. Gudipati, J. Castillo-Rogez, *The Science of Solar System Ices* (Springer, New York, 2013)

M.S. Gudipati, J. Daverkausen, G. Hohlneicher, Higher excited states of aromatic hydrocarbons: polarized VUV fluorescence-excitation spectra of anthracene and pyrene in argon matrices at 15 K using synchrotron radiation. Chem. Phys. **173**, 143–157 (1993)

M.S. Gudipati, J.P. Dworkin, X.D.F. Chillier, L.J. Allamandola, Luminescence from vacuum-ultraviolet-irradiated cosmic ice analogs and residues. Astrophys. J. **583**, 514–523 (2003). doi:10.1086/345349

E. Gullikson, Hot-electron diffusion lengths in the rare-gas solids. Phys. Rev. B, Condens. Matter **37**, 7904–7906 (1988). doi:10.1103/PhysRevB.37.7904

G.B. Gumenchuk, A.N. Ponomaryov, I.V. Khyzhniy, S.A. Uyutnov, E.V. Savchenko, V.E. Bondybey, Triggering of relaxation cascades in pre-irradiated RGS by chemiluminescent reactions. Phys. Proc. **2**, 441–447 (2009). doi:10.1016/j.phpro.2009.07.029

H.D. Hagstrum, Rev. Mod. Phys. **23**, 185 (1951)

T.M. Halasinski, F. Salama, L.J. Allamandola, Investigation of the ultraviolet, visible, and near-infrared absorption spectra of hydrogenated polycyclic aromatic hydrocarbons and their cations. Astrophys. J. **628**, 555–566 (2005). doi:10.1086/430631

T. Henning, F. Salama, Carbon in the universe. Science **282**, 2204 (1998). doi:10.1126/science.282.5397.2204

H. Hijazi, H. Rothard, P. Boduch, I. Alzaher, F. Ropars, A. Cassimi, J.M. Ramillon, T. Been, B.B. d'Etat, H. Lebius, et al., Interaction of swift ion beams with surfaces: sputtering of secondary ions from LiF studied by XY-TOF-SIMS. Nucl. Instrum. Methods Phys. Res., Sect. B, Beam Interact. Mater. Atoms **269**, 1003–1006 (2011). doi:10.1016/j.nimb.2010.12.062

H. Hijazi, H. Rothard, P. Boduch, I. Alzaher, A. Cassimi, F. Ropars, T. Been, J. Ramillon, H. Lebius, B. Band'Etat, et al., Electronic sputtering: angular distributions of $(LiF)_nLi^+$ clusters emitted in collisions

of Kr (10.1 MeV/u) with LiF single crystals. Eur. Phys. J., D, At. Mol. Opt. Phys. **66**(3), 68 (2012). doi:10.1140/epjd/e2012-20545-3

H. Hijazi, H. Rothard, P. Boduch, I. Alzaher, T. Langlinay, A. Cassimi, F. Ropars, T. Been, J. Ramillon, H. Lebius, B. Ban-d'Etat, et al., Electronic sputtering of (LiF) by Kr (10 MeV/u): size dependent energy distributions of $(LiF)_nLi^+$ clusters with LiF single crystals. Eur. Phys. J. D, At. Mol. Opt. Plasma Phys. (2013)

J.M. Hollis, F.J. Lovas, P.R. Jewell, Interstellar glycolaldehyde: the first sugar. Astrophys. J. Lett. **540**, 107–110 (2000). doi:10.1086/312881

S. Ioppolo, H.M. Cuppen, C. Romanzin, E.F. van Dishoeck, H. Linnartz, Laboratory evidence for efficient water formation in interstellar ices. Astrophys. J. **686**, 1474–1479 (2008). doi:10.1086/591506

S. Ioppolo, M.E. Palumbo, G.A. Baratta, V. Mennella, Formation of interstellar solid CO_2 after energetic processing of icy grain mantles. Astron. Astrophys. **493**, 1017–1028 (2009). doi:10.1051/0004-6361:200809769

S. Ioppolo, H.M. Cuppen, E.F. van Dishoeck, H. Linnartz, Water formation at low temperatures by surface O_2 hydrogenation. I. Characterization of ice penetration. Phys. Chem. Chem. Phys. **12**, 12065 (2010). doi:10.1039/c0cp00250j

S. Ioppolo, Y. van Boheemen, H.M. Cuppen, E.F. van Dishoeck, H. Linnartz, Surface formation of CO_2 ice at low temperatures. Mon. Not. R. Astron. Soc. **413**, 2281–2287 (2011). doi:10.1111/j.1365-2966.2011.18306.x

P. Iza, L.S. Farenzena, E.F.. da Silveira, Effects of projectile track charging on the H-secondary ion velocity distribution. Nucl. Instrum. Methods Phys. Res., Sect. B, Beam Interact. Mater. Atoms **256**, 483–488 (2007). doi:10.1016/j.nimb.2006.12.070

T. Jalowy, R. Neugebauer, M. Hattass, J. Fiol, F. Afaneh, J. Pereira, V. Collado, E. Da Silveira, H. Schmidt-Böcking, K. Groeneveld, Dynamics of secondary ion emission: novel energy and angular spectrometry. Nucl. Instrum. Methods Phys. Res., Sect. B, Beam Interact. Mater. Atoms **193**(1), 762–767 (2002). doi:10.1016/S0168-583X(02)00900-X

T. Jalowy, T. Weber, R. Dörner, L. Farenzena, V. Collado, E. Da Silveira, H. Schmidt-Böcking, K. Groeneveld, Initial velocity of secondary ions from XY-TOF technique, simultaneous calibration by residual gas ionization. Int. J. Mass Spectrom. **231**(1), 51–58 (2004)

C. Jäger, H. Mutschke, T. Henning, F. Huisken, From PAHs to solid carbon, in *EAS Publications Series*, ed. by C. Joblin. A.G.G.M. Tielens EAS Publications Series, vol. 46 (2011), pp. 293–304. doi:10.1051/eas/1146031

R.E. Johnson, J. Schou, Sputtering of inorganic insulators, in *Symposium on the Occasion of the 250th Anniversary of the Royal-Danish-Academy-of-Sciences-and-Letters: Fundamental Processes in Sputtering of Atoms and Molecules (SPUT92)*, ed. by P. Sigmund. Mat. Fys. Medd. Dan. Vid. Selsk., vol. 43, (1993), pp. 403–493

P.V. Johnson, R. Hodyss, D.K. Bolser, R. Bhartia, A.L. Lane, I. Kanik, Ultraviolet-stimulated fluorescence and phosphorescence of aromatic hydrocarbons in water ice. Astrobiology **11**, 151–156 (2011). doi:10.1089/ast.2010.0568

R. Jost, *NATO ASI Series C Mathematical and Physical Sciences*, vol. 483 (Kluwer Academic, Norwell, 1996), p. 249.

J.K. Jørgensen, C. Favre, S.E. Bisschop, T.L. Bourke, E.F. van Dishoeck, M. Schmalzl, Detection of the simplest sugar, glycolaldehyde, in a solar-type protostar with ALMA. Astrophys. J. Lett. **757**, 4 (2012). doi:10.1088/2041-8205/757/1/L4

R. Kalish, A. Reznik, K.W. Nugent, S. Prawer, The nature of damage in ion-implanted and annealed diamond. Nucl. Instrum. Methods Phys. Res., Sect. B, Beam Interact. Mater. Atoms **148**, 626–633 (1999). doi:10.1016/S0168-583X(98)00857-X

H.D. Kang, R. Preuss, T. Schwarz-Selinger, V. Doser, Decomposition of multicomponent mass spectra using Bayesian probability theory. J. Mass. Spectrom. **37**, 748–754 (2002). doi:10.1002/jms.335

I. Khyzhniy, E.V. Savchenko, S. Uyutnov, A. Ponomaryov, V. Bondybey, Exoelectron emission from solid nitrogen. Radiat. Meas. **45**, 353–355 (2010). doi:10.1016/j.radmeas.2009.11.020

H.G. Kjaergaard, T.W. Robinson, K.A. Brooking, Calculated CH-stretching overtone spectra of naphthalene, anthracene and their cations. J. Phys. Chem. **104**, 11279–11303 (2000). doi:10.1021/jp002686n

R.F. Knacke, Y.H. Kim, W.M. Irvine, An upper limit to the acetylene abundance toward BN in the orion molecular cloud. Astrophys. J. **345**, 265–267 (1989). doi:10.1086/167902

S. Kuma, H. Nakahara, M. Tsubouchi, A. Takahashi, M. Mustafa, G. Sim, T. Momose, A.F. Vilesov, Laser induced fluorescence spectroscopy of tetracene with large Ar, Ne, and H_2 clusters in superfluid He nanodroplets. J. Chem. Phys. A **115**, 7392–7399 (2011). doi:10.1021/jp203341r

V.S. Langford, A.J. McKinley, T.I. Quickenden, Luminescent photoproducts in UV-irradiated ice. Acc. Chem. Res. **33**, 665–671 (2000)

S. Leach, M. Vervloet, A. Desprès, E. Bréheret, J.P. Hare, T.J. Dennis, H.W. Kroto, R. Taylor, D.R.M. Walton, Electronic spectra and transitions of the fullerene C60. Chem. Phys. **160**, 451–466 (1992). doi:10.1016/0301-0104(92)80012-K

C. Lee, Y. Fong, M. Tsaic, I. Wing, R. Wue, S. Lee, Study of the luminescence of H_2O and D_2O ices induced by charged-particle bombardment. Appl. Surf. Sci. **255**, 4716–4719 (2009)

L. Lieszkovsky, A.R. Filippelli, C.R. Tilford, Meteorological characteristics of a group of quadrupole partial-pressure analyzers. J. Vac. Sci. Technol. A **8**, 3838–3854 (1990). doi:10.1116/1.576458

H. Linnartz, J.-B. Bossa, J. Bouwman, H.M. Cuppen, S.H. Cuylle, E.F. van Dishoeck, E.C. Fayolle, G. Fedoseev, G.W. Fuchs, S. Ioppolo, K. Isokoski, T. Lamberts, K.I. Öberg, C. Romanzin, E. Tenenbaum, J. Zhen, Solid state pathways towards molecular complexity in space, in *IAU Symposium*. IAU Symposium, vol. 280 (2011), pp. 390–404. doi:10.1017/S1743921311025142

M.J. Loeffler, R.A. Baragiola, Photolysis of solid NH_3 and NH_3-H_2O mixtures at 193 nm. J. Chem. Phys. **133**, 214506 (2010). doi:10.1063/1.3506577

M.J. Loeffler, R.A. Baragiola, Isothermal decomposition of hydrogen peroxide dihydrate. J. Chem. Phys. **115** 5324 (2011). doi:10.1021/jp200188b

M.J. Loeffler, R.A. Baragiola, Blistering and explosive desorption of irradiated ammonia-water mixtures. Astrophys. J. **744** 102 (2012). doi:10.1088/0004-637X/744/2/102

M.J. Loeffler, U. Raut, R.A. Baragiola, Enceladus: a source of nitrogen and an explanation for the water vapor plume observed by Cassini. Astrophys. J. Lett. **649**, 133–136 (2006). doi:10.1086/508459

C. Lu, J. Vac. Sci. Technol. **12**, 578 (1975)

C. Lu, *Applications of Piezoelectric Quartz Crystal Microbalances* (Elsevier, Amsterdam, 1984). Chap. 2.

Z.G. Lu, P. Campbell, X.-C. Zhang, Free-space electro-optic sampling with a high-repetition-rate regenerative amplified laser. Appl. Phys. Lett. **71**, 593–595 (1997). doi:10.1063/1.119803

G. Malenkov, Liquid water and ices: understanding the structure and physical properties. J. Phys. Condens. Matter **21**, 283101 (2009)

V. Mennella, M.E. Palumbo, G.A. Baratta, Formation of CO and CO_2 molecules by ion irradiation of water ice-covered hydrogenated carbon grains. Astrophys. J. **615**, 1073–1080 (2004). doi:10.1086/424685

K.M. Merrill, B.T. Soifer, Spectrophotometric observations of a highly absorbed object in Cygnus. Astrophys. J. Lett. **189**, 27 (1974). doi:10.1086/181456

F. Meyer, P. Harris, C. Taylor, H. Meyer III, A. Barghouty, J. Adams, Sputtering of lunar regolith simulant by protons and singly and multicharged ar ions at solar wind energies. Nucl. Instrum. Methods Phys. Res., Sect. B, Beam Interact. Mater. Atoms **269**(11), 1316–1320 (2011)

B.P. Michael, J.A. Nuth III, L.U. Lilleleht, Zinc crystal growth in microgravity. Astrophys. J. **590**, 579–585 (2003). doi:10.1086/374918

E.H. Mitchell, M.J. Schaible, U. Raut, D. Fulvio, C.A. Dukes, R.A. Baragiola, in 43rd Lunar and Planetary Sci. Conf., vol. 2363 (2012)

N. Miyauchi, H. Hidaka, T. Chigai, A. Nagaoka, N. Watanabe, A. Kouchi, Formation of hydrogen peroxide and water from the reaction of cold hydrogen atoms with solid oxygen at 10 K. Chem. Phys. Lett. **456**, 27–30 (2008). doi:10.1016/j.cplett.2008.02.095

M.H. Moore, R.L. Hudson, Far-infrared spectra of cosmic-type pure and mixed ices. Astron. Astrophys. Suppl. Ser. **103**, 45–56 (1994)

G.M. Muñoz Caro, W.A. Schutte, UV-photoprocessing of interstellar ice analogs: new infrared spectroscopic results. Astron. Astrophys. **412**, 121–132 (2003). doi:10.1051/0004-6361:20031408

G.M. Muñoz Caro, U.J. Meierhenrich, W.A. Schutte, B. Barbier, A. Arcones Segovia, H. Rosenbauer, W.H.-P. Thiemann, A. Brack, J.M. Greenberg, Amino acids from ultraviolet irradiation of interstellar ice analogues. Nature **416**, 403–406 (2002)

G.M. Muñoz Caro, A. Jiménez-Escobar, J.Á. Martín-Gago, C. Rogero, C. Atienza, S. Puertas, J.M. Sobrado, J. Torres-Redondo, New results on thermal and photodesorption of CO ice using the novel Interstellar astrochemistry chamber (ISAC). Astron. Astrophys. **522**, 108 (2010). doi:10.1051/0004-6361/200912462

H. Mutschke, S. Zeidler, T. Posch, F. Kerschbaum, A. Baier, T. Henning, Far-infrared spectra of hydrous silicates at low temperatures. providing laboratory data for Herschel and ALMA. Astron. Astrophys. **492**, 117–125 (2008). doi:10.1051/0004-6361:200810312

Y. Oba, N. Miyauchi, H. Hidaka, T. Chigai, N. Watanabe, A. Kouchi, Formation of compact amorphous H_2O ice by codeposition of hydrogen atoms with oxygen molecules on grain surfaces. Astrophys. J. **701**, 464–470 (2009). doi:10.1088/0004-637X/701/1/464

A. Oliva-Florio, R.A. Baragiola, M.M. Jakas, E.V. Alonso, J. Ferron, Noble-gas ion sputtering yield of gold and copper-dependence on the energy and angle of incidence of the projectiles. Phys. Rev. B **35**, 2198–2204 (1987). doi:10.1103/PhysRevB.35.2198

T.C. Owen, T.L. Roush, J.L. Elliot, L.A. Young, C. Debergh, B. Schmitt, T.R. Geballe, R.H. Brown, M.J. Bartholomew, Surface ices and the atmospheric composition of Pluto. Science **261**, 745–748 (1993). doi:10.1126/science.261.5122.745

K.I. Öberg, G.W. Fuchs, Z. Awad, H.J. Fraser, S. Schlemmer, E.F. van Dishoeck, H. Linnartz, Photodesorption of CO ice. Astrophys. J. Lett. **662**, 23–26 (2007). doi:10.1086/519281
K.I. Öberg, A.C.A. Boogert, K.M. Pontoppidan, G.A. Blake, N.J. Evans, F. Lahuis, E.F. van Dishoeck, The c2d spitzer spectroscopic survey of ices around low-mass young stellar objects. III. CH_4. Astrophys. J. **678**, 1032–1041 (2008). doi:10.1086/533432
K.I. Öberg, E.C. Fayolle, H.M. Cuppen, E.F. van Dishoeck, H. Linnartz, Quantification of segregation dynamics in ice mixtures. Astron. Astrophys. **505**, 183–194 (2009a). doi:10.1051/0004-6361/200912464
K.I. Öberg, R.T. Garrod, E.F. van Dishoeck, H. Linnartz, Formation rates of complex organics in UV irradiated CH_3OH-rich ices. I. Experiments. Astron. Astrophys. **504**, 891–913 (2009b). doi:10.1051/0004-6361/200912559
K.I. Öberg, H. Linnartz, R. Visser, E.F. van Dishoeck, Photodesorption of ices. II. H_2O and D_2O. Astrophys. J. **693**, 1209–1218 (2009c). doi:10.1088/0004-637X/693/2/1209
K.I. Öberg, E.F. van Dishoeck, H. Linnartz, Photodesorption of ices. I. CO, N_2, and CO_2. Astron. Astrophys. **496**, 281–293 (2009d). doi:10.1051/0004-6361/200810207
K.I. Öberg, A.C.A. Boogert, K.M. Pontoppidan, S. van den Broek, E.F. van Dishoeck, S. Bottinelli, G.A. Blake, N.J. Evans II, The spitzer ice legacy: ice evolution from cores to protostars. Astrophys. J. **740**, 109 (2011). doi:10.1088/0004-637X/740/2/109
M.E. Palumbo, Formation of compact solid water after ion irradiation at 15 K. Astron. Astrophys. **453**, 903–909 (2006). doi:10.1051/0004-6361:20042382
G. Pascoli, A. Polleux, Condensation and growth of hydrogenated carbon clusters in carbon-rich stars. Astron. Astrophys. **359**, 799–810 (200)
J. Pereira, E. da Silveira, Axial energy distributions of Li^+ and F_- desorbed from LiF surfaces by fast ion impact. Appl. Surf. Sci. **390**(1), 158–163 (1997)
A. Ponomaryov, G. Gumenchuk, E. Savchenko, V.E. Bondybey, Radiation effects, energy storage and its release in solid rare gases. Phys. Chem. Chem. Phys. **9**, 1329–1340 (2007). doi:10.1039/b616441b
K.M. Pontoppidan, A.C.A. Boogert, H.J. Fraser, E.F. van Dishoeck, G.A. Blake, F. Lahuis, K.I. Öberg, N.J. Evans II, C. Salyk, The c2d spitzer spectroscopic survey of ices around low-mass young stellar objects. II. CO_2. Astrophys. J. **678**, 1005–1031 (2008). doi:10.1086/533431
T. Posch, F. Kerschbaum, H. Richter, H. Mutschke, Solid state features in the Herschel-pacs-range, in *ESA Special Publication*, ed. by A. Wilson ESA Special Publication, vol. 577 (2005), pp. 257–260
T. Posch, A. Baier, H. Mutschke, T. Henning, Carbonates in space: the challenge of low-temperature data. Astrophys. J. **668**, 993–1000 (2007). doi:10.1086/521390
P.B. Price, O.V. Nagornov, Y.D. He, P. Miocinovic, A. Richards, K. Woschnagg, B. Koci, V. Zagorodnov, Temperature profile for glacial ice at the South Pole: Implications for life in a nearby subglacial lake. Proc. Natl. Acad. Sci. USA **99**(12), 7844–7847 (2002). doi:10.1073/pnas.082238999
R.H. Prince, G.N. Sears, F.J. Morgan, Fluorescence of ice by low energy electrons. J. Chem. Phys. **64**, 3978–3984 (1976). doi:10.1063/1.432030
T.I. Quickenden, S.M. Trotman, D.F. Sangster, Pulse radiolytic studies of the ultraviolet and visible emissions from purified H_2O ice. J. Chem. Phys. **77**, 3790–3802 (1982). doi:10.1063/1.444352
C.V. Raman, K.S. Krishnan, A new type of secondary radiation. Nature **121**, 501–502 (1928). doi:10.1038/121501c0
U. Raut, M. Fama, B.D. Teolis, R.A. Baragiola, Characterization of porosity in vapor-deposited amorphous solid water from methane adsorption. J. Chem. Phys. **127**, 204713 (2007). doi:10.1063/1.2796166
U. Raut, D. Fulvio, M.J. Loeffler, R.A. Baragiola, Radiation synthesis of carbon dioxide in ice-coated carbon: implications for interstellar grains and icy moons. Astrophys. J. **752**, 159 (2012). doi:10.1088/0004-637X/752/2/159
J. Remy, L. Biennier, F. Salama, Plasma structure in a pulsed discharge environment. Plasma Sources Sci. Technol. **12**, 295–301 (2003). doi:10.1088/0963-0252/12/3/301
J. Remy, L. Biennier, F. Salama, Plasma in a pulsed discharge environment. IEEE Trans. Plasma Sci. **33**(2), 554–555 (2005). doi:10.1109/TPS.2005.845937
A. Rice, Y. Jin, X.F. Ma, X.-C. Zhang, D. Bliss, J. Larkin, M. Alexander, Terahertz optical rectification from (110) zinc-blende crystals. Appl. Phys. Lett. **64**, 1324–1326 (1994). doi:10.1063/1.111922
C.L. Ricketts, C.S. Contreras, R.L. Walker, F. Salama, The coupling of a reflectron time-of-flight mass spectrometer with a cosmic simulation chamber: a powerful new tool for laboratory astrophysics. Int. J. Mass Spectrom. **300**, 26–30 (2011). doi:10.1016/j.ijms.2010.11.017
C. Romanzin, S. Ioppolo, H.M. Cuppen, E.F. van Dishoeck, H. Linnartz, Water formation by surface O_3 hydrogenation. J. Chem. Phys. **134**, 084504 (2011)
N.J. Sack, R.A. Baragiola, Sublimation of vapor-deposited water ice below 170 K, and its dependence on growth conditions. Phys. Rev. B **48**, 9973–9978 (1993). doi:10.1103/PhysRevB.48.9973
F. Salama, PAHs in astronomy—a review, in *IAU Symposium*, ed. by S. Kwok, S. Sandford IAU Symposium, vol. 251 (2008), pp. 357–366. doi:10.1017/S1743921308021960

F. Salama, E.L.O. Bakes, L.J. Allamandola, A.G.G.M. Tielens, Assessment of the polycyclic aromatic hydrocarbon-diffuse interstellar band proposal. Astrophys. J. **458**, 621 (1996). doi:10.1086/176844

F. Salama, G.A. Galazutdinov, J. Krełowski, L. Biennier, Y. Beletsky, I.-O. Song, Polycyclic aromatic hydrocarbons and the diffuse interstellar bands: a survey. Astrophys. J. **728**, 154 (2011). doi:10.1088/0004-637X/728/2/154

S.A. Sandford, L.J. Allamandola, T.R. Geballe, Spectroscopic detection of molecular-hydrogen frozen in interstellar ices. Science **262**, 400–4004 (1993). doi:10.1126/science.11542874

A. Sassara, G. Zerza, M. Chergui, S. Leach, Absorption wavelengths and bandwidths for interstellar searches of C_{60} in the 2400–4100 å region. Astrophys. J. Supp. Ser. **135**, 263–273 (2001). doi:10.1086/323533

G. Sauerbrey, Verwendung von Schwingquarzen zur Wgung dnner Schichten und zur Mikrowgung. Z. Phys. **155**, 206–222 (1959)

E.V. Savchenko, G.B. Gumenchuk, E.M. Yurtaeva, A.G. Belov, I.V. Khyzhniy, M. Frankowski, M.K. Beyer, A.M. Smith-Gicklhorn, A.N. Ponomaryov, V.E. Bondybey, Anomalous low-temperature desorption from preirradiated rare gas solids. J. Lumin. **112**, 101–104 (2005). doi:10.1016/j.jlumin.2004.09.004

E.V. Savchenko, A.G. Belov, G.B. Gumenchuk, A.N. Ponomaryov, V.E. Bondybey, Oxygen-driven relaxation processes in pre-irradiated Ar cryocrystals. Low Temp. Phys. **32**, 1078–1081 (2006). doi:10.1063/1.2389016

E.V. Savchenko, I.V. Khyzhniy, G.B. Gumenchuk, V.E. Bondybey, Relaxation emission of electrons and photons from rare-gas solids: correlation and competition between TSL and TSEE. Phys. Status Solidi C **4**, 1088–1091 (2007). doi:10.1002/pssc.200673809

E.V. Savchenko, G. Zimmerer, V.E. Bondybey, Electronically induced modification of atomic solids and their relaxation probed by luminescence methods. J. Lumin. **129**, 1866–1868 (2009). doi:10.1016/j.jlumin.2009.01.040

E.V. Savchenko, I.V. Khyzhniy, S.A. Uyutnov, G.B. Gumenchuk, A.N. Ponomaryov, M.K. Beyer, V.E. Bondybey, Formation of $(Xe_2H)^*$ centers in solid Xe via recombination: nonstationary luminescence and internal electron emission. Low Temp. Phys. **36**, 407–410 (2010a). doi:10.1063/1.3432249

E.V. Savchenko, I.V. Khyzhniy, S.A. Uyutnov, G.B. Gumenchuk, A.N. Ponomaryov, V.E. Bondybey, Relaxation of charged and neutral particles in doped atomic solids: TSL, OSL, TSEE, OSEE and their interconnection. IOP Conf. Ser., Mater. Sci. Eng. **15**, 012082 (2010b). doi:10.1088/1757-899X/15/1/012082

E.V. Savchenko, I.V. Khyzhniy, S.A. Uyutnov, G.B. Gumenchuk, A.N. Ponomaryov, V.E. Bondybey, Radiation effects in atomic cryogenic solids. Nucl. Instrum. Methods Phys. Res., Sect. B, Beam Interact. Mater. Atoms **268**, 3239–3242 (2010c). doi:10.1016/j.nimb.2010.05.098

E.V. Savchenko, I.V. Khyzhniy, S.A. Uyutnov, G.B. Gumenchuk, A.N. Ponomaryov, M.K. Beyer, V.E. Bondybey, Charging effects in an electron bombarded ar matrix and the role of chemiluminescence-driven relaxation. J. Phys. Chem. **A 115**, 7258–7266 (2011). doi:10.1021/jp2004419

E.V. Savchenko, I.V. Khyzhniy, S.A. Uyutnov, G.B. Gumenchuk, A.N. Ponomaryov, V.E. Bondybey, Charging effect and relaxation processes in electron bombarded cryogenic solids. Nucl. Instrum. Methods Phys. Res., Sect. B, Beam Interact. Mater. Atoms **277**, 131–135 (2012). doi:10.1016/j.nimb.2011.12.042

E. Schindhelm, K. France, G.J. Herczeg, E. Bergin, H. Yang, A. Brown, J.M. Brown, J.L. Linsky, J. Valenti, Lyα dominance of the classical T Tauri far-ultraviolet radiation field. Astrophys. J. Lett. **756**, 23 (2012). doi:10.1088/2041-8205/756/1/L23

J. Schou, H. Sørensen, P. Børgensen, The measurement of electron-induced erosion of condensed gases: experimental methods. Nucl. Instrum. Methods Phys. Res., Sect. B, Beam Interact. Mater. Atoms **5**, 44–57 (1984). doi:10.1016/0168-583X(84)90568-8

B.J. Selby, T.I. Quickenden, G. Freeman, Isotopic effects on the time-dependences of 420 nm ice luminescence excited by UV light. React. Kinet. Catal. Lett. **47**, 686–698 (2006). doi:10.1134/S0023158406050065

K. Sellgren, M.W. Werner, J.G. Ingalls, J.D.T. Smith, T.M. Carleton, C. Joblin, C_{60} in reflection nebulae. Astrophys. J. Lett. **722**, 54–57 (2010). doi:10.1088/2041-8205/722/1/L54

E. Seperuelo Duarte, A. Domaracka, P. Boduch, H. Rothard, E. Dartois, E.F. da Silveira, Laboratory simulation of heavy-ion cosmic-ray interaction with condensed CO. Astron. Astrophys. **512**, 71 (2010). doi:10.1051/0004-6361/200912899

J. Shi, B.D. Teolis, R.A. Baragiola, Irradiation-enhanced adsorption and trapping of O^{-2} on nanoporous water ice. Phys. Rev. B **79**, 235422 (2009). doi:10.1103/PhysRevB.79.235422

J. Shi, U. Raut, J.-H. Kim, M. Loeffler, R.A. Baragiola, Ultraviolet photon-induced synthesis and trapping of H_2O_2 and O_3 in porous water ice films in the presence of ambient O_2: implications for extraterrestrial ice. Astrophys. J. Lett. **738**, 3 (2011). doi:10.1088/2041-8205/738/1/L3

J. Shi, M. Fama, B.D. Teolis, R.A. Baragiola, Ion-induced electrostatic charging of ice at 15–160 K. Phys. Rev. B **85**, 035424 (2012). doi:10.1103/PhysRevB.85.035424

D. Sicilia, S. Ioppolo, T. Vindigni, G.A. Baratta, M.E. Palumbo, Nitrogen oxides and carbon chain oxides formed after ion irradiation of CO:N_2 ice mixtures. Astron. Astrophys. **543**, 155 (2012). doi:10.1051/0004-6361/201219390

P.H. Siegel, THz instruments for space. IEEE Trans. Antennas Propag. **55**, 2957–2965 (2007). doi:10.1109/TAP.2007.908557

H. Singh, J.W. Coburn, D.B. Graves, Appearance potential mass spectrometry: discrimination of dissociative ionization products. J. Vac. Sci. Technol., A, Vac. Surf. Films **18**, 299–305 (2000). doi:10.1116/1.582183

R.G. Smith, G. Robinson, A.R. Hyland, G.L. Carpenter, Molecular ices as temperature indicators for interstellar dust: the 44- and 62-m lattice features of H_2O ice. Mon. Not. R. Astron. **271**, 481–489 (1994)

J.D.T. Smith, B.T. Draine, D.A. Dale, J. Moustakas, R.C. Kennicutt Jr., G. Helou, L. Armus, H. Roussel, K. Sheth, G.J. Bendo, B.A. Buckalew, D. Calzetti, C.W. Engelbracht, K.D. Gordon, D.J. Hollenbach, A. Li, S. Malhotra, E.J. Murphy, F. Walter, The mid-infrared spectrum of star-forming galaxies: global properties of polycyclic aromatic hydrocarbon emission. Astrophys. J. **656**, 770–791 (2007). doi:10.1086/510549

C. Stehl, C. Joblin, L. d'Hendecourt, Foreword. EAS Publ. Ser. **58**, 1–3 (2012)

G. Strazzulla, G.A. Baratta, Carbonaceous material by ion irradiation in space. Astron. Astrophys. **266**, 434–438 (1992)

G. Strazzulla, G.A. Baratta, M.E. Palumbo, Vibrational spectroscopy of ion-irradiated ices. Spectrochim. Acta **57**, 825–842 (2001)

X.F. Tan, F. Salama, Cavity ring-down spectroscopy and theoretical calculations of the $S_1(^1B_{3u}) \leftarrow S_0(^1A_g)$) transition of jet-cooled perylene. J. Chem. Phys. **122**, 084318 (2005). doi:10.1063/1.1851502

B.D. Teolis, M. Fama, R.A. Baragiola, Low density solid ozone. J. Chem. Phys. **127**, 074507 (2007a). doi:10.1063/1.2762215

B.D. Teolis, M.J. Loeffler, M. Fama, R.A. Baragiola, Infrared reflectance spectroscopy on thin films: interference effects. Icarus **190**, 274–279 (2007b). doi:10.1063/1.2762215

A.G.G.M. Tielens, W. Hagen, J.M. Greenberg, Interstelar ice. J. Phys. Chem. **87**, 4220–4229 (1983). doi:10.1021/j100244a049

A.G.G.M. Tielens, *The Physics and Chemistry of the Interstellar Medium* (Cambridge University Press, Cambridge, 2005)

A.G.G.M. Tielens, Interstellar polycyclic aromatic hydrocarbon molecules. Annu. Rev. Astron. Astrophys. **46**, 289–337 (2008). doi:10.1146/annurev.astro.46.060407.145211

Y. Ueno, R. Rungsawang, I. Tomita, K. Ajito, Quantitative measurements of amino acids by terahertz time-domain transmission spectroscopy. Anal. Chem. **78**, 5424–5428 (2006). doi:10.1021/ac060520y

F. van der Tak, The first results from the Herschel-HIFI mission. Adv. Space Res. **49**, 1395–1407 (2012). doi:10.1016/j.asr.2012.02.027

E.F. van Dishoeck, B. Jonkheid, M.C. van Hemert, Photoprocesses in protoplanetary disks. Faraday Discuss. **133**, 231–243 (2006). doi:10.1039/B517564J.

E.F. van Dishoeck, J.K. Jørgensen, Star and planet-formation with ALMA: an overview. Astrophys. Space Sci. **313**, 15–22 (2008). doi:10.1007/s10509-007-9600-y

E.F. van Dishoeck, L.E. Kristensen, A.O. Benz, E.A. Bergin, P. Caselli, J. Cernicharo, F. Herpin, M.R. Hogerheijde, D. Johnstone, R. Liseau, B. Nisini, R. Shipman, M. Tafalla, F. van der Tak, F. Wyrowski, Y. Aikawa, R. Bachiller, A. Baudry, M. Benedettini, P. Bjerkeli, G.A. Blake, S. Bontemps, J. Braine, C. Brinch, S. Bruderer, L. Chavarría, C. Codella, F. Daniel, T. de Graauw, E. Deul, A.M. di Giorgio, C. Dominik, S.D. Doty, M.L. Dubernet, P. Encrenaz, H. Feuchtgruber, M. Fich, W. Frieswijk, A. Fuente, T. Giannini, J.R. Goicoechea, F.P. Helmich, G.J. Herczeg, T. Jacq, J.K. Jørgensen, A. Karska, M.J. Kaufman, E. Keto, B. Larsson, B. Lefloch, D. Lis, M. Marseille, C. McCoey, G. Melnick, D. Neufeld, M. Olberg, L. Pagani, O. Panić, B. Parise, J.C. Pearson, R. Plume, C. Risacher, D. Salter, J. Santiago-García, P. Saraceno, P. Stäuber, T.A. van Kempen, R. Visser, S. Viti, M. Walmsley, S.F. Wampfler, U.A. Yıldız, Water in star-forming regions with the Herschel space observatory (WISH). I. Overview of key program and first results. Publ. Astron. Soc. Pac. **123**, 138–170 (2011). doi:10.1086/658676

E.F. van Dishoeck, R. Visser, Molecular photodissociation, submitted to *Modern Concepts in Laboratory Astrochemistry*, ed. by S. Schlemmer, H. Mutschke, Th. Giesen (Springer, Berlin, 2013)

L. Verstraete, The role of PAHs in the physics of the interstellar medium, in *EAS Publications Series*, ed. by C. Joblin, A.G.G.M. Tielens EAS Publications Series, vol. 46 (2011), pp. 415–426. doi:10.1051/eas/1146043

R.A. Vidal, B.D. Teolis, R.A. Baragiola, Angular dependence of the sputtering yield of water ice by 100 keV proton bombardment. Appl. Surf. Sci. **588**, 1 (2005). doi:10.1016/j.susc.2005.05.007

D.R. Vij, *Luminescence of Solids* (Plenum, New York, 1998), p. 427

X. Xie, J. Dai, X.-C. Zhang, Coherent control of THz wave generation in ambient air. Phys. Rev. Lett. **96**(7), 075005 (2006). doi:10.1103/PhysRevLett.96.075005

T. Yada, K. Norizawa, M. Hirai, C. Yamanaka, M. Ikeya, Optically stimulated luminescence study on gamma-irradiated ice frozen from H_2O and D_2O. Jpn. J. Appl. Phys. **41**, 5874–5880 (2002)
B.C. Wang, J.C. Chang, H.C. Tso, H.F. Hsu, C.Y. Cheng, Theoretical investigation the electroluminescence characteristics of pyrene and its derivatives. J. Mol. Struct., Theochem **629**, 11–20 (2003)
N. Watanabe, A. Kouchi, Efficient formation of formaldehyde and methanol by the addition of hydrogen atoms to CO in H_2O–CO ice at 10 K. Astrophys. J. Lett. **571**, 173–176 (2002). doi:10.1086/341412
M.S. Westley, R.A. Baragiola, R.E. Johnson, G.A. Baratta, Photodesorption from low-temperature water ice in interstellar and circumsolar grains. Nature **373**, 405–407 (1995). doi:10.1038/373405a0
M.S. Westley, G.A. Baratta, R.A. Baragiola, Density and index of refraction of water ice films vapor deposited at low temperatures. J. Chem. Phys. **108**, 3321–3327 (1998). doi:10.1063/1.475730
A. Winkler, J.T. Yates, Capillary array dosing and angular desorption distribution measurements: a general formalism. J. Vac. Sci. Technol., A, Vac. Surf. Films **6**, 2929–2933 (1998). doi:10.1116/1.575453
P.M. Woods, G. Kelly, S. Viti, B. Slater, W.A. Brown, F. Puletti, D.J. Burke, Z. Raza, On the formation of glycolaldehyde in dense molecular cores. Astrophys. J. **750**, 19 (2012). doi:10.1088/0004-637X/750/1/19
Q. Wu, X.-C. Zhang, Free-space electro-optic sampling of terahertz beams. Appl. Phys. Lett. **67**, 3523–3525 (1995). doi:10.1063/1.114909
A. Wucher, Sputtering: experiment, in *Ion Beam Science: Solved and Unsolved Problems*, eds. by P. Sigmund. Mat. Fys. Medd. Dan. Vid. Selsk., vol. 52 (2007), pp. 405–432
G. Zasowski, F. Kemper, D.M. Watson, E. Furlan, C.J. Bohac, C. Hull, J.D. Green, Spitzer infrared spectrograph observations of class I/II objects in Taurus: composition and thermal history of the circumstellar ices. Astrophys. J. **694**, 459–478 (2009). doi:10.1088/0004-637X/694/1/459
X.-C. Zhang, J. Xu, *Introduction to THz Wave Photonics* (Springer, New York, 2010), pp. 1–246. doi:10.1007/978-1-4419-0978-7
W.J. Zheng, R.I. Kaiser, Formation of hydroxylamine (NH_2OH) in electron irradiated ammonia-water ices. J. Phys. Chem. **114**, 5251–5255 (2010)